Modelling Dynamic Postural Stability Margins during Fixed-Support Balance Recovery

by

Keaton Alexander Inkol

A Thesis

presented to

The University of Guelph

In partial fulfilment of requirements
for the degree of

Master of Science

in

Human Health and Nutritional Sciences

Guelph, Ontario, Canada

ABSTRACT

MODELLING DYNAMIC STABILITY MARGINS DURING FIXED-SUPPORT BALANCE RECOVERY

Keaton Alexander Inkol
University of Guelph, 2018

Advisor:
Dr. Lori Ann Vallis

This dissertation is an investigation into the use of whole-body center of mass (CoM) dynamics for evaluation of balance control following robotic platform perturbations evoking fixed base of support postural strategies. Two primary purposes were identified: i) ascertain the effects of anthropometric model reductions on estimations of extrapolated CoM-based margins of stability (MoS); and ii) develop a biomechanical model to evaluate changes in dynamic MoS when accounting for both a counterbalance postural strategy and platform perturbation. Experimental data collection and analyses (kinematics) of young adults responding to perturbations in addition to forward dynamics simulations of the proposed model suggested the following: i) the degree of anthropometric simplicity sufficient for CoM estimates depends on the perturbations utilized; ii) counterbalance strategies produce a larger feasible MoS relative to those derived using an inverted pendulum model. Thus, these findings highlight the importance of considering the postural task/mechanics when using CoM based stability metrics.

ACKNOWLEDGEMENTS

Foremost, I would like to thank my advisor Dr. Lori Ann Vallis. Lori, your guidance and support throughout my years in the Gait Lab has been truly invaluable. You've been essential in my development as both a scientist and individual. In the future, I hope to be able to balance work and personal life as well as you have – it's admirable – and look forward towards collaborating again.

I would like to thank the professors that have been a part of both my advisory and defence committee. To both Dr. Lori Ann Vallis and Dr. Stephen Brown, thank you for guidance and feedback during the completion of my thesis. To, Dr. John Zettel, thank you for your time and the thought-provoking questions asked during my defence. All three of you have helped me develop into a better critical thinker as I move towards the beginning of my doctoral program.

To my fellow Gait Lab members: David Shulman, Becky Breau, and Emily McIntosh. I'm thankful for all the times you helped me navigate through the challenges that grad school can throw at you and glad to have made a lifelong friendship in each of you. I look forward to seeing you all succeed in the future. I'd also like to extend a thanks to those in the Brown, Bent, Power, and Srbely labs for their friendship and for being a great group to grab a beer with.

To Mom, Dad, Kelsey and Jordon, I appreciate your support and encouragement (and for the roof over my head) throughout the completion of my Master's degree. To Alisha, thank you for sticking around through the highs and lows. You've been an amazing supporter throughout this entire process.

TABLE OF CONTENTS

LIST OF TABLES

LIST OF FIGURES

LIST OF SYMBOLS AND ABBREVIATIONS

Chapters 1 & 2. General Introduction, Review of the Literature

BoS	Base of support
CNS	Central nervous system
CoM	Centre of mass
EMG	Electromyography
IP	Inverted pendulum
CoP,μ	Centre of pressure (position; m)
ODE	Ordinary differential equation
$c, \dot{c}, \ddot{c}$	Uniplanar position (m), velocity (m/s), and acceleration (m/s^2) of CoM
I	Moment of inertia from IP model ($I \approx m\ell^2$; kg·m^2)
m	Total body mass (excluding BoS; kg)
g	Gravitational acceleration (9.81 m/s^2)
ℓ	IP length (m)
FSR	Feasible Stability Region
xCoM, χ	Extrapolated centre of mass (m)
ω_0	Eigenfrequency of non-inverted pendulum ($\omega_0 = \sqrt{g/\ell}$; s^{-1})
MoS, ξ	Margin of stability (m)
b_i	Position of *i*th BoS boundary (m)
NLP	Nonlinear programming
DC	Direct Collocation

Chapter 4. Does simplifying the anthropometric model used to estimate center of mass …

$\boldsymbol{c}$	Whole-body CoM position vector (3D; cm)
$\bar{\boldsymbol{c}}_i$	CoM position vector (3D) of *i*th segment (cm)
ρ_i	Mass proportion (of total mass) of *i*th segment (%)
WFM	Winter full anthropometric model (modified; 13-segments)
NAr	WFM model excluding arm segments

HTP	Head, trunk, and pelvis segments
CoMp	Pelvis CoM
AP	Anteroposterior
ML	Mediolateral
$b_{\max}/b_{\min}$	Maximum/minimum BoS boundaries in plane (cm)
$\mathrm{MoS}_{\mathrm{peak}}$	Minimum MoS at peak platform velocity (cm)
r	Cross-correlation coefficient
ε_{S}	Absolute error term for simplified model (NAr, HTP, CoMp; cm)
ξ_{WFM}, ξ_{S}	MoS of WFM or simplified model (NAr, HTP, CoMp; cm)
RMS	Root mean square error (cm)
ME	Maximum absolute error (cm)
ANOVA	Analysis of variance

Chapter 6. Estimating optimal dynamic stability margins for lateral fixed-support strategies …

$\{c_{t_0}\}$	Set of initial horizontal CoM positions normalized to BoS length
S	Standing task – no perturbation (bilateral, double-support configurations)
$\mathrm{P}_{\mathrm{mid}}$	Perturbation task – initialize at platform velocity $\dot{p}_x = 0.435$ m/s
$\mathrm{P}_{\mathrm{peak}}$	Perturbation task – initialize at platform velocity $\dot{p}_x = 0.870$ m/s
S′, S″	Variant of S configurations for single limb support initialization (left ′ or right ″ leg)
t_0, t_f	Initial and final time of simulations (or initial/final node when discretized)
c_{t_0}, $\dot{c}_{t_0}$	Initial horizontal CoM position and velocity (*normalized*)
fBoS	Fixed-BoS control strategy (e.g. counterbalance)
ΔBoS	Change in BoS control strategy
$\bar{\bar{c}}$	Instantaneous horizontal CoM position, normalized to BoS ($[c - b_R]\ell_b^{-1}$)
b_R, b_L	Right/left BoS boundaries (head 5th metatarsals; m)
$\boldsymbol{q}$, $\dot{\boldsymbol{q}}$, $\ddot{\boldsymbol{q}}$	Generalized coordinates, velocities, and accelerations (vector)
p_x, $\dot{p}_x$, $\ddot{p}_x$	Uniplanar platform position (m), velocity (m/s), and acceleration (m/s^2)
φ_i, $\dot{\varphi}_i$, $\ddot{\varphi}_i$	Angular position (rad), velocity (rad/s), and acceleration (rad/s^2) of ith segment about AP axis
$\boldsymbol{Q}$	Column vector of generalized forces (conservative + non-conservative; N or N·m)

$\boldsymbol{\mathcal{J}}$	Bilateral stance constraint force(s) matrix
$\boldsymbol{M}$	Inertial mass matrix
$\boldsymbol{C}$	Coriolis/centripetal force matrix
$\boldsymbol{G}$	Gravitational toppling vector
λ	Vector of Langrage multipliers associated with bilateral stance
F_p	Horizontal force applied to platform/support-surface (N)
τ_j	Sum of active and passive joint torques (actuation) applied to jth joint (N·m)
γ_j	Active torque at jth joint; sum of agonist (A) and antagonist (ANT) torques (N·m)
B_j, K_j	Damping (N·m·s rad^{-1}) and elastic (N·m rad^{-1}) coefficients of the jth joint
$\boldsymbol{a}$	Vector of muscle activations a (1)
$\tau_{\max}$	Maximum feasible joint torque from muscle group (N·m)
$\boldsymbol{u}$	Vector of neural excitations u that correspond to muscles in $\boldsymbol{a}$ (1)
t_A,t_D	Activation/deactivation time constants for muscle activation dynamics (s)
η	Smoothing parameter for muscle dynamics (1)
$\boldsymbol{\Phi}$	Vector of holonomic, equality, constraint function(s)
ℓ_i	Length of ith segment (m)
a_y	Right ankle height (m)
$\boldsymbol{q}_{t_0}$	Initial value of $\boldsymbol{q}$ for simulations (reference configuration)
m	Total body mass (kg)
Ev	Eversion about ankle
In	Inversion about ankle
Ab	Abduction about hip
Ad	Adduction about hip
ℓ_P, ℓ_F, ℓ_b	Width of pelvis/foot and resultant BoS in simulations ($\ell_b = \ell_P + \ell_F$; m)
K_A, B_A, K_H, B_H	Elastic (N·m rad^{-1}) and damping (N·m·s rad^{-1}) coefficient of ankle/hip joints (A/H)
ζ	Cost function for trajectory (parameter) optimization
h_k	Step size from node k to $k+1$ (s)
$\dot{\boldsymbol{x}}, f_k$	Evolution function of dynamical system ($d\boldsymbol{x}/dt$)
$\boldsymbol{x}_k, \boldsymbol{u}_k$	State and control vectors at node k
$\boldsymbol{x}_{\min}$, $\boldsymbol{x}_{\max}$	Minimum and maximum state boundaries within simulations
c_{RC}, $\boldsymbol{q}_{RC}$	Reference configurations, value of $\boldsymbol{q}$ at t_0 that yields a specific value of c

$\lfloor\varphi_i,\varphi_k\rfloor_{\min}$, $\lfloor\varphi_i,\varphi_k\rfloor_{\max}$	Minimum and maximum relative joint angles permissible within simulations
F_x, F_y	Horizontal and vertical ground reaction force components under stance limb (N)
$\ddot{c}_{x,i}, \ddot{c}_{y,i}$	Horizontal and vertical accelerations of ith segment CoM for calculating F_x, F_y
$\boldsymbol{z}$	Vector of parameterized state and control trajectories (plus t_f)

Appendices

LCS	Local (segmental) coordinate system
GCS	Global coordinate system or reference frame
(x, y, z)	3D position vector in LCS
(x', y', z')	Transformed position vector (x, y, z) within GCS
$\boldsymbol{R}$, $\boldsymbol{o}$	Rotation matrix and linear position of LCS in GCS
b_R,b_L,b_A,b_P	Right, left, anterior, and posterior BoS boundaries
EOM	Equations of motion
T	Net kinetic energy of body (J)
V	Net potential energy of body (J)
L	Lagrangian; net difference between T and V (J)
N	Number of segments within biomechanical system
n	Number of degrees of freedom
$\boldsymbol{q}$, $\dot{\boldsymbol{q}}$, $\ddot{\boldsymbol{q}}$	Generalized coordinates, velocities, and accelerations (vector)
m_i	Mass of ith segment (kg)
$\boldsymbol{I}_i$	Inertia tensor of ith segment
$\boldsymbol{r}_i$,$\dot{\boldsymbol{r}}_i$	3D Position (m) and velocity (m/s) of ith segment CoM in GCS
$\boldsymbol{\varphi}_i$, $\dot{\boldsymbol{\varphi}}_i$	Angular position (rad) and velocity (rad/s) of ith segment CoM in GCS
g	Acceleration due to gravity (9.81 m/s^2)
$\bar{\ell}_i$	Length from ith segment origin to CoM (m)
ℓ_i	Total length of ith segment (m)
Φ_j	jth holonomic constraint function ($\Phi_j = 0$)
λ_j	jth Lagrange multiplier corresponding to Φ_j
Q_i	Generalized force corresponding to q_i (N or N·m)

d	Number of constraint functions (length of Φ)
$\boldsymbol{M}$	Inertial mass matrix
$\boldsymbol{C}$	Coriolis/centripetal force matrix
$\boldsymbol{G}$	Gravitational toppling vector
$\boldsymbol{Q}$	Generalized force vector for conservative/non-conservative forces
$\boldsymbol{\mathcal{J}}, \dot{\boldsymbol{\mathcal{J}}}$	Jacobian matrix of $\Phi(q)$ and its time derivative
λ	Vector of Lagrange multipliers corresponding to $\boldsymbol{\mathcal{J}}$
$\boldsymbol{\Psi}_i$	Jacobian of linear CoM velocity of ith segment as function of $\dot{q}$
$\boldsymbol{\Upsilon}_i$	Jacobian of angular CoM velocity of ith segment as function of $\dot{q}$
M_{ij}, C_{ij}	Element ij within inertial matrix $\boldsymbol{M}$ or Coriolis/centripetal force matrix $\boldsymbol{C}$
I_i	Moment of inertia about z axis (AP) of ith segment (kg·m^2)
h, w	Height or width dimension of trunk segment
$c_y\big\vert_{\bar{c}=0.5}$	Height of CoM evaluated at a normalized horizontal CoM position of 0.5

LIST OF APPENDICES

Chapter 1. General Introduction

Maintenance of upright posture within bipedal mechanics is an inherently challenging task. Gravitational toppling of linked segments coupled with a narrow base of support (BoS; e.g. location of area in contact with support-surface) presents a continuous source of instability. The challenge of standing may be further amplified upon application of some external force that increases the demand of the central nervous system (CNS) to prevent a total loss of balance, i.e. a fall. These destabilizing forces (perturbations) can be applied through various means including a push, contact with a slippery low-friction surface, or an obstacle on the ground. Even movements of self (internal perturbations; e.g., reaching, forceful respiration) must be corrected either proactively or reactively (if proactive responses are insufficient) to maintain upright balance (Jeong 1991; Aimola et al. 2011). Although not typically of concern for healthy young individuals, successful execution of corrective responses can present a much greater motor control challenge within work environments that require manual labour and can also present challenges for older adult and clinical populations (e.g., post-stroke). For example, unintentional falls resulted in approximately 85% of hospitalizations for Canadian senior citizens from 2008-2009 (73,190 total; CIHI 2010). The care and surgical interventions that follow injuries have be noted as a large source of expenditure for the Canadian healthcare system (Papadimitropoulos et al. 1997). Given the general trend towards an increase in the percent of the Canadian population above 65 years of age (Statistics Canada 2010), attenuating the likely concurrent increase in fall-related injuries within the coming decades requires pre-emptive actions aimed to improve our understanding of balance recovery.

For biomechanists, research questions involving balance control are approached from multiple perspectives. Researchers may be interested in the physiological changes that are closely linked to high fall-risk populations, e.g. muscle fibre contractile properties, motor excitability, muscle adiposity, etc. (Miljkovic et al. 2015; Addison et al. 2017). Similarly, pathologically-induced structural changes to the skeletal system such as arthritis may also be associated with an increased fall-risk. These changes can affect the mechanical properties of

osseous tissue (e.g. stiffening) and/or yield chronic pain (Armstrong et al. 2005; Stanmore et al. 2013). In contrast to the aforementioned area(s) of focus, others may be interested in the underlying motor control that maintains upright balance or coordinates it with additional tasks (e.g. locomotion, obstacle avoidance, reach and grasp; Cinelli et al. 2008; Zettel et al. 2008; Huntley et al. 2017c; Worden and Vallis 2017). For example, many older adults have diminished cognitive capabilities despite the evident link between allocation of cognitive resources and balance control (Maki and McIlroy 2007; Zettel et al. 2008; Inkol et al. 2018a). It may be the case then that paradigms focused primarily on these higher-level processes represent a vital course of study for falls prevention strategies.

One tool that can be used effectively to further our insight into balance control is biomechanical modelling (e.g. musculoskeletal, mathematical). It is able to incorporate elements of the approaches mentioned *a priori* that are used to investigate balance control. It also allows for highly structured (through hypothetical) balance-recovery scenarios. Used by many research groups, these models can be used to design controllers that reflect CNS behaviour using physiologically-realistic actuators or sensory integration (van der Kooij et al. 2001; Micheau et al. 2003) or to derive optimal control solutions for certain mechanical behaviours (Kuo 1995, 2005; Yang et al. 2007; Versteeg et al. 2016). Modelling can also provide insight into the role of specific components or biological parameters within a control system. By adjusting the contributions of these components within the defined control system (bounded by biologically accepted norms), these models may then yield numerical evaluations of balance, or other tasks, that can be applied to experimental data (e.g. Hof et al. 2005). Though there are caveats, especially given the approximations of a system as complex as the human body, modeling is an inherently valuable tool in biomechanics. Advances in computational processing power and affordability have further made biomechanical modelling a feasible area of investigation for many researchers.

The following sections within this thesis will examine the concepts introduced above, primarily regarding biomechanical modelling, in greater detail. Chapter 2 will provide a review of the literature related to balance recovery and applications of biomechanical modelling to this area of the literature. The objectives of this thesis will then be introduced prior to dissemination

of the two experiments completed (Chapters 3-6). Chapter 7 will involve a general discussion of the experimental results presented with a focus on connecting the outcomes of the two studies, contributions to the current literature, and future directions.

Chapter 2. Review of the Literature

2.1 Balance Recovery Strategies

2.1.1 Overview of Categories

Balance within a bipedal system (e.g. humans) requires maintenance of the whole-body center of mass (CoM) within the available boundaries of the BoS. During quiet standing, a combination of viscoelastic tissue properties surrounding the ankle joint and low magnitude muscle synergies maintain this relationship (Winter et al. 1998; Masani et al. 2003; Casadio et al. 2005). However, responding to an external perturbation requires active changes to the CNS output to compensate for instability (falling). Perturbations may exist in many forms; to address our specific research questions we have chosen to focus on perturbations that involve sudden acceleration(s) of the BoS induced by robotic platform translations (*unless noted otherwise*). These translations effectively place an individual within a non-inertial reference frame and provide high degree of experimenter controllability of perturbation characteristics, e.g. peak velocity, displacement, etc. A comparable scenario would be an individual standing on a bus that suddenly accelerates within any given direction. In order to prevent a fall following these perturbations, the CNS executes proactive and/or reactive balance control strategies characterized by patterns of muscle activity that produce corrective adjustments to posture and the whole-body CoM (Horak and Nashner 1986).

It should be noted that this method of postural response induction is not without flaws. Assuming the platform operates with multiple degrees of freedom, it is possible to introduce unpredictability within an experimental paradigm through manipulation of perturbation magnitude and/or direction. This may beneficially mitigate anticipatory effects often associated with alternative methods (Bhatt et al. 2006, 2013; Martelli et al. 2015). However, unique to *active* platform perturbations, controlled changes in acceleration direction during a single

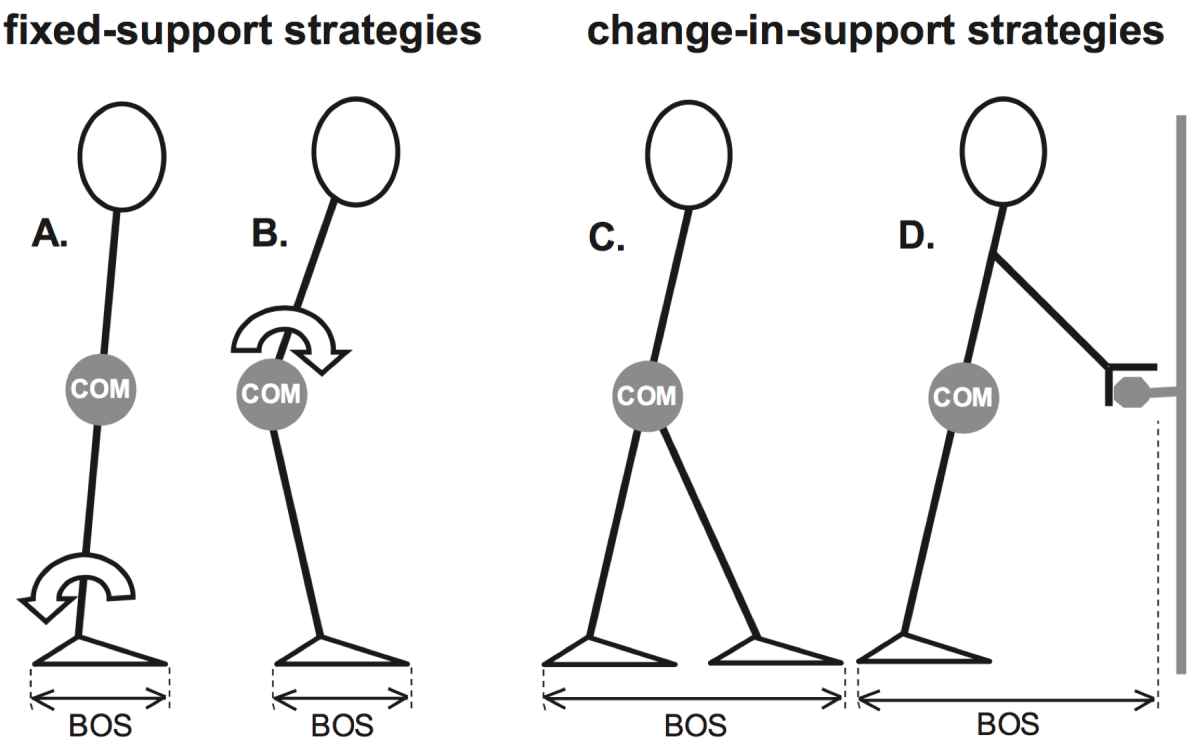

Figure 2.1 Schematic outlining the fixed-BoS and change in BoS balance recovery strategies within the sagittal plane (termed "fixed-support" and "change-in-support" respectively). Note that (**A**) and **(B)** demonstrate the difference between the ankle and hip strategy; the latter is similar to the counterbalance strategy within the frontal plane. Reprinted from *Neurologic Clinics*, Vol. 23, Maki and McIlroy, Change-in-support balance reactions in older persons: an emerging research area of clinical importance, 751-783, Copyright (2005), with permission from Elsevier.

perturbation must inherently influence the characteristics of recovery as noted by Egerton et al. (2011).

The following subsections will highlight two general categories of balance control strategies: fixed BoS and change in BoS. Additionally, the directional dependence of response characteristics will be summarized.

2.1.2 Fixed Base of Support Strategies

The general objective of balance recovery strategies is to effectively minimize relative motion between the CoM and BoS. Maki and McIlroy (1997) suggested that, depending on how the system is constrained, this objective is realised through two general classes of control strategies: fixed BoS (e.g. sway) and change in BoS (e.g. reactive stepping). These strategies are outlined in **Figure 2.1**, adapted from Maki and McIlroy (2005). However, the constraints that result in selection of these strategies are complex as they involve cognitive factors (e.g. task instructions; Maki et al. 1996) as well as task and environmental conditions (e.g. obstructed foot-path, Zettel et al. 2002a, b; limited BoS, Horak and Nashner 1986; perturbation magnitude, Diener et al. 1988; Maki et al. 1996).

Fixed BoS strategies were examined in the classic study conducted by Horak and Nashner (1986); the researchers used sagittal perturbations to evoke different responses via limitations of the planar area enveloped by the BoS. Using this experimental paradigm coupled with surface electromyography (EMG) of postural muscles, they observed stereotypical *patterns* of muscle activation (termed synergies) that changed with alterations of BoS characteristics. Although responses to forward and backward perturbations differed in terms of the specific muscles used, the patterns within normal and short BoS conditions were similar (e.g. bottom-up versus top-down). The ankle strategy was noted for its inverted pendulum sway-like characteristics while the hip strategy generated counter-rotations of the trunk and lower limbs in relation to perturbation direction (**Figure 2.1 A** and **B**). The former would play an important role within the formation of numerous important biomechanical models of postural stability (see Chapter 2.2). We should also note that Horak and Nashner (1986) observed learning effects

associated with these strategies; participants would undergo a period of transition between strategies following changes in BoS size. This suggests that although these strategies can be identified within some general dichotomy, the execution can be variable and is an important factor to acknowledge in the study of motor control.

2.1.3 Change in Base of Support Strategies

Under many circumstances it may not be feasible to maintain both a fixed BoS and upright balance. For example, a substantially large magnitude of CoM momentum relative to that of the BoS may require a change in the characteristics of the BoS itself to prevent a fall. As shown in **Figure 2.1**, these change in BoS strategies may range from execution of a step or a grasping a handrail (Maki and McIlroy 1997, 2005; Maki et al. 2000). At minimum, they promote stability through expansion of the BoS boundaries. Addition of corrective "braking" impulses to CoM momentum generated via ballistic interaction between end-effector (e.g. foot) and contact-surface (e.g. ground) further promote the stability of these control strategies. This is functionally similar to the transient execution of gait termination (Bishop et al. 2003; Peterson et al. 2011).

Spatial-temporal trajectory of the stepping limb is essential in successful execution of the reactive stepping change in BoS variant. A similar scenario would be the importance of timing and location of foot placement for simultaneous progression and stability within the gait cycle (Bauby and Kuo 2000; Millard et al. 2009). In the scenario a perturbation is experienced, the BoS must be repositioned quickly and of a sufficient distance in relation to the state of CoM motion. If necessary, multiple steps may be taken as observed in older adults following lateral waist pulls (Bair et al. 2016). For locomotor tasks, reactive stepping may simply integrate itself within the gait cycle (Marigold et al. 2003; Moyer et al. 2009; Inkol et al. 2018b)

2.1.4 Responses in the Frontal Plane

Many of the previous studies referenced for generalizations of the fixed and change in BoS balance recovery strategies were focused primarily on perturbation acting in the sagittal plane (Do et al. 1982; Horak and Nashner 1986; Hoshiyama et al. 1993; Rogers et al. 1996; Zettel et al. 2002a). Studies that have specified their focus balance control in relation to frontal perturbations

(e.g. Maki et al. 1996; Egerton et al. 2011; Bair et al. 2016; Addison et al. 2017) have addressed primarily the lateral change in BoS strategies due to their various subcategorizations. Much of the early work addressing these lateral balance control strategies was disseminated within the well-known publications by Maki, McIlroy and colleagues. However, fewer studies have focused on how fixed-BoS manifests uniquely within the frontal plane.

As noted prior, the observations of Horak and Nashner (1986) highlighted that despite differences in the muscle groups utilized between forwards and backwards perturbations, *patterns* or *synergies* of muscle activity for opposing directions were near mirror images. However, when considering lateral balance, different anatomical degrees of freedom, characteristics of the BoS, and capabilities of the musculoskeletal system can influence the manifestation of balance recovery. For example, the knee joint is relatively "locked" within the frontal plane due to its revolute nature in the orthogonal plane. One of the biggest factors in differentiating balance control strategies evoked in the frontal plane from the sagittal plane is the occurrence of loading and unloading of the lower limbs. Activation of hip abductors/adductors can actively control the loading under each limb as necessary (Winter 1995). Perturbations may themselves produce *passive* unloading of the limb opposite to the direction of balance-loss (Maki et al. 1996, 2000). In this context, passive unloading refers to the decrease in limb loading not resulting from application of CNS-controlled, active joint torques. An early study by Brunt et al. (1992) exposed healthy young adults to perturbations that involved rotations of the support-surface about the anteroposterior axis. These were designed specifically to passively load a specific limb. Using surface EMG, they observed large changes in tibialis posterior within the loaded limb but little activity within the unloaded limb. This finding is in contrast to the observations of Horak and Nashner (1986) who reported bilateral coordinated symmetric muscle activity following the application of sagittal plane perturbations. Brunt et al. (1992) also noted contributions of ankle dorsiflexors (tibialis anterior) in *both* limbs; this was suggested to stabilize the limb due to the reciprocal actions of tibialis posterior, i.e. plantarflexion. It should be be noted that this same study surprisingly ignored activity of hip abductors and adductors. As outlined by Winter et al. (1995), the total body sway in the frontal plane is effectively a summation of both hip and ankle net joint moments. Notably, Winter et al. (1998) suggested that

control of hip musculature is most important in these scenarios as excessive ankle inversion-eversion moments would produce rolling of the foot segment.

Lateral fixed BoS strategies may also reflect a hip strategy similar to that reported following a sagittal plane perturbation. For the frontal plane, this strategy may be characteristically termed a counterbalance strategy. This strategy has been noted in balance recovery scenarios such as following a lateral waist pull (Egerton et al. 2011), quiet standing (Federolf et al. 2013), slacklining (Mildren et al. 2018), and even in mathematical models of unilateral standing balance (Hof 2007). However, it is often not the focus of research despite its unique characteristics. For example, it is common for the body to transition from bipedal to unilateral stance following a lateral perturbation; in this instance, the trunk and unloaded lower limb perform counter-rotations about the pelvis (Hof 2007). The trunk and unloaded limb can then be returned to an upright posture (or alternatively unilateral stance/single support may be maintained). Unlike that observed commonly for sagittal plane control strategies, the unloaded foot is not used to effectively expand the BoS but rather to influence whole-body CoM dynamics. Hof (2007) suggested that this strategy promotes stability through conservation of angular momentum and exploitation of the trunk/lower limb's large inertial properties. The result is the ability to navigate the CoM outside the BoS (briefly) by approximately 4 cm (Otten 1999; Hof 2007).

As mentioned prior, stepping characteristics of lateral balance recovery are also inherently unique. Execution of a lateral step to prevent falling has numerous potential subcategories. Two of these options include the following: unload the initial support/loaded limb to step laterally or manoeuvre the unloaded limb (ipsilateral to fall direction) around the supporting limb (Maki et al. 2000; Mille et al. 2005; Egerton et al. 2011; Bair et al. 2016). Cleary either scenario can present an issue for high fall-risk populations such as older adults where reductions in neuromuscular function can result in further perturbations to the system during single leg stance, an inherently unstable posture (Addison et al. 2017; Sivakumaran et al. 2018). The potential for lower-limb collisions to occur with short medial or cross-over steps of the unloaded limb can also present danger. Selection between the two subcategories of responses introduced above has been related to lower hip abductor torque generation and higher

intramuscular adipose content (Addison et al. 2017). Surprisingly, the theoretically more prolonged and demanding step reaction (i.e. cross-over) is more often executed in older adults, while younger adults often elect to (briefly) unload the limb initially supporting their weight and execute a lateral recovery step (Mille et al. 2005; Bair et al. 2016).

2.2 Postural Stability

In Chapter 2.1, we introduced the balance control strategies that are typically executed to prevent falling. The following section will address applications of mathematical and biomechanical modelling used to enhance our understanding of balance control and stability. Attention will be primarily directed towards the models used to derive CoM position-velocity based boundaries for numerical evaluations of balance and stability.

2.2.1 General Methods for Evaluating Stability

The concept of stability, while at its core presents a straightforward idea, is quite challenging to quantify when applied to a biological system. Often, nonlinear time-series analyses are utilized to reconstruct system dynamics with time series data and then are used to evaluate stability via orbital or local stability metrics (e.g. Lyapunov exponents; Bradley and Kantz 2015). Regarding local metrics, stability for aperiodic movement patterns is established according to the response following small perturbations to the system that return it towards periodic pattern(s) (Ali and Menzinger 1999; Bradley and Kantz 2015). This method has been used to quantify stability for tasks including trunk rotations (Beaudette et al. 2014) and locomotion (Dingwell and Kang 2007; Worden et al. 2016). However, a critical component remains in the application of local stability; the tasks must be cyclical in nature. For this reason, quantifying stability for execution of a transient balance recovery strategy following a singular, *large* perturbation poses a challenge. There are a multitude of postural recovery strategies that may be evoked (see Chapter 2.1) and learning effects/habituation with the addition of fatigue and repetition should influence any periodicity (Horak and Nashner 1986; Bhatt et al. 2006; Inkol et al. 2018b). Variability of performance outcomes (e.g. O'Connor et al. 2012) have been suggested as an indirect measures of stability; though, they do not necessarily correlate well local stability metrics (Dingwell et al.

2001). Conversely, the concept and application of dynamic stability margins provides an additional perspective on the analysis of balance. Given the underlying nature of balance control in terms of regulating the whole-body CoM , many authors have suggested identifying the maximum, functional BoS boundaries within which the CoM may be maneuvered (i.e. stable regions) as a means of capturing dynamic stability. Discussed in Chapter *2.2.3,* these boundaries evaluate the CoM-BoS relationship according to position-velocity metrics and have shown promising results in prediction of unstable movement strategies (Patton et al. 1999; Yang et al. 2008). Biomechanical modelling has been used extensively to estimate these boundaries prior to applications to experimental data. The following sections will provide a brief history in the development of a few central models upon which the dynamic stability margin concept is based.

2.2.2 Inverted Pendulum Model

Frequently throughout the biomechanics literature, the inverted pendulum (IP) model is used to explore the control and execution of balance control strategies. Many researchers in biomechanics or engineering will adopt this model or n-link variations in the development of controls for upright balance akin to bipedal stance or gait (Peterka 2003; Kuo 2005; Millard et al. 2012; Suzuki et al. 2012). By expanding the degrees of freedom within the IP model, it can be used to inherently address strategies beyond the ankle strategy (Winter 1995; Pai and Patton 1997) which may include the knee/hip strategy (Iqbal and Pai 2000; Suzuki et al. 2012).

Winter (1995) notably popularized applications of the single segment IP model for quiet standing scenarios. The rationale of the IP was based on the ankle strategy for balance control; net ankle moments produced through plantar- and dorsiflexor activity control CoM accelerations. He summarized this relationship between the whole-body CoM and center of pressure (CoP) – the point of application of the integrated sum of pressure(s) acting on the BoS – using the following second-order ordinary differential equation (ODE):

$$-I\frac{\ddot{c}}{\ell} = (\mu - c)mg \tag{2.1}$$

Pendulum mass m, length ℓ, and moment of inertia I define the inertial properties of the linearized inverted pendulum dynamics. The primary source of instability within this model is then the toppling produced by gravitational acceleration g. Note that the diacritic dot notation defines the time derivatives of any element,

$$\dot{x} \equiv \frac{dx}{dt}, \qquad \ddot{x} \equiv \frac{d^2x}{dt^2}. \tag{2.2}$$

Within the IP model, a method of control must exist for countering gravity. Equation 2.1 describes a scenario in which the acceleration of the CoM $\ddot{c}$ is manipulated through changes in CoP position μ with respect to CoM position c; μ is adjusted through changes in the net ankle moment/torque. This model is detailed visually in **Figure 2.2A** (adapted from Hof et al. 2005). Winter et al. (1998) would continue to build upon the IP model as a means to understand balance control suggesting the importance of elastic ankle stiffness in maintaining upright balance in addition to validating the proposed model through analyses of experimental data (Winter et al. 1998, 2001; Gage et al. 2004). Specifically, Gage et al. (2004) reported a very high correlation between CoM sway and segmental CoM-CoP. A poor relationship would suggest alternate mechanisms of control rather than that driven by ankle moments as highlighted in Equation 2.1. Furthermore, Winter's suggestion of ankle stiffness as a means of low-input balance control was not entirely unopposed. Authors including Morasso and Sanguineti (2002) and Casadio et al. (2005) suggested that this model was an oversimplification of the control system. They noted sources of error within the determinant of critical stiffness such as the assumption of static motoneuron activation levels during quiet stance. Despite this, Winter and his colleagues' work provided the primary foundation upon which stability margins were developed.

Though the IP remains a widely used model in biomechanics, it is not without its limitations. Inherently, its applications are restricted to certain movements that may not necessarily coincide with the dynamic tasks that are most likely to cause a fall or provide a greater challenge (e.g. large magnitude perturbations). Even with quiet standing, Sasagawa et al. (2009) countered Gage et al. (2004) highlighting the inverse relationship between ankle and hip joint accelerations suggesting quiet dynamics may be better approximated as a double pendulum.

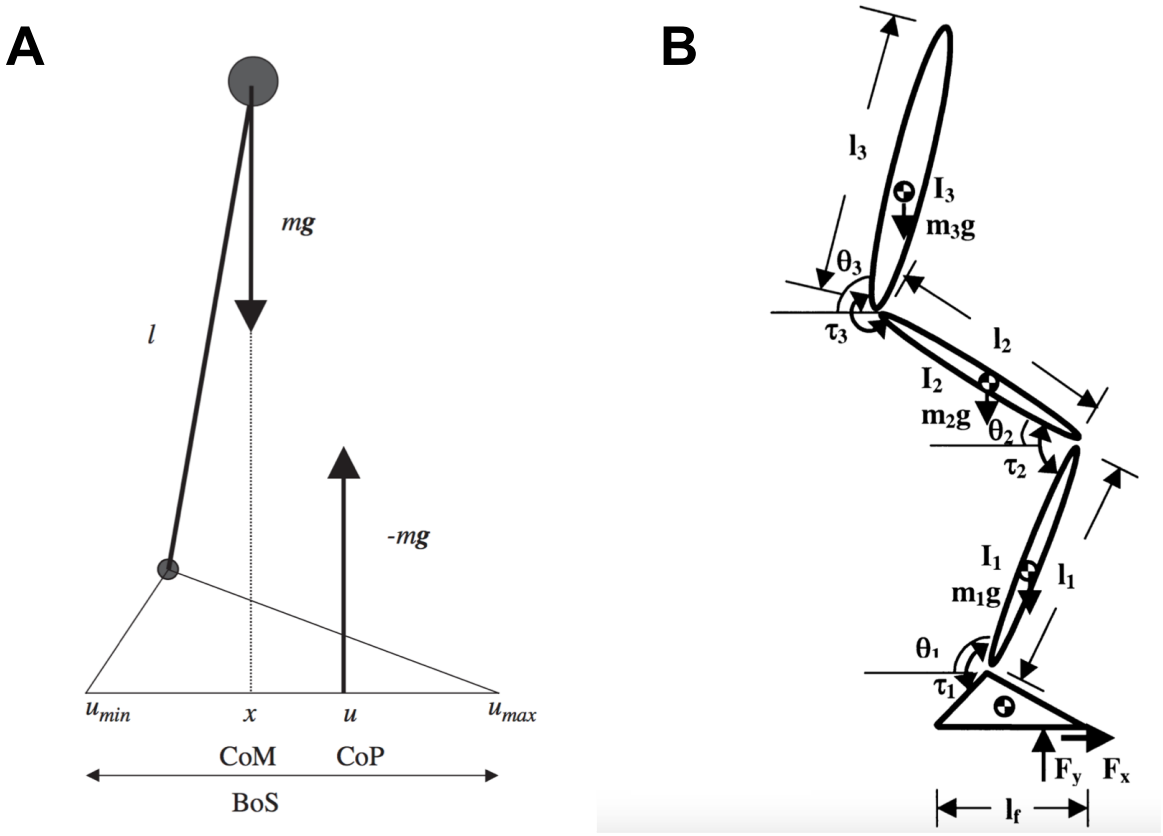

Figure 2.2 (A) Inverted pendulum model of human stance in the sagittal plane reprinted from *J Biomech*, Vol. 38, Hof et al., The condition for dynamic stability, 1-8, Copyright (2005), with permission from Elsevier. (**B**) Multi-link segment model of human stance reprinted from *J Biomech*, Vol. 33, Iqbal and Pai, Predicted region of stability for balance recovery: motion at the knee joint can improve termination of forward movement, 1619-1627, Copyright (2000), with permission from Elsevier.

Therefore, the primary benefit of the IP model is its ability to present complex dynamics with a high degree of simplicity that, in many cases, can provide a good approximation of balancing tasks (Hof et al. 2010; Fujimoto et al. 2017).

2.2.3 Dynamic Stability Margins

Following much of the work by Winter, researchers began to consider that *both* the CoM position and its instantaneous velocity may influence the boundaries that define stable postures; not just the static position of the CoM within the BoS. Pai and Patton (1997) notably suggested that there was an interaction between CoM state (position and velocity) that influenced the ability to maintain stability. Using the IP model and simplified estimates of control, Pai and Patton (1997) proposed "feasible stability regions" (FSR) within the CoM phase-space (**Figure 2.3A**). The FSR address unstable IP dynamics for two scenarios: *i*) the CoM is within the BoS but the outward CoM velocity is of substantial magnitude; *ii*) the CoM is outside the BoS and the inward velocity is *not* of substantial magnitude. Case *i* defines what is denoted as the upper boundary of stability while case *ii* defines the lower boundary. These definitions of stability are inherently dependent on the future state of the system, i.e. the system *will become* unstable and is therefore unstable. Furthermore, the existence of both a discrete upper and lower boundary velocity at any given CoM position is dependent on both the definition of the BoS boundaries and the CoM position within said boundaries.

Pai would continue this work adopting their initial approach to derive the FSR for additional scenarios that include unexpected sagittal perturbations (Pai and Iqbal 1999; Pai et al. 2000), multi-segment responses, hip recovery strategies (Iqbal and Pai 2000), gait (Yang et al. 2007, 2009), and gait perturbations (i.e. slips, Yang et al. 2008). Successful validation of these boundaries within experimental data sets, primarily to predict initiation of a change in BoS, were also disseminated by this group (Pai et al. 1998, 2000; Patton et al. 1999). Notable most amongst these studies was the validation of an adjusted, IP-based FSR that accounted for the sagittal plane support-surface translations used in Maki et al. (1996) (Pai et al. 2000). Specifically, they acknowledged the velocity boundaries in the direction of fall induced by a perturbation (e.g. forwards fall following backwards translation). Temporal dependence of the FSR on the

perturbation's acceleration waveform was reported, an example of which was the larger upper boundary observed during the perturbation's deceleration phase when compared to that at onset of acceleration.

Over the course of the decade in which the work by Pai and colleagues was completed, the methodology was frequently altered by other scientists. Particularly, there was a general change in the methods used to approximate these boundaries (e.g. using predefined control trajectories, trajectory optimizations). In this regard, it is important to set a base interpretation of the resulting stability margins in terms of the methodology used. Given the prioritization of trajectory optimizations, especially in later iterations (Yang et al. 2007, 2008, 2009), it may be best to use the term *optimal* FSR. Note that this relates to the boundaries being the optimized measure, not the optimization/management of the CoM within the FSR. It establishes that these boundaries define incidence in which the following criteria can be met: the body behaves with similar mechanics to the model utilized and the CNS is able to yield a similar response to that derived via programmed trajectory optimization. The latter is intriguing as it should theoretically vary between anticipatory/volitional and reactive movements where the limitations of the neuromuscular system are most evident (e.g. neural delays).

In 2005, Hof and colleagues presented their own variation of the dynamic CoM stability margins. Rather than numerically determining the boundaries for dynamic stability as Pai and Patton (1997) had done, Hof et al. (2005) presented an analytical solution to the second-order ODE for the IP model (Equation 2.1). This solution yielded the formulation of the extrapolated CoM (xCoM) χ:

$$\chi = c + \frac{\dot{c}}{\omega_0}. \tag{2.3}$$

Here, CoM position c is extrapolated according to the CoM velocity $\dot{c}$ normalized to ω_0, the eigenfrequency of the non-inverted pendulum of length ℓ (i.e. $\omega_0 = \sqrt{g/\ell}$). The work presented by Hof et al. (2005) has been implemented by many researchers through the proposed dynamic margin of stability (MoS) metric which effectively presents the position of the xCoM within the

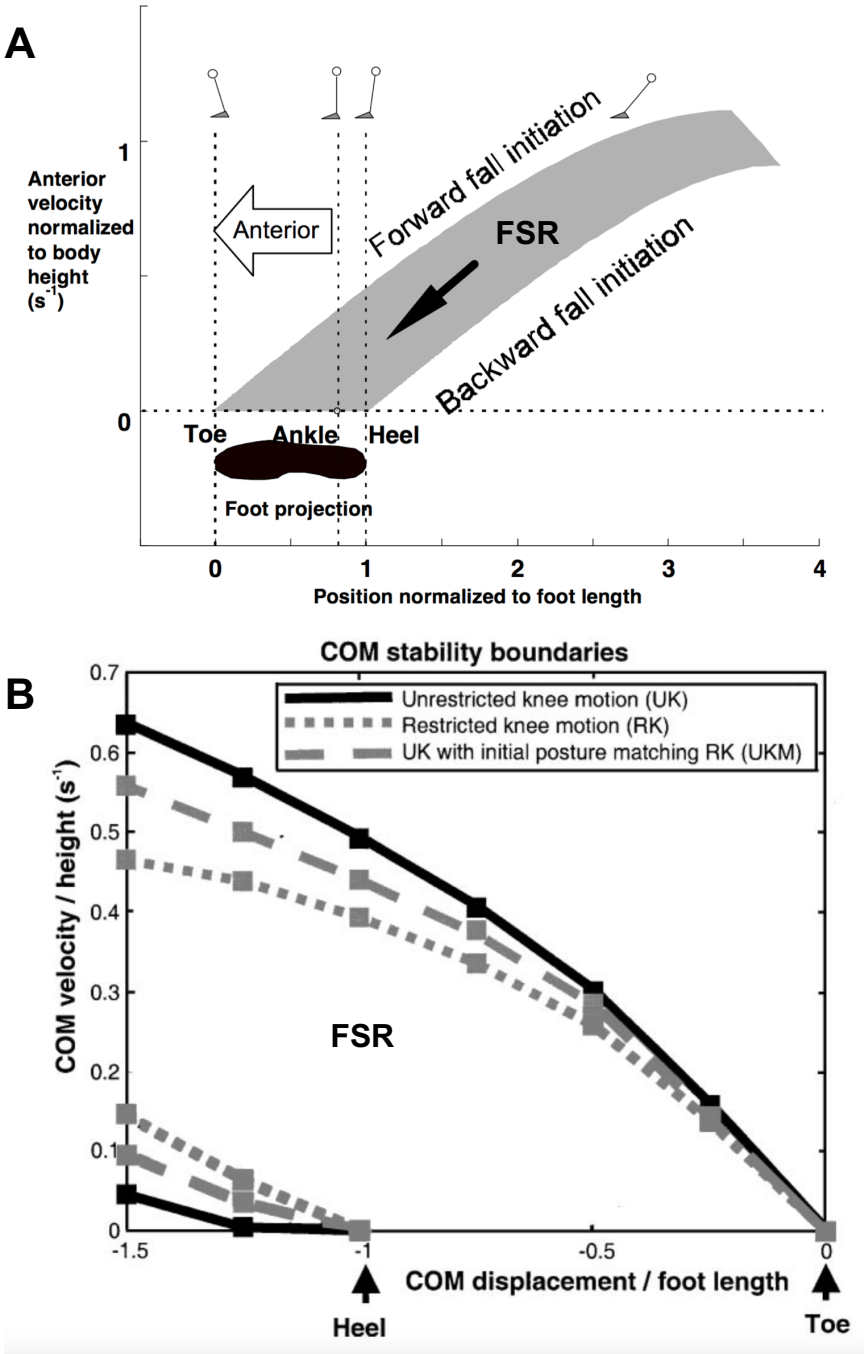

Figure 2.3 Anterior feasible stability regions (FSR) for the sagittal models described in **Figure 2.2**: (**A**) the inverted pendulum reprinted from *J Biomech*, Vol. 30, Pai and Patton, Center of mass velocity-position predictions for balance control, 347-354, Copyright (1997), with permission from Elsevier. (**B**) the multi-segment, hip/knee strategy model reprinted from *J Biomech*, Vol. 33, Iqbal and Pai, Predicted region of stability for balance recovery: motion at the knee joint can improve termination of forward movement, 1619-1627, Copyright (2000), with permission from Elsevier.

FSR of Patton and Pai (1997). This measure can be expressed *generally* as

$$\xi = \min \{b_i - \chi\}_{i=1}^{N} \tag{2.4}$$

Briefly, the MoS ξ provides the minimum position of the xCoM within the set of BoS boundaries b; the N boundaries vary depending on the BoS's geometric approximation. A negative MoS would suggest that a recovery strategy, not bound by IP mechanics, is required to maintain balance; it does *not* simply imply a change in BoS (due to falling) is required. Examples of strategies outside the bounds of the IP model include the hip strategy, large arm movements, and counterbalancing using the lower limbs (Hof et al. 2005; Hof et al. 2007). Alternatively, the MoS with respect to a specific boundary, rather than all boundaries, is another common application of this measure (i.e. $N = 1$). An example of this type of scenario would be position of the CoM or xCoM with respect to the trailing heel during walking (You et al. 2001; Inkol et al. 2018b)

Several studies investigating balance have implemented the xCoM and MoS (Rosenblatt and Grabiner 2010; Hurt et al. 2011; Fujimoto et al. 2015; Worden and Vallis 2016; Inkol et al. 2018b). The innate benefit of this measure is its ease of use in quantifying the dynamic state of the CoM. The linear CoM transformation (Equation 2.3) and its specified position within the BoS (Equation 2.4) is arguably simpler to execute and interpret relative to the FSR alone; however, this simplicity could be argued as a drawback. While it may be practical to apply Hof's model for certain scenarios, specifically the MoS, it may only be only a modest measure of stability across the spectrum of postural strategies. This may be predominantly attributed to the assumption that the CoP is an effective determinant of balance control. However, there are efforts to improve the fidelity of xCoM-based metrics. It was recently proposed that the nature of the mathematical approach (e.g. controlling $d\chi/dt$) can account for the concept of neural delay within the confines of the dynamic MoS (Hof and Curtze 2016). Given that changes in CoM velocity are often viewed as an important factor in the neural control of movement, this perspective improves the physiological rationale of the MoS as a feasible model of dynamic stability.

It is pertinent to mention that the majority of models and study discussed within this section prioritized balance within the sagittal plane. A limitation evident within the biomechanics-related literature is the abundance of studies that focus on recovery strategies within the sagittal plane; unique frontal plane strategies discussed in Chapter *2.1.4* are not often addressed. Few studies have addressed stability within the frontal plane and these were primarily concerned with either gait (Bauby and Kuo 2000; Yang et al. 2009; Hof et al. 2010) or small perturbations to stance (Rietdyk 1999). The counterbalance strategy, evoked following larger perturbations, has been well established within the sagittal plane (e.g. hip strategy, modeled as double pendulum) but, to our knowledge, no studies have noted its components within the frontal plane outside of quiet unilateral stance (Hof 2007; Federolf et al. 2013) or have established the FSR for such motor behaviour. It may be that the linear boundaries of the IP-based FSR (**Figure 2.3A**) do not fully explain the dynamics of a lateral counterbalance. Rather, the boundaries may be non-linear (**Figure 2.3B**) across a range of CoM positions like that observed by Iqbal and Pai (2000). The unique properties of a multi-link pendulum strategy within the frontal plane identify as the large wobbling mass of the trunk and unloaded limb. As such these factors should theoretically influence the FSR like other, higher degree-of-freedom sagittal models (Iqbal and Pai 2000; Yang et al. 2007). Although Yang et al. (2009) suggested the IP model was a good approximate to higher-order models, the counterbalance dynamics need to be addressed. Furthermore, the method of evoking the lateral counterbalance strategy should be included within evaluations of the FSR, especially if that method is a support-surface perturbation (Pai et al. 2000).

2.2.4 Experimental CoM Estimations

It is apparent that the overarching theme of balance recovery is the demand to manipulate *whole-body* CoM position and velocity in relation to that of the BoS. Within experimental data sets, it is then inherently necessary to provide appropriate estimates of this CoM trajectory. Many studies have addressed the concept of both CoM estimations using single segments (Hahn and Chou 2003; Yang and Pai 2014; Tisserand et al. 2016b), reduced anthropometric models (Huntley et al. 2017b; Jamkrajang et al. 2017), or different models entirely (Catena et al. 2017). Typically, the results of the studies have suggested a high degree of fidelity in whole-body CoM estimates

by tracking the pelvis segment given the task in question is gait (Yang and Pai 2014; Huntley et al. 2017b). Conversely, (Hahn and Chou 2003) suggested poor ability of the pelvis (or trunk) in identifying older adults with balance disorders using mediolateral CoM based metrics.

Given the recent popularization of Hof's xCoM-based stability metrics within the literature (e.g. MoS and time-to-contact, Hof et al. 2005), researchers have begun to address the effects of reduced models on xCoM trajectories. This is especially important due to its dependence on both position and velocity (Equation 2.3). It is appropriate to note here that that prior studies examining estimates of the xCoM have focused on execution of volitional tasks (e.g. jumping, Jamkrajang et al. 2017). To our knowledge, only Tisserand et al. (2016b) has examined balance recovery, though not that involving a fixed BoS. They observed poor xCoM estimates using a pelvis model, primarily in the mediolateral direction, for change in BoS balance recovery.

2.3 Balance Recovery and Estimates of Motor Control

The following section will provide a brief overview of the motor control strategies associated with the maintenance of balance in response to both local, and large global perturbations. Due to the inherent complexity associated with this area of the literature, and the breadth of available hypotheses, this section will maintain a narrow focus on primarily the 'degrees of freedom problem' (Bernstein 1967) and its integration into dynamic systems theory. The concept of optimal control theory and trajectory optimization within models designed to examine balance control will also be presented.

2.3.1 Degrees of Freedom Problem

The control of human movement by the CNS requires highly complex processes that remain largely enigmatic within the scientific community. Unlike many robots (e.g. serial manipulators), the human body is not necessarily specialized for any single task. Rather we are able to complete a variety of complex motor tasks (e.g. walking, running) in addition to learning many others (e.g. throwing, playing musical instruments). Nikolai Bernstein (1967) famously addressed this notion by posing the degrees of freedom problem. He outlined that the musculoskeletal system is highly

redundant, physiologically, anatomically and kinematically. A clear example of this is a joint actuated by multiple muscles that share a common function (e.g. biceps brachii and brachialis at the elbow). At the whole-body level, humans may also complete various goal-oriented tasks in a seemingly infinite number of ways (e.g. reaching towards a handle). Despite the redundancies that exist at multiple levels, the CNS is able to produce highly coordinated sets of actions that complete instructed tasks with typically little error (Thelen 2000). Bernstein proposed that sets of motor synergies (modules) within higher centers of the CNS reduced these redundancies by essentially forming clusters of *effectors* (e.g. groupings of motor units) rather than controlling the system according to individual muscles or motor units.

Another important concept introduced by Bernstein (1967) within the framework of motor control theory was the utilization of system dynamics to dictate motor actions. An example provided by Thelen (2000) is the passive, resonant properties of viscoelastic tissues in the transfer of energy during gait. Having the dynamics of a task instructing the CNS as opposed to the CNS generating strictly pre-meditated patterns of movement inherently reduces the complexity of motor control. Integration of available afferent (sensory) information is then critical to produce any movement intended with minimal error (Thelen 2000). The application of dynamic systems theory to motor control is largely based on this overarching concept. As individuals transition through childhood and adolescence and the dynamics of their body change, they converge on certain attractor states that coincide with successful patterns of movement (Hinton and Vallis 2016). In relation to balance control, we raise the question of what the attractor may be used to maintain upright balance. Given there are multiple postural strategies whose use are dependent on fluctuating system constraints (Horak and Nashner 1986; Maki et al. 1996) or objectives (Kuo 1995; Versteeg et al. 2016), multiple attractor states may exist and are thus contextually dependent.

2.3.2 Optimal Control: A Solution to Motor Redundancy?

Dynamic numerical optimization has often been used to address the problems associated with generation of motor patterns in completion of a task. Given this is a very large body of literature, we will provide only a very general overview to address a few key components in the analysis of balance control. Forward dynamics simulations provide a means by which the motion of the

body may be inferred through joint moments predicted through definition of an optimal control objective/cost. The cost function minimized (e.g. metabolic energy expenditure, Anderson and Pandy 2001) is often related to a potential goal of the CNS within any given scenario. One particular application of optimization in balance control is in combination with closed-loop feedback systems (i.e. optimal estimation models). Researchers such as Kuo (1995, 2005) and van der Kooij et al. (2001) have proposed control systems in which a multi-component controller (similar to the CNS) processes and integrates afferent information for state estimates (e.g. vestibular and proprioception) with system dynamics to estimate a given output (feedback) according to an objective functions. This can be related back to dynamic systems theory in the narrow sense that afferent information is used to instruct the CNS on the necessary descending input.

Another commonly used method by which we can address the issue of motor redundancy is through conversion of the optimal control problem into a nonlinear programming (NLP) problem. This method is especially powerful when applied to musculoskeletal models that contain musculoskeletal *and* kinematic redundancies with system dynamics akin to a biological system. It has been used in a similar context as optimal estimation models to generate different postural responses following a perturbation (e.g. hip and ankle synergies). In fact, recently, Versteeg et al. (2016) addressed the applications of NLP to reactive postural control by implemented an initial neural delay of 100 ms, adopted from Nashner et al. (1989), within their optimization routine. Ankle and hip strategies were generated by their musculoskeletal model via adjustments of the weighted cost function that detailed components such as tissue stress and CoM excursions. Conversely, the use of NLP may be of increasing importance in addressing more theoretical concepts such as the FSR. As discussed prior, assessment of the FSR for single-support during gait was facilitated using NLP (Yang et al. 2007, 2008, 2009). These authors utilized a direct, single shooting based method originally proposed by Pandy et al. (1992) to determine the capabilities of their biomechanical models. These capabilities were the maximum relative CoM velocities the system was able to terminate for specific local CoM positions. For consideration, inclusion of a neural delay (Versteeg et al. 2016) with a muscle activation ODE (Pandy et al. 1992; Yang et al. 2009; De Groote et al. 2016) in NLP may then provide FSR that better reflect the limitations of neuromuscular system in responding to external perturbations.

Above, the concept of direct shooting was introduced. As outlined by Pandy et al. (1992) for its applications to motor control (i.e. single shooting) and for general cases of trajectory optimizations by Betts (2010), direct shooting involves parameterization of control trajectories via definition of a mesh or nodal points. This provides a discretization of the continuous time series trajectory(ies) to be estimated. The given objective for any simulation of optimal control is then considered a function of these control parameters. Betts (2010) compared this method to shooting a cannon and then adjusting the angle of the shot iteratively until the target is hit (hence the name). A alternative method of NLP also outlined in detail by Betts (2010) is direct collocation (DC). Also utilized by many biomechanists, it requires parameterization of *both* state and control trajectories such that the objective is a function of both. Discrete states and controls are defined according to a series of linear and nonlinear equality/inequality algebraic constraint equations. These may include the system equations of motion, anatomical bounds, etc.. Porsa et al. (2016) noted that using DC was a highly efficient means of trajectory optimization when applied to vertical jumping simulations in comparison to direct shooting (i.e. reduced processing time). However, a caveat of DC is the requirement for an initial guess detailing both state and control trajectories as opposed to just the latter as necessary in direct shooting.

Chapter 3. Thesis Objectives

The following thesis consists of two studies included as separate entries. A common objective of each study included quantifying the state of bipedal standing stability as introduced in Chapters *2.2.3* and *2.2.4*. The specific objectives are outlined as follows:

Study 1. Experimentally determine the fidelity of a simplified model compared to a standard anthropometric model (Winter et al. 1998) in the calculations of dynamic MoS (Hof et al. 2005) during fixed-BoS balance recovery. There is limited understanding in how reducing the complexity of an anthropometric model affects the fidelity of xCoM and dynamic MoS estimates during these transient tasks. It is necessary then to address this question for researchers who wish to use simplified models to address research questions involving special populations (e.g. older adults) and/or researchers who wish to reduce the duration of experimental setup or analyses. It was hypothesized that increasingly simplified estimates of CoM kinematics would reduce accuracy of the MoS for fixed-BoS balance recovery responses. Accuracy was quantified as the difference between a given simplified model's outcomes and those of an anthropometric model commonly used for the study of balance and gait.

Study 2. Develop a bipedal, mathematical model and trajectory optimization routine that define the FSR necessary to calculate dynamic MoS during execution of lateral fixed-BoS postural strategies. There has been little use of exclusively frontal plane models of postural control in the scientific literature; especially following support-surface perturbations. The assumption that the body behaves mechanically akin to the IP may only hold true within limited scenarios; this is likely not the case for lateral counterbalancing strategies. Thus, a higher degree of freedom model is necessary to test whether the FSR of the IP model is similar to that for lateral counterbalancing. It was hypothesized that our model would highlight expanded boundaries within the FSR in comparison to the Hof et al. (2005) model. This would suggest larger feasible CoM velocities that lateral counterbalancing may correct

at an array of CoM positions and thus a more stable postural strategy. Additionally, coupling distinct events within an active perturbation waveform with our model would have a direct effect on the FSR thus highlighting the dependency of evaluating MoS on the perturbation used to trigger balance recovery (Pai et al. 2000).

In general, this thesis prioritized examination of the methodology used within balance and posture research with the intention of refining common outcome measures such that they reflect the mechanics of the underlying motor behaviours. Unique objectives and hypotheses for each study are highlighted in greater detail within the introduction of corresponding Chapters (4 and 6).

Chapter 4. Does simplifying the anthropometric model used to estimate center of mass position-velocity affect the dynamic margin of stability for fixed-support strategies that follow a support-surface perturbation?

Published in Gait & Posture. (2018). 62; 434-439. DOI: 10.1016/j.gaitpost.2018.03.050

4.1 Introduction

Maintaining the centre of mass (CoM) of the body within the base of support (BoS) boundaries is a critical component of upright balance (Winter et al. 1998); however, quantifying the ability to balance is a challenging task. Hof et al. (2005) proposed a dynamic measure of postural stability, the dynamic margin of stability (MoS), which accounts for both position and velocity of the CoM (i.e. extrapolated CoM; xCoM). While their model is not the first to consider CoM position and its time derivative (Pai and Patton 1997; Pai and Iqbal 1999), it provides a single measure of dynamic stability that is relatively simple to implement and has been frequently used to quantify stability for a variety of tasks (e.g. obstacle avoidance Worden et al. 2016, perturbed balance Hasson et al. 2008) and clinical populations (Peebles et al. 2016; van Meulen et al. 2016).

A primary factor associated with evaluations of MoS is the ability to estimate whole-body CoM position. One commonly used approach combines kinematic analyses with anthropometric models to estimate segmental CoM; these are weighted and summed to provide an estimate of whole-body CoM (Winter et al. 1998). Often researchers will simplify anthropometric models to include a subset of body-segments (e.g. head, trunk and pelvis) for ease of use (i.e. reduced number of markers, decreased setup time) in addition to fewer steps in data processing (Hahn and Chou 2003; Kubo and Ulrich 2006; Yang and Pai 2014; Tisserand et al. 2016b; Worden et al. 2016; Huntley et al. 2017b; Jamkrajang et al. 2017; Havens et al. 2018). One well-known and commonly used anthropometric model within many gait and posture-based research laboratories (Rietdyk et al. 1999; Perry et al. 2001; Worden et al. 2016; Huntley et al.

2017b) is the Winter et al. (1998) model, which considers the "whole-body" to be fourteen rigid segments, each defined by anatomical landmarks and a proportion of total body mass.

The ability to accurately quantify balance recovery mechanisms is critical for many research teams. Previous work has explored the effectiveness of simplified marker setups in reproducing "whole-body" CoM/xCoM kinematics derived from a full anthropometric model during volitional activities (Hahn and Chou 2003; Yang and Pai 2014; Tisserand et al. 2016b; Huntley et al. 2017b; Jamkrajang et al. 2017; Havens et al. 2018); however, there remains a limited understanding of how they impact the study of reactive responses (Yang and Pai 2014; Tisserand et al. 2016b). Reducing the number of segments used to examine whole-body stability (via kinematic analyses) may be necessary when equipment limitations (e.g. camera angles), time constraints, or setbacks within collected data sets (e.g. marker occlusion) do not permit the use of a detailed model. As suggested by Jamrakang et al. (2017), simplifying a model may also permit a detailed analysis of single segment kinematics (e.g. trunk) while retaining similar "whole-body" estimates.

Therefore, the purpose of the current study was to explore the impact of simplifying a single anthropometric model (Winter et al. 1998) used to estimate "whole-body" CoM on calculations of MoS. The fidelity of these simplified CoM estimates was challenged further as these calculations were applied to data acquired following a support-surface perturbation which evoked rapid fixed-support postural strategies. Given the results of Yang and Pai (2014) and Tisserand et al. (2016b), we hypothesized that increasingly simplified estimates of "whole-body" CoM would decrease accuracy of the estimates of (or increase difference between) full anthropometric model MoS during the postural task. As our focus was on the resulting measures of stability, our analyses were conducted within, rather than between the different perturbation conditions present.

4.2 Methods

4.2.1 Participants

Ten healthy young adults (5 males; mean ± SD, age: 22.5±1.78 years; height: 1.71±0.09 m; weight: 72.4±12.0 kg) participated in the current study. Individuals were free from self-reported musculoskeletal or neurological conditions that could affect their ability to maintain balance. They did not report taking any medications that could impact motor control and had normal or corrected to normal vision. All participants gave written consent to participate; the study was approved by the institutional research ethics board.

4.2.2 Experimental Protocol

Data collected and analyzed were a subset of a larger experimental protocol that included 104 trials. Participants were fitted with a suspended safety harness and asked to stand barefoot on a robotic motion platform (5 x 2 m; Shelley Automation, Cambridge, ON, Canada). Foot position was traced and kept approximately hip-width apart throughout. Sixteen trials were analyzed for the current study; four for each direction of perturbation used. All trials included a support-surface perturbation that evoked a fixed-BoS postural response (displacement, peak velocity, and acceleration adapted from Maki et al. 1996) within the sagittal [forward/backward] or frontal plane [left/right] (**Table 4.1**). Participants were instructed not to take a step and were free to use their arms as necessary, excluding grasping the harness. Randomization of experimental trials into four blocks mitigated the effects of anticipation on postural responses; conditions were evenly distributed amongst blocks and demonstrations were given prior to data collection.

Kinematic data were collected using a 12-camera Optitrack system (100 Hz; NaturalPoint, Corvallis, OR, USA). Rigid bodies of three to four reflective markers were fastened to body segments (feet, thighs, pelvis) and single markers covered in retro-reflective tape were then digitized relative to these fixed rigid bodies. Markers were placed on anatomical landmarks following the criterion outlined in Winter et al. (1998); seven additional markers were used to digitize BoS boundaries (e.g. toe, head of fifth metatarsal, heel) and track motion of the robotic platform. For more details outlining the marker setup used, refer to Appendix 9.1.

4.2.3 Data Processing and Centre of Mass Estimation

Data analyses were completed with Visual3D software (Version 6, C-Motion Inc., Germantown, MD, USA). Physical marker trajectories were first interpolated then low-pass filtered using a fourth order, dual-pass Butterworth filter (cut-off: 6 Hz). Within each trial, four models consisting of N body segments (i.e. variations of the 14-segment Winter et al. 1998 model) were used to estimate position vector $\boldsymbol{c}$ of the "whole-body" (net) CoM using the following equation:

$$\boldsymbol{c} = \sum_{i}^{N} \bar{\boldsymbol{c}}_i \rho_i \tag{4.1}$$

where $\bar{\boldsymbol{c}}_i$ (segment CoM position) and $\boldsymbol{c} \in \mathbb{R}^3$ (anteroposterior, AP; mediolateral, ML; vertical) and ρ_i is the mass-proportion constant of the i^{th} segment (**Table 4.2**). The first model variation was the Winter full model (WFM) that used 13 segments in place of the original 14; the second and third trunk segments were combined due in part to the safety harness occluding the ribs. The three other, simplified models reduced components of the WFM via bilateral segment exclusion; specifically, exclusion of arm segments (NAr; similar to (Havens et al. 2018), inclusion of only head, trunk and pelvis (HTP; similar to Worden et al. 2016), or only the pelvis (CoMp; similar to Yang and Pai 2014). Position of the xCoM χ (AP, ML) for each model was calculated using the following equation:

$$\chi = c + \frac{\dot{c}}{\omega_0} \tag{4.2}$$

where c, $\dot{c}$ was the uniplanar CoM position and velocity. The scalar ω_0 was the eigenfrequency of the non-inverted pendulum; the latter was calculated as 1.24 or 1.34 times trochanteric height depending on the plane on interest (Hof et al. 2005). Note that $\dot{c}$ was relative to the robotic platform's velocity.

4.2.4 Margin of Stability

Comparisons of CoM models for each condition were focused within the anatomical direction corresponding to the direction of perturbation (e.g. AP MoS analyzed for backwards

Table 4.1 Each direction of perturbation (and the respective magnitude: displacement, Δx; peak velocity, $\dot{x}$; acceleration, $\ddot{x}$) utilized in the experimental protocol (see Maki et al. 1996). Note that values under $\ddot{x}$ indicate the magnitude of acceleration only; the values were equal and opposite during acceleration and deceleration phases of the square-wave perturbation waveform.

Perturbation Direction	Perturbation Magnitude		
	Δx (cm)	Peak $\dot{x}$ (cm/s)	$\ddot{x}$ (cm/s^2)
Forward	7	22	73
Backwards	9	30	100
Left	9	29	96
Right	9	29	96

Table 4.2 Whole-body center of mass (CoM) used for the margin of stability calculations were derived from the following segments/mass proportions ($\boldsymbol{\rho}$ adapted from Winter et al. 1998) for each model variant (full model, WFM; full model excluding arm segments, NAr; head, trunk and pelvis, HTP; pelvis, CoMp). Definitions of individual segment CoM in relation to the position of anatomical landmarks captured were also adopted from Winter et al. (1998). The "Trunk #" notation below indicates the specific trunk segment utilized for estimation of total CoM; the total trunk consists of four separate segments. The resulting CoM positions during quiet standing are also presented (calculated during ten seconds of quiet standing with respect to the xiphoid process). Negative values in the sagittal plane indicate the posterior direction; in the frontal plane, they indicate the left direction. Note that values are presented as mean ± SEM.

	Full Model	Simplified Models		
	WFM	NAr	HTP	CoMp
Segment Mass Proportions (ρ)				
Head	0.081	0.090	0.140	-
Trunk 4	0.136	0.151	0.234	-
Trunk 2+3	0.143	0.159	0.247	-
Trunk 1	0.078	0.087	0.134	-
Pelvis	0.142	0.158	0.245	1.000
Upper Arm (*2)	0.028	-	-	-
Forearm (*2)	0.022	-	-	-
Thigh (*2)	0.100	0.110	-	-
Shank (*2)	0.060	0.067	-	-
TOTAL	1.000	1.000	1.000	1.000
CoM Directions (cm)				
Anteroposterior (AP)	-12.19 (0.36)	-10.95 (0.34)	-8.89 (0.30)	-5.36 (0.49)
Vertical	-25.19 (1.06)	26.09 (1.04)	-4.19 (0.77)	-24.64 (1.29)
Mediolateral (ML)	0.07 (0.27)	1.01 (0.26)	0.05 (0.23)	0.24 (0.41)

perturbations). At each instant of time, AP or ML MoS ξ was evaluated specifically within the lab Cartesian reference frame using a simplified geometric interpretation of the BoS as follows:

$$\xi = \min\{b_{\max} - \chi,\ \chi - b_{\min}\}. \quad 4.3$$

Specifically, MoS was the minimum distance between position of the xCoM within the direction of interest and the corresponding BoS boundaries ($b_{\max}/b_{\min}$). Representative data detailing the trajectory output are displayed in **Figure 4.1** (top).

Instantaneous MoS for each model was highlighted at the model-specific event at which xCoM had experienced the largest magnitude of displacement in the direction opposite to that of the perturbation (MoS_{peak}; e.g. forward following a backward perturbation, see **Figure 4.1,** top). Similar measures (e.g. peak CoM/CoP excursion) have been used as a metric for postural task performance in protocols fixated on balance recovery (Norrie et al. 2002). For analyses of simplified model performance (i.e. ability to estimate WFM MoS), data was windowed within a two-second period originating at perturbation onset. This two-second period was necessary to capture the entirety of the perturbation (length ≈ 0.60s) in addition to the altered postural sway that follows cessation of platform translation (Norrie et al. 2002). Within windowed sequences of data, characteristics of signal trajectory between WFM and simplified MoS were compared via zero-lag cross correlation coefficients (*r*). Similar trajectories would be expected to provide correlation values close to +1. Additionally, element-wise error for each of the three simplified models ε_S was evaluated as follows:

$$\varepsilon_S = |\ \xi_{WFM} - \xi_S\ | \quad 4.4$$

where ξ_{WFM} and ξ_S were the discrete time series WFM and simplified model derived MoS respectively. From sequences of ε_S of length *T*, root mean square error (RMS) and maximum error (ME) were evaluated as $\text{RMS} = \left(\frac{1}{T}\sum_i^T \varepsilon_{i,S}^2\right)^{1/2}$ and $\text{ME} = \max(\varepsilon_S)$. Error metrics provided a reference for the average bias observed between simplified and WFM model (RMS) in addition to boundaries (ME) within which the simplified models accurately estimated WFM MoS (Yang and Pai 2014; Huntley et al. 2017b; Havens et al. 2018).

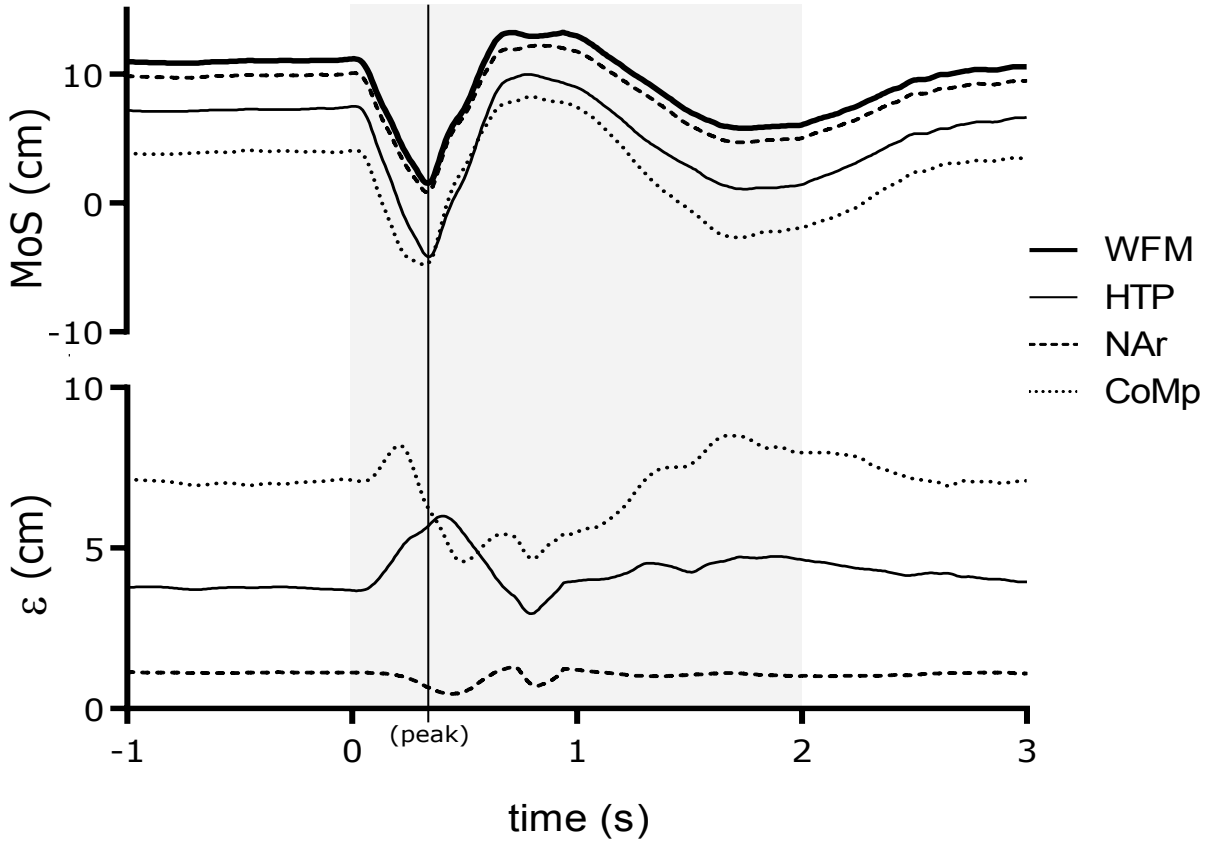

Figure 4.1 A single, representative trial time series illustrating the anteroposterior margin of stability (MoS; *top*) and error (ε; *bottom*) following a backwards perturbation (i.e. translation of the support-surface). Data from all variations of the Winter et al. (1998) anthropometric model explored in this study are illustrated. The grey-tinted region of the figure highlights window over which peak MoS (MoS_{peak}), error metrics (RMS and maximum error), and cross-correlations were evaluated; see text for more details. Note that the peak instant shown is for the full Winter et al. (1998) model (WFM).

4.2.5 Statistical Analyses

Statistical analyses were completed using R statistical environment (Version 3.4, R Core Team, Vienna, Austria). For each participant, outcomes were averaged within factors to avoid inflation of the statistical degrees of freedom; factors were model (WFM, NAr, HTP, CoMp) crossed with each perturbation direction (16 total).

One-way ANOVAs with repeated measures were performed to examine the effect of model on MoS_{peak} (all four models included) and error metrics (r, RMS, ME; WFM not included as factor) within each perturbation condition. In the case Mauchly's sphericity test failed ($p < 0.05$), a Greenhouse-Geisser correction was used to adjust factor/error degrees of freedom and the resulting p-value. When significance was found within an ANOVA, pairwise comparisons between models were performed using paired t-tests with p-values adjusted via Bonferroni corrections. For all tests performed, statistical significance was set to p-value < 0.05.

4.3 Results

For a single participant, an incorrect postural response (i.e. stepping) was evoked in two trials; these trials were excluded from subsequent analyses. The CoM position calculated during quiet standing using each model variation is presented in **Table 4.2**. The mean (± SE) for r, RMS, and ME within each perturbation condition in addition to their corresponding to CoM model main effects (ANOVA results) are displayed in **Table 4.3**. Main effects of CoM model on MoS_{peak} are detailed within the following sections in-text.

4.3.1 Backward Perturbations

A main effect of CoM model was detected for AP MoS_{peak} ($F(1.45, 13.04) = 118.6$, $p < 0.01$; see **Figure 4.2A**). Each of the NAr ($p = 0.02$), HTP ($p < 0.01$), and CoMp ($p < 0.01$) resulted in significantly different MoS_{peak} from WFM. Between simplified models, NAr produced different MoS_{peak} relative to HTP ($p < 0.01$) and CoMp ($p < 0.01$); no difference existed between HTP and CoMp ($p = 1.00$). Use of NAr produced the lowest RMS (HTP, $p < 0.01$; CoMp, $p < 0.01$) and ME (HTP, $p < 0.01$; CoMp, $p < 0.01$) in addition to the greatest r values (HTP, $p = 0.04$; CoMp,

$p = 0.04$). In terms of WFM estimations, HTP performed next best based on its lower RMS ($p < 0.01$) and ME ($p < 0.01$) relative to CoMp despite no significant difference in r ($p = 0.051$) between the two.

4.3.2 Forward Perturbations

A main effect of CoM model was detected for AP MoS_{peak} ($F(1.14, 10.23) = 5.26$, $p = 0.04$; see **Figure 4.2B**). Interestingly, only the difference between WFM and NAr derived MoS_{peak} was significant ($p < 0.01$). However, analyses of RMS, ME, and r revealed numerous pairwise differences between simplified models. The NAr model produced the lowest RMS (HTP, $p < 0.01$; CoMp, $p < 0.01$), ME (HTP, $p < 0.01$; CoMp, $p < 0.01$), and the greatest values of r (HTP, $p < 0.01$; CoMp, $p < 0.01$). While not as close to WFM as NAr, HTP produced larger values of r ($p = 0.02$) and reduced RMS ($p < 0.01$) and ME ($p < 0.01$) relative to CoMp. Again, CoMp yielded the largest difference in MoS estimates compared to WFM. This was most clear given the low r between CoMp and WFM; the lowest observed within the current study.

4.3.3 Left Perturbations

A main effect of CoM model was detected for ML MoS_{peak} ($F(1.53, 13.73) = 32.87$, $p < 0.01$; see **Figure 4.2C**). Values of MoS_{peak} calculated using the WFM were different from both NAr ($p < 0.01$) and HTP ($p < 0.01$), though not from CoMp ($p = 1.00$). Again, considering MoS_{peak}, both NAr and CoMp were different from HTP ($p < 0.01$), though not from each other ($p = 1.00$). In terms of error metrics and correlations, no main effects were observed, leaving MoS_{peak} as the sole outcome measure to rank model performance.

4.3.4 Right Perturbations

A main effect of CoM model was detected for ML MoS_{peak} ($F(1.28, 11.55) = 58.1$, $p < 0.01$; see **Figure 4.2D**). Similar to the left perturbations, MoS_{peak} calculated using the WFM were different from both NAr ($p < 0.01$) and HTP ($p < 0.01$), though not from CoMp ($p = 0.79$). While both NAr and CoMp were different from HTP ($p < 0.01$), they were not different from each other ($p = 0.16$). Additionally, HTP again provided the highest values of r (NAr, $p < 0.01$;

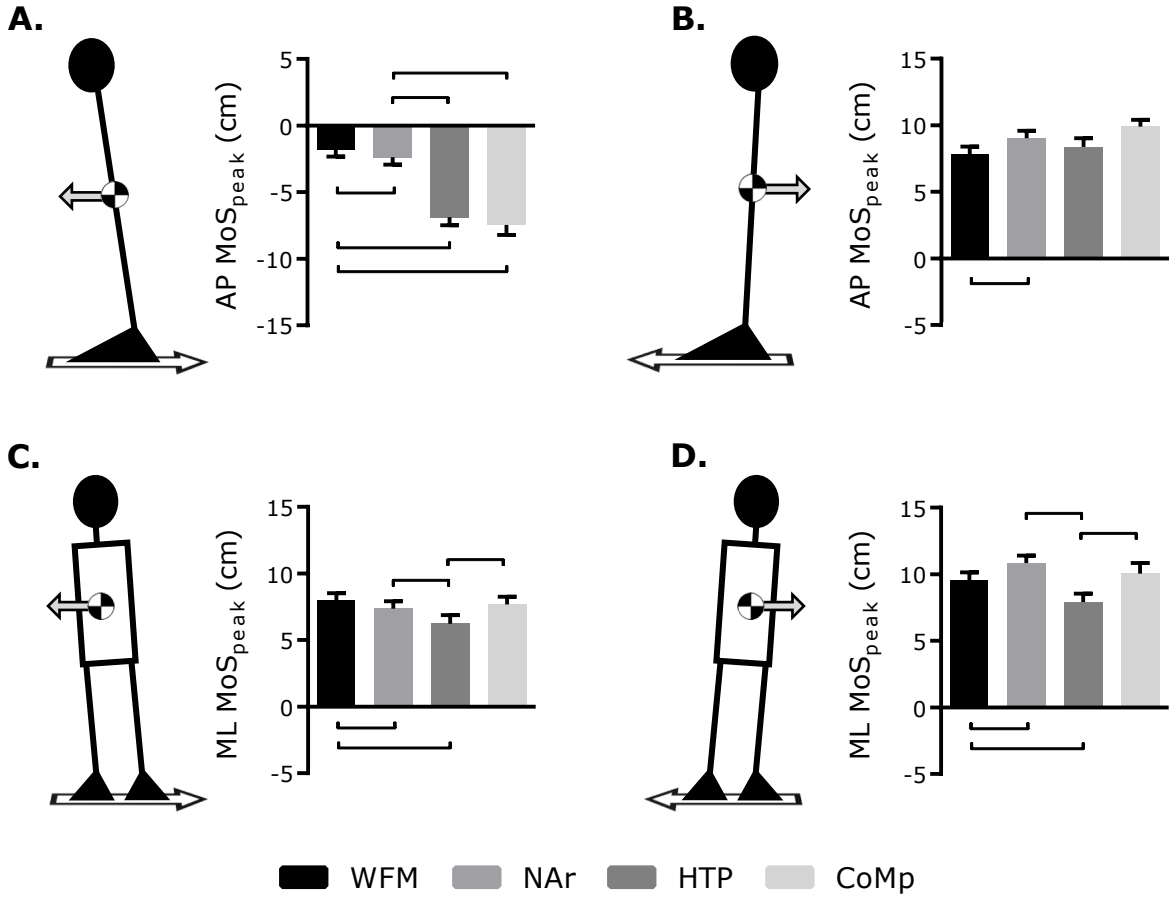

Figure 4.2 Effects of model simplification on margin of stability at peak extrapolated center of mass displacement opposite to perturbation direction (MoS_{peak}) following a A) backwards and B) forwards, C) left and D) right support surface translation. For A and B, MoS was calculated in the anteroposterior direction (AP); for C and D, this measure was calculated in the mediolateral (ML) direction. Significant differences between the full Winter et al. (1998) model (WFM) and simplified variations of said model are identified by open top brackets (⊔); differences between simplified models are identified by open bottom brackets (⊓). Values are expressed as mean (± SE)

Table 4.3 Cross correlation coefficients (*r*), RMS error (RMS) and maximum error (ME) expressed as mean (± SE) for each of the simplified models (NAr, HTP, and CoMp). Results of the one-way repeated measures ANOVAs performed to examine the effect of center of mass model are present as well.

Perturbation Direction	Variable	Center of Mass Model			ANOVA results	
		NAr	HTP	CoMp	*F*	*p*
Backwards	*r*	0.993 (0.002)[ab]	0.986 (0.002)	0.900 (0.031)	9.14	< 0.01*
	RMS (cm)	1.04 (0.04)[ab]	3.78 (0.18)[c]	5.86 (0.39)	118	< 0.01*
	ME (cm)	1.36 (0.07)[ab]	5.75 (0.34)[c]	7.74 (0.39)	165	< 0.01*
Forwards	*r*	0.825 (0.031)[ab]	0.614 (0.078)[c]	0.162 (0.150)	18.2	< 0.01*
	RMS (cm)	1.10 (0.06)[ab]	2.63 (0.17)[c]	5.79 (0.40)	136	< 0.01*
	ME (cm)	1.56 (0.11)[ab]	3.74 (0.23)[c]	7.68 (0.53)	128	< 0.01*
Left	*r*	0.965 (0.004)[a]	0.993 (0.002)[c]	0.953 (0.009)	15.8	< 0.01*
	RMS (cm)	0.89 (0.02)	0.78 (0.06)	0.89 (0.09)	1.25	0.31
	ME (cm)	1.56 (0.36)	2.05 (0.17)	2.11 (0.20)	1.37	0.28
Right	*r*	0.932 (0.006)[a]	0.991 (0.002)[c]	0.908 (0.028)	7.65	0.02*
	RMS (cm)	0.95 (0.02)	0.69 (0.05)	0.94 (0.14)	3.88	0.07
	ME (cm)	1.43 (0.06)[ab]	1.90 (0.13)	2.42 (0.35)	8.36	0.01*

Note: model / error degrees of freedom = (2, 18)

[*] Significant main effect of model ($p < 0.05$)

Significant differences between pairs: [a] NAr and HTP; [b] NAr and CoMp; [c] HTP and CoMp

CoMp, $p = 0.037$); NAr and CoMp were not different ($p = 1.00$). Despite this, NAr produce lower ME relative to HTP ($p < 0.01$) and CoMp ($p = 0.03$), though no differences could be detected for RMS.

4.4 Discussion

The purpose of the current study was to examine the effects of simplifying an anthropometric model used to derive whole-body xCoM position estimates on the MoS following support-surface perturbations. As hypothesized, the simplified model that retained most components of the WFM (a commonly used 13-segment full body model) excluding only those segments of little mass/contribution (NAr) yielded the best estimates of MoS. The CoM models that excluded the arms and legs (HTP) or used the pelvis only (CoMp), consistently yielded significantly different MoS values (CoMp more often than HTP), though these observed biases existed predominantly for sagittal plane perturbation conditions.

In the case of forwards and backwards perturbations, model simplifications yielded the most substantial effects on evaluations of the dynamic MoS. Using NAr provided the closest estimates of WFM MoS according to error (RMS ≤ 1.10cm, ME ≤ 1.56cm) and signal correlations ($r \geq 0.832$). It was followed by HTP and CoMp; the latter being the model variant that differed the most from the WFM. This hierarchy was most clear following forward perturbations where correlations across simplified models varied by a large degree (0.162–0.825). Considering MoS_{peak}, NAr remained the best model again followed by HTP and CoMp; though this was only clear for backwards perturbations. To clarify, following forward perturbations, only NAr was statistically different from WFM despite the larger mean MoS produced by CoMp. In this case, the lack of difference from CoMp can be explained by an inconsistent within-subject trend associated with that model.

Unlike sagittal perturbations, all models provided acceptable estimates of MoS following frontal plane perturbations (right and left). If it is assumed that the resulting postural sway from a perturbation is similar to that of an inverted pendulum, then segments along the length of the pendulum (e.g. trunk vs legs) should yield predictably different results. For example, MoS_{peak}

following lateral perturbations and evaluated using the HTP is lower than all other models that estimate a CoM closer to the axis of rotation (i.e. ankles). Despite this, over the two-second period of balance recovery isolated, HTP was associated with the best correlations and lowest RMS. This outcome suggests that this model can provide even more appropriate estimates of WFM on average relative to the more complex NAr model. It may be that following the instant of MoS_{peak} in these scenarios, independent sway between the HTP and the combined lower limbs yield a HTP CoM trajectory that better resembles that of the WFM.

In general, our results suggest that use of the NAr variation of WFM provided the best approximations of WFM MoS. Havens et al. (Havens et al. 2018) reported similar fidelity and estimations of a whole-body CoM model using a trunk + legs CoM model during a walking / turning task. In their healthy, young adult population, there was a minimal influence of arm segments in MoS calculations, likely due to the small mass proportion from the upper limbs. It is unknown at this time if this relationship is the same for other populations (e.g. older adults who may use larger arm responses to complete these tasks; (Tang and Woollacott 1998).

Both HTP and CoMp performed well following frontal perturbations, with HTP producing good estimates of WFM MoS. However, these models performed poorly for sagittal plane perturbations. It is possible that a proportion of the error (RMS, ME, and MoS_{peak}) observed within these conditions can be explained by a vector offset to some segment local coordinate system such as the pelvis akin to that reported by Yang and Pai (Yang and Pai 2014). However, the time-varying nature of this error as illustrated in **Figure 4.1.** (*top*) suggests that this solution may not be infallible. The complex coordination required for repositioning multiple body segments following a perturbation may also be a key factor driving these observed differences. The AP boundaries of the BoS are a fraction of those in the ML direction. With less space to manipulate the center of pressure and xCoM, postural strategies that utilize counter-rotations of the trunk/pelvis are used (Horak and Nashner 1986; Hof 2007). In this scenario, the actions of the trunk/pelvis poorly reflect the integrated whole-body strategy in terms of CoM motion as reflected by the different estimates of HTP and CoMp models. While some authors have suggested the pelvis reflects 'true' CoM motion following a perturbation, this prior research was conducted in gait where a primary goal is to maintain constant forward momentum (Yang

and Pai 2014). Similar that reported in the current study, Tisserand et al. (2016b) observed a low fidelity of a pelvis model in estimating sagittal CoM and xCoM. Though within their protocol, a change in base of support was an acceptable postural response to a multi-planar applied external perturbation and likely attributed to their additional observations of poor CoM estimates in the frontal plane. Therefore, in the scenario presented in the current study we recommend that researchers account for both the lower limbs and trunk/pelvis in the Winter et al. (1998) CoM estimates prior to calculating stability metrics.

As mentioned prior, it is difficult to directly relate our observations with different experimental paradigms (e.g. postural control during gait). The current work, in addition to previously published work, assists in providing a framework for future research questions that employ similar experimental measures and setup. With more researchers utilizing the xCoM and MoS (or its temporal variant) to quantify dynamic stability (Delabastita et al. 2016; Peterson et al. 2016; Tisserand et al. 2016a; Caderby et al. 2017; Huntley et al. 2017a), the potential use of a reduced-marker setup that would require a smaller camera volume, reduced time-dedication, and a lower risk of poor data quality is beneficial. Future work will explore correction of simplified CoM models within similar conditions as a potential workaround for the issues made evident within our results. Finally, it is important to acknowledge that while we consider segmental CoM calculations acquired using kinematic data to be the "gold-standard", this method is not without assumptions that must be acknowledged (e.g. wobbling mass, older-adult cadaver-based anthropometric data, etc. (Pearsall et al. 1994; Winter et al. 1998; Gittoes and Kerwin 2006). Additionally, the current study highlighted the modifications of a single anthropometric model that is functionally different to other common anthropometric models (Catena et al. 2017). The current study explored how different reductions of the Winter model (Winter et al. 1998) impact the ability to track MoS during a dynamic task; in the future this exploration could be expanded to include the reduction of other whole body estimates of CoM.

4.5 Conclusion

In summary, the degree to which the anthropometric model may be simplified to estimate whole-body CoM is context specific. The present study indicates that for young adults, a Winter full

model is not necessary for calculating MoS during complex, fixed base of support tasks. The NAr model provides good estimates of MoS derived using the full model, though specific research questions may necessitate tracking of arm movements. When examining frontal perturbations that evoke a fixed-BoS response, it is reasonable to use a simplified pelvis CoM (or estimates of the combined head+trunk+pelvis) alone to approximate MoS. If sagittal plane perturbations are being used, at minimum the no arms model should be made use of as our work demonstrates that combined head, trunk, pelvis and pelvis only estimates of CoM dynamics produce larger magnitude MoS biases with respect to the Winter full model.

4.6 Acknowledgments

The authors would like to acknowledge funding provided by a NSERC Discovery Grant (awarded to LAV), Ontario Graduate Student scholarship and NSERC summer student fellowship (awarded to KAI) and Canadian Foundation for Innovation and Ontario Research Fund Research Infrastructure grants for equipment. The authors would also like to extend their appreciation to Dr. John Zettel for use of laboratory equipment and thank Tim Worden and Rhianna Malcolm for assistance with experimental design and data collection.

Chapter 5. Review of Objectives

In Study 1 (Chapter 4), we addressed the first objective of this thesis:

i. Experimentally determine the fidelity of simplifications made to a standard anthropometric model (Winter et al. 1998) on calculations of the dynamic MoS (Hof et al. 2005) for fixed-support balance recovery.

It was established that reducing complexity of anthropometric models can produce large errors in estimated CoM dynamics (xCoM); though this was dependent on the strategy evoked and plane of motion studied. The modelling concepts that underlie the FSR that may be used to calculate dynamic MoS now require attention as we translate these metrics towards more complex, biomechanical balance recovery strategies.

The following chapter will address the second objective of this thesis:

ii. Develop a bipedal, mathematical model and trajectory optimization routine that define the FSR necessary to calculate dynamic MoS during execution of lateral fixed-BoS postural strategies.

If the aim of a MoS-based metric is to reflect the system dynamics for bipedal balance, then it is critical for researchers to diverge frontal and sagittal MoS; anatomical differences and the number of degrees of freedom must be adjusted accordingly to ensure the fidelity of these postural control models (e.g. execution of counter-rotations). Furthermore, as we were interested in testing the robustness of our proposed model under a challenging postural perturbation (of the support surface via a robotic platform perturbation), it was critical that we also address the time-dependent influence of the support-surface perturbation waveform characteristics on the FSR.

Chapter 6. Estimating dynamic stability margins for lateral fixed-support strategies using trajectory optimization.

6.1 Introduction

Fundamentally, upright balance is considered the ability to maintain position of the whole-body centre of mass (CoM) within the available boundaries of the base of support (BoS). These boundaries may include the areas of contact between the individual and a support-surface (e.g. ground, railing, etc.). During the past few decades, many researchers interested in the underlying CNS control of balance factor the nature of this relationship into their outcome measures (Rosenblatt and Grabiner 2010; Lugade et al. 2011; Welch and Ting 2014; Huntley et al. 2017a; Inkol et al. 2018a). To this end, a commonly cited objective within many of these studies is to gain a deeper understanding of the mechanisms that lead to falls across populations (e.g. healthy young people, older adults, individuals recovering from a stroke) using various experimental paradigms such as obstacle crossing (Worden and Vallis 2016) and balance recovery (Bierbaum et al. 2013; Inkol et al. 2018a). Inherently, the fidelity of these results hinges largely upon the assumption that the underlying biomechanical model reflects mechanics of the task used such that meaningful interpretations or conclusions may be disseminated.

Motor strategies that prevent falling are of noted importance in relation to balance control due to their role as a defence mechanism. For example, older adults exhibit a greater likelihood of instability due to lower limb collision following a lateral support-surface perturbation (Rogers and Mille 2003). If they do fall, ground impact and fracture of the hip/pelvis is a common outcome (Cummings and Melton 2002). Young adults are typically able to avoid these injuries through reduction of the magnitude of impact (Hsiao and Robinovitch 1998). Balance recovery strategies can be classified as a change in BoS or fixed-BoS (i.e. no recovery step is taken); the latter will be of focus within the current study. As noted by Horak and Nashner (1986) and Maki et al. (1996), adding constraints to the system (e.g. task instructions, reducing BoS size, increasing the magnitude of perturbation) can result in substantial changes to the characteristics of a fixed-BoS response. Naturally, these changes may alter the observable degrees of freedom

as evident within the transition from an ankle to hip strategy. For the latter, divergence in the torque profiles between ankles and hips is necessary (e.g. opposite directions of rotation) as opposed to prioritizing control about a single axis of rotation (Horak and Nashner 1986). Execution of the hip strategy is then able to effectively counter-rotate body segments relative to CoM motion to produce a stable outcome (Hof et al. 2005; Hof 2007).

An often-used paradigm for investigations into biped stability and balance is mathematical modelling and simulation. Early mechanical models of balance suggested that quiet stance operates akin to that of an inverted pendulum (IP) in which ankle synergies produce joint moments that control sway of the CoM within the BoS (i.e. ankle strategy; Winter 1995; Winter et al. 1998). Patton and Pai (1997) expanded upon this model establishing the importance of CoM position-velocity dynamics in identifying the theoretical boundaries within which upright balance may persist ("feasible stability region"; FSR). The boundaries that define the FSR address two unstable scenarios: the CoM is above the BoS but has substantial outward velocity (exceeds *upper* boundary); the CoM is outside of the BoS and does not have substantial inward velocity (less than the *lower* boundary). Similar experiments were conducted by this group using models of increased degrees of freedom and different tasks (e.g. IP with a support-surface perturbation, Pai and Iqbal 1999; gait+slip, Yang et al. 2008) and by additional researchers deriving analytical solutions (Hof et al. 2005; Hof and Curtze 2016). The extrapolated CoM (xCoM) concept introduced by (Hof et al. 2005), an analytical solution to the original FSR (Patton and Pai 1997), has become increasingly popular in many gait and posture-related studies. However, the proposed dynamic margin of stability (MoS) measure derived from the linearized FSR (i.e. the maximum stable xCoM excursions) is largely based on quiet standing with relatively low magnitude external perturbations at most. For more appropriate evaluations of balance recovery, it is necessary to adjust the MoS within the direction of balance loss induced by support-surface perturbation. Prior research has identified the temporal dependence of the FSR on active perturbation acceleration waveforms (Pai et al. 2000). For example, the upper boundary velocities at the onset of the deceleration (negative) phase of the perturbation should be larger than those at the earlier stages of acceleration.

Within Study 1 (Chapter 4) of this thesis, use of Hof's MoS produced negative values following small-scale perturbations; similar observations have also been noted by other researchers (Hof et al. 2005; Rosenblatt and Grabiner 2010). Fundamentally, negative values suggest the model itself was unstable; but does not suggest that the individual was unstable (i.e. fell). Rather, it suggests that individuals must use mechanisms external to the IP model (e.g. take a step, counter-rotations, use future perturbation accelerations, etc.) in order to maintain stability, upon which multitudes of options exist. These ambiguous interpretations raise the question of whether an individual is truly unstable or if alternatively, they have successfully adopted a strategy in which the FSR was larger. If the latter is true, as suggested by Iqbal and Pai (2000), definition of these margins would assist in discerning the potential of viable postural strategies. Executing a control strategy that permits larger instantaneous velocities and does not require a change in BoS may be intrinsically beneficial in terms of producing a more adaptable system for fall prevention.

Prior work, acknowledged above, has investigated and modelled balance control within the sagittal plane primarily. Less has been documented regarding lateral balance strategies with a *fixed* BoS; especially for those responses that represent a lateral counterbalance (Egerton et al. 2011; Federolf et al. 2013). This strategy is the frontal plane equivalent of a hip strategy but is uniquely dependent on the active/passive loading and unloading of the legs that occurs as a result of our bipedal anatomy. Models consisting of multi-segment chains do exist for estimating stability margins (Iqbal and Pai 2000) but operate within just the sagittal plane. Only a few published studies have attempted to model control strategies for specifically maintaining lateral balance (Hof 2007; Yang et al. 2009; Bingham et al. 2011; Nishihori et al. 2012). These studies have disseminated the ability for the CoM to move approximately 4 cm outside of the physical BoS boundaries during unilateral balancing (Otten 1999; Hof 2007). Given the association between lateral instability and increased falls risk with older adults (e.g. during activities of daily living such as reaching towards an object, Huntley et al. 2017) in addition to the existence of mechanisms of lateral balance control outside of the scope of the IP model, a more focused approach to lateral *dynamic* MoS is essential (Lord et al. 1999; Maki et al. 2000).

Estimating dynamic FSR for complex systems in and of itself provides a unique and difficult challenge. It relies on some consideration of how the CNS controls a highly redundant system for which a simple and universally-accepted explanation does not exist. Many forward dynamics-based simulations estimate the FSR using anything from predefined torque-time profiles (Pai and Patton 1997; Pai and Iqbal 1999) to trajectory optimization (Yang et al. 2007, 2008, 2009). These studies have often ignoring the possibility of coactivation of agonist-antagonist pairs that may alter performance of balance recovery (Brunt et al. 1992). The direct-shooting solution proposed by Pandy et al. (1992) is interesting as it has been used previously in models of volitional motor tasks (e.g. jumping) and replicating experimental data (Anderson and Pandy 2001; Porsa et al. 2016). It requires the optimal control problem to be redefined as a nonlinear programming (NLP) problem by parameterization of control trajectories; solutions can be estimated computationally using numerous algorithms (e.g. gradient-based search, simulated annealing, etc.). A more computationally efficient method of trajectory optimization alternative to direct-shooting is direct collocation (DC; Porsa et al. 2016). Unlike the shooting method, this approach towards forward dynamics requires parameterization of both control *and* state trajectories. Trajectories may be bound via linear/non-linear constraints. In the case of the FSR, the problem to be solved involves maximization/minimization of the initial horizontal CoM velocity at any given CoM position to define discrete boundaries. This is contrary to other cases of optimal control that aim to mimic biological phenomenon, e.g. minimizing CoM displacement following perturbation (Kuo 2005; Versteeg et al. 2016). While balance control itself is not strictly volitional, these solutions may provide important information pertaining to the capabilities of the human body in fall prevention

The ***purpose*** of the current experiment was to utilize DC to estimate the FSR for fixed-BoS counterbalance strategies. We executed these simulations during standing with or without the addition of a support-surface perturbation. For the latter condition, we examined two evenly spaced time points within the platform acceleration waveform to initialize the simulation in order to estimate the temporal and task dependence of these stability margins. We then utilized the newly identified FSR via our model and those provided by Hof et al. (2005) to compare the calculated MoS within experimental data. We *hypothesized* that the MoS for our proposed

system would in fact be larger than that suggested by Hof et al. (2005) due to the addition of a counterbalance mechanism that benefits postural stability. Analysis of experimental data sets would reflect this hypothesis through significantly larger values of MoS during quiet standing and following a perturbation when compared with results based on the Hof et al. (2005) model. We further hypothesized that the upper FSR boundary approximated at peak platform velocity (deceleration onset) would be a larger magnitude than both the no perturbation and early platform accelerations (preceding peak velocity) FSR (Pai et al. 2000). The MoS evaluated using these FSR would best reflect the stability of the individual based on the presence of positive or negative values. If our model does in fact describe mechanics outside of the IP model; then IP-based MoS will not be appropriate and must then be modified.

6.2 Experimental Methods

6.2.1 Subjects

Experimental data were collected from ten healthy young adults (5 Males, 5 Females; mean ±SD Age: 22.5 ± 1.78 years; Height: 1.71 ± 0.09 m, Weight: 72.4 ± 12.0 kg); informed, written consent was provided by each subject prior to participation. Subjects were free of self-reported neuromuscular conditions (i.e., injury or disease) that could influence their ability to maintain balance. This experiment was approved by the University of Guelph Research Ethics Board.

6.2.2 Data Collection

The data collected was a subset of the data collected as outlined within Study 1 in addition to (Inkol et al. 2018a). Briefly, participants were suspended using a safety harness and stood barefoot on a pair of strain-gauge force plates (0.90 m x 0.60 m; AMTI, Inc; Watertown, MA) embedded within a 5 x 2 m robotic platform (Shelley Automation, Cambridge, ON). Within each trial of the 104-trial protocol, support-surface translations (i.e. perturbations) were triggered to evoke balance recovery. Eight variations of perturbations were utilized: four directions (forward, backward, left, right) by two magnitudes (small and large). Perturbation magnitudes were assigned a “small” or “large” value according to the work by Maki et al. (1996); these values have been used in prior related studies (Perry et al. 2001; Zettel et al. 2002a, 2008; Huntley et al.

2017a). The goal of the small magnitudes was to evoke strictly fixed BoS responses (e.g. CoM sway), while the large magnitudes were purposed to evoke a reactive stepping response. Instructions to "*maintain upright balance without taking a step*" were provided to participants prior to testing to increase the likelihood of appropriate response execution. Note that despite our original intentions, the fixed BoS counter-balance strategies were unexpectedly evoked following primarily large magnitude lateral perturbations. As the simulations performed prioritized rightward loss of balance (Chapter *6.2.3*), trials that evoked this scenario using large, left directed perturbations were isolated and analyzed within the current study.

During testing, the 3D position of markers surrounded in retroreflective tape were captured using 12 Optitrack cameras (100 Hz; NaturalPoint, Corvallis, OR, USA). Markers were affixed to bony, anatomical landmarks according to the anthropometric model outlined in Winter et al. (1998). Rigid clusters of markers were also strapped to several segments (pelvis, thighs, feet) to facilitate the tracking of digitized landmarks relevant to each segment. This method involved definition of a local coordinate system for each segment using three non-colinear markers within the corresponding fixed cluster. Refer to Appendix 9.1 for further details related to the marker setup.

6.2.3 Forward Dynamics Simulations

Forward dynamics simulations were used to estimate the FSR associated with the mechanics of the lateral counterbalance strategy. The bipedal biomechanical model used is displayed in **Figure 6.1** and detailed in Chapter *6.3*. A schematic of the routine used to approximate these stable boundaries under different conditions is outlined in **Figure 6.2A**. Briefly, a set of different initial whole-body CoM positions were defined with respect to the right boundary of the BoS and normalized to a standardized BoS width (**Figure 6.2B**). The latter was assumed to be equivalent to a hip-width stance in which the ankle joint centres were in line with the hip joints. Each initial, horizontal CoM position c_{t_0}, an element of the set $\{c_{t_0}\}$ = {0, 0.25, 0.50, 0.75, 1.00, 1.25, 1.50}, was associated with a reference configuration related to the model's vector of generalized coordinates (**Figure 6.3**). These reference configurations fell under the following categories: double support (S); single support with either the left leg (S′) or right leg (S″) as the support

limb. Only the S condition was permitted to initialize stance using double support dynamics (see Chapters 6.3-4). The S′, S″ postures were included primarily to test the model under more extreme conditions; they do not necessarily translate to real-world scenarios. Lastly, for future reference, c_{t_0}= 0 indicates position of the CoM over the right, physical BoS boundary where as c_{t_0}= 1 is over the left boundary.

Once reference configurations were determined and an initial guess for balance recovery trajectory(ies) was compiled via experimental data (Chapter *6.4.1*), two general simulation conditions were defined. One had no translations of the support-surface (standing, S); the other required CoM control *during* a fixed-size perturbation. The perturbations used were identical to those of the experimental paradigm of Study 1 (though not included in text): a square wave acceleration waveform; acceleration magnitude = 2.9 m/s^2; peak velocity = 0.87 m/s; displacement = 0.26 m. Simulations were initiated at two different starting velocities within the perturbation's acceleration phase (P1, 0.435 m/s; P2, 0.870 m/s; see **Figure 6.2C** top). The results were the FSR specific to events P1 (P_{mid}) and P2 (P_{peak}). For convenience, the FSR for perturbation conditions detailed only CoM positions between 0 and 1 and thus had only an upper boundary.

Trajectory optimization via DC was used to approximate the maximum or minimum, rightward, initial CoM velocity that could be corrected within each condition at each value of c_{t_0}. Maximum and minimum velocities corresponded to the upper and lower FSR boundaries respectively. Note that the lower boundaries were assumed to be zero if c_{t_0} was within the physical standardized BoS and the reference configuration was an S-type ($0 \leq c_{t_0} \leq 1$). Scenarios in which S′/S″ single-support configurations were used ($1 \leq c_{t_0} \leq 1.50$) were the only cases in which lower boundaries were estimated. This portion of the experiment is outlined in greater detail in Chapter *6.4.2*.

6.2.4 Experimental Data Analyses

Analyses of study 1 experimental were completed within Visual3D (Version 6, C-Motion Inc., Germantown, MD, USA) and MATLAB (Version 9.4, The MathWorks Inc., Natick, MA, USA).

As mentioned prior, we analyzed only the large magnitude, left perturbation conditions within our data set to apply the FSR estimated within our simulations and by Hof et al. (2005). Kinematic data from each participant were initially examined to categorize the postural responses evoked within each trial (4 total); the two categories were reactive stepping to expand the BoS within the direction of balance loss (ΔBoS) or maintenance of a fixed, right BoS boundary (fBoS). The fBoS trials were inherently associated with the counterbalance strategy. For reference purposes, representative rightward MoS trajectories (calculated using the xCoM) from one subject that utilized an fBoS strategy and another that required ΔBoS are displayed in **Figure 6.2C** (bottom). Gaps within marker trajectories due to occlusion were interpolated via cubic-spline; data were further processed using a low-pass, zero-lag Butterworth filter (fourth order; cut-off = 6 Hz). Whole-body CoM position was then estimated using a thirteen-segment variation of the Winter et al. (1998) anthropometric model and Equation 4.1. Note that two trunk segments were lumped within this model as a result of persistent occlusion of the rib markers by the safety harness. Lateral velocity of the CoM was estimated using the finite central difference across three frames of data (Δt = 0.02 s).

The MoS ξ developed from both our model and Hof et al. (2005) (i.e. Hof) was evaluated as the difference between instantaneous xCoM position within experimental data and maximal (stable) xCoM position estimated from simulations. These maximal positions were determined from the FSR generated from either simulations or the Hof model using the following equation:

$$\xi = \omega_0^{-1}(\dot{c} - \dot{c}_{\max}|_{\bar{\bar{c}}}) \qquad 6.1$$

The first term was the non-inverted pendulum eigenfrequency $\omega_0 = \sqrt{g/\ell}$ where g was gravitational acceleration and ℓ was 1.34 times trochanteric height (Hof et al. 2005). The second term was the difference between experimental lateral CoM velocity $\dot{c}$ and maximum feasible velocity $\dot{c}_{\max}$ evaluated at $\bar{\bar{c}}$, the CoM position (as proportion of measured BoS length) with respect to the right BoS boundary: $\bar{\bar{c}} = \frac{(c-b_R)}{|b_R-b_L|}$. Here, b_R, b_L were right/left BoS positions (bilateral head of fifth metatarsals).

To generate Hof model's FSR for the set of c_{t_0} used in simulations, our model's anthropometric parameters (height and BoS width) were incorporated within the defining equation for xCoM (Equation 4.2). The resulting $\dot{c}_{\max}$ could then be evaluated for c_{t_0} as $\dot{c}_{\max}|_{c_{t_0}} = \omega_0(c_{t_0}\ell_b)$, which defines that the maximum feasible excursions of xCoM are then equal to the normalized c_{t_0}. The final step prior to evaluating the MoS in Equation 6.1 was estimation of a continuous FSR. For each of the Hof, S, P_{mid}, and P_{peak} discrete FSR, a cubic spline was fit to approximate each maximal velocity for CoM positions from 0 to 1 using increments of 0.01 (approximately 0.4 mm unnormalized).

Calculations of the MoS were completed during a 10 s quiet standing trial (using averaged values of c and $\dot{c}$) via FSR derived from Hof and the S condition simulations. The MoS during perturbation trials at P1 and P2 events was evaluated using all three of the Hof, S, and corresponding P-based FSR (i.e. P_{mid} at P1, P_{peak} at P2).

6.2.5 Statistical Analyses

As mentioned prior, comparisons between applications of the FSR derived from Hof et al. (2005) and the proposed standing/perturbation models (S, P_{mid}, P_{peak}) were facilitated by calculating the MoS within experimental data, i.e., the adapted lateral MoS. Statistical analyses was completed within SPSS software (Version 24, IBM Corporation, Armonk, NY, USA). Mixed-design ANOVAs were performed to examine the differences between each underlying model/solution (*within-subject*; Hof, S, P_{mid}, P_{peak}) and postural strategy evoked (*between-subject*; ΔBoS, fBoS) on calculated MoS. For quiet standing, only Hof and S MoS were compared; for perturbations (P1, P2 events), Hof, S, and the corresponding P event MoS were compared. When significant main effects were obtained, post-hoc testing was performed using Bonferroni corrections. Significance for all tests was set to $p < 0.05$.

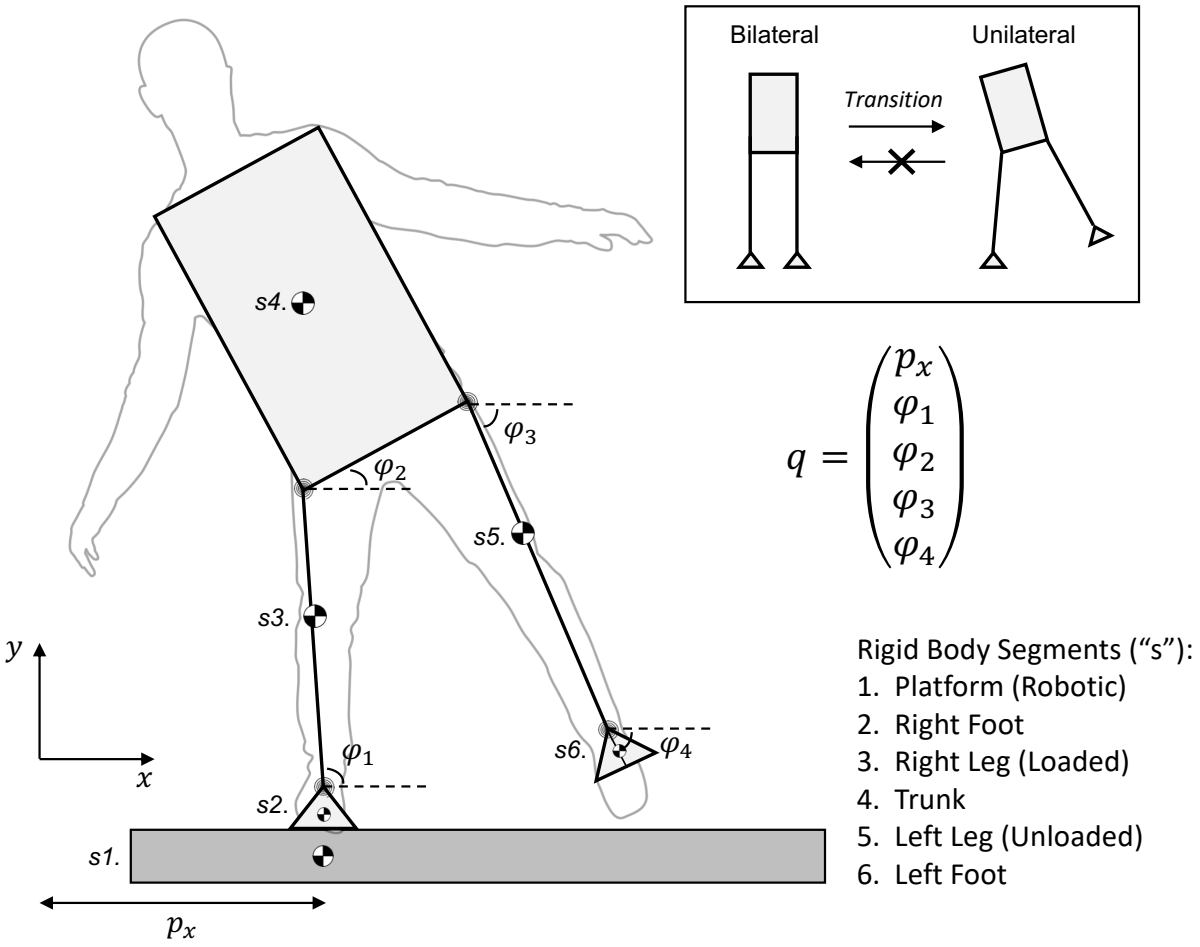

Figure 6.1 The proposed six segment, bipedal biomechanical model (segments labelled) utilized to estimate lateral dynamic margins of stability with the addition of a counterbalance strategy. Included are the definitions of the generalized coordinates $\boldsymbol{q}$. The model was permitted to transition from bipedal to unilateral stance only; the reverse direction was not a feasible scenario (inlay).

6.3 Mathematical Model

6.3.1 Equations of Motion

The two-dimensional system used to model the lateral counterbalance recovery strategies is outlined in **Figure 6.1**. It was a multi-link system consisting of six rigid bodies (linked segments) and five degrees of freedom that defined the generalized coordinates of the system

$$\boldsymbol{q} = (p_x, \varphi_1, \varphi_2, \varphi_3, \varphi_4)^T \in \mathbb{R}^5. \quad 6.2$$

Segments within our model included the robotic platform, free to move within any prescribed lateral direction (p_x), and the five body segments (e.g. trunk, legs, feet; $\varphi_1, \dots, \varphi_4$) within the defined inertial reference frame. A reminder that the perturbations considered were leftward, unidirectional translations of the platform. As the BoS (i.e. feet in contact with platform) was assumed to be fixed to the platform via static friction, it was not included within $\boldsymbol{q}$ though was considered within the system dynamics. Links within the biomechanical component of the model were connected by frictionless hinge joints, each of which contained a viscoelastic, torsional spring that introduced additional energy (stored) and damping (Farley and Morgenroth 1999; Suzuki et al. 2012). We assumed that these springs/dampers would tend towards null velocities and a general pseudo-anatomical upright position (i.e. $\boldsymbol{q}_{t_0}$ at c = 0.50)

The ordinary differential equations (ODE) that provided the dynamic equations of motion for each system were derived and organized using Euler-Lagrangian dynamics such that

$$\boldsymbol{Q} + \boldsymbol{\mathcal{J}}(\boldsymbol{q})^T\lambda = \boldsymbol{M}(\boldsymbol{q})\ddot{\boldsymbol{q}} + \boldsymbol{C}(\boldsymbol{q}, \dot{\boldsymbol{q}})\dot{\boldsymbol{q}} + \boldsymbol{G}(\boldsymbol{q}) \quad 6.3$$

Matrices $\boldsymbol{M}$, $\boldsymbol{C}$, and column vector $\boldsymbol{G}$ contained information pertaining to the orientation-dependent inertia, Coriolis/centrifugal force(s), and gravitational toppling moments respectively (see Appendix 9.2). The non-conservative forces of the control vector $\boldsymbol{Q}$ for forward dynamics were as follows:

$$\boldsymbol{Q} = \begin{pmatrix} F_p \\ \tau_1 - \tau_2 \\ \tau_2 - \tau_3 \\ \tau_3 - \tau_4 \\ \tau_4 \end{pmatrix} \quad 6.4$$

Each joint (1-4) was provided a pair of simple agonist/antagonist "muscles". These were effectively single muscle equivalents that could actuate joints through direct applications of torque. Net torque of the j^{th} joint (τ_j) was therefore comprised of active and passive (viscous and elastic) components that were a function of *relative* joint angular position and velocity. This behaviour is explained through the following equations:

$$\tau_j = \gamma_j - B_j\lfloor\dot{\varphi}_i, \dot{\varphi}_k\rfloor - K_j\lfloor\varphi_i, \varphi_k\rfloor, \quad \gamma_j = \gamma_j^{\mathrm{A}} + \gamma_j^{\mathrm{ANT}} \quad 6.5$$

The notation $\lfloor i, k \rfloor$ indicates the relative joint angles/angular velocity between linked segments i and k. Elastic (K) and viscous (B) spring/damping coefficients, properties of the torsional springs, were adopted and adjusted from the literature (see *Chapter 6.3.2*).

The two muscles per joint (i.e. agonist [A], antagonist [ANT] pair) determined the active components of torque γ_j. The torque generated for either A or ANT, $\gamma_j^{\mathrm{A|ANT}}$, was determined via the muscle/actuator's activation a and maximum permissible torque $\tau_{\max}$ (see **Table 6.1**):

$$\gamma_j^{\mathrm{A|ANT}} = (a\tau_{\max})_j^{\mathrm{A|ANT}}, \quad a \in [0,1]. \quad 6.6$$

Muscle activation itself was controlled via neural excitation u. The first-order ODE that defined this dynamic relationship was adapted from the musculoskeletal model by De Groote et al. (2016) which smoothly transitioned between activation states via a hyperbolic tan function (tanh):

$$\dot{a} = \tilde{a}\left[\frac{1}{t_A(0.5 + 1.5a)}\,[0.5 + 0.5\tanh(\eta\tilde{a})] + \frac{0.5 + 1.5a}{t_D}\,[0.5 - 0.5\tanh(\eta\tilde{a})]\right] \quad 6.7$$

Above, $\tilde{a} \equiv u - a$, η was a smoothing parameter (0.1), and t_A/t_D were activation/deactivation time constants respectively (0.015 s, 0.060 s). Like a, values of $u \in [0,1]$. Therefore, the index

of elements within vector $\boldsymbol{a} \in \mathbb{R}^8$ (activations of all eight muscles) were controlled during simulations by the equivalent index of control vector $\boldsymbol{u} \in \mathbb{R}^8$.

Additional components to Equation 6.3 were the vector of Lagrange multipliers λ and matrix $\boldsymbol{\mathcal{J}}$, the Jacobian of the holonomic constraint functions $\boldsymbol{\Phi}(\boldsymbol{q}) = 0$. These equality constraints were defined to include basic ground contact forces applied the left foot rigid body and form a closed chain (McGrath et al. 2017); they were only applied at initialization of S-type reference configurations in which the model was oriented in double support (**Figure 6.3**). For S′ and S″, the left side of Equation 6.3 contained only the vector $\boldsymbol{Q}$. The constraint equations maintained the left foot's vertical position on the platform (Φ_1), horizontal position as fixed distance s from the right foot (Φ_2), and eliminated foot-roll (Φ_3):

$$\Phi_1 = \mathrm{a}_y + \sum_{i=1}^{4} \ell_i \sin(\varphi_i) \tag{6.8}$$

$$\Phi_2 = p_x - s + \sum_{i=1}^{4} \ell_i \cos(\varphi_i) \tag{6.9}$$

$$\Phi_3 = \frac{1}{2}\pi + \varphi_4 \tag{6.10}$$

Within the above equations, a_y is the height of the right foot's ankle and ℓ_i indicates the length of the *i*th segment. These constraints were state dependent and the transition from double to single support (see **Figure 6.1** inlay) was a simple logical switch triggered when $\lambda_{\Phi_1} < 0$. Once in unilateral stance, the model was not permitted to revert back to avoid the influence of further foot contact dynamics on the counterbalance responses generated.

For more details regarding the operations used to solve for the equations of motion, refer to Appendix 9.2 and 9.3. Note that Mathematica software (Version 11.3, Wolfram Research Inc., Champaign, Il) was used to check for errors in the equations of motion via symbolic mathematics.

6.3.2 Model Parameters

An overview of the model parameters used is provided in **Table 6.1**. Simple 2D geometric interpretations of segment shape were used to reduce system complexity (e.g. boxes for trunk and BoS). Segment inertial parameters such as mass, moment of inertia, and length were estimated using the anthropometric tables provided by (Winter 2009) and originally determined by Dempster (1955). The platform itself was given a substantial mass (10^8 kg) to nullify the impact of postural sway on its own momentum. This assisted in replicating the system within our laboratory in which a pre-calculated force could be applied via electric motors to generate a given acceleration waveform of the robotic platform. Additional components that governed system behaviour included values of spring/damping coefficients, peak isokinetic joint torques (ankles, Karatsolis et al. 2009; hips, Sugimoto et al. 2014), and passive joint ranges of motion (Boone and Azen 1979). Note that due to the lack of published values of K and B for rotations in the frontal plane, we adopted and scaled-down values from the sagittal-plane double pendulum designed by Suzuki et al. (2012). Gains for B between joints/planes were adjusted proportionately to the architecture of the muscle groups that actuated each joint. For example, the ratio of physiological cross-sectional area between hip ab-/adductors and flexors/extensors (Ward et al. 2009) defined the adjustments of B from Suzuki et al. (2012). Values of K were only a fraction of the Suzuki et al. (2012) values as the sagittal plane estimates of stiffness demanded a much larger BoS than that offered by a single foot width.

6.4 Optimization Routine

A schematic of the optimization routine used within the current study for estimation of the lateral FSR is outlined in **Figure 6.2A**.

6.4.1 Reference Configurations and Initial Guess

Reference configurations of $\boldsymbol{q}$ (i.e. $\boldsymbol{q}_{t_0}$) that corresponded to a given initial CoM c_{t_0} within each simulation were assessed using NLP in combination with the segmental averaging method of CoM estimation (Equation 4.1). The problem defined was constrained according to anatomical

limits of the model (i.e. joint ranges of motion, see **Table 6.1**). Initial CoM positions from 0 to 1.50 were assigned values of $\boldsymbol{q}_{t_0}$ that initialized the model in double support (S) or single support (left limb S′; right limb S″). A reminder that the resulting $\boldsymbol{q}_{t_0}$ for each initial CoM position in addition to the scenarios not considered are illustrated in **Figure 6.3**; values and definitions of c_{t_0} in relation to the standardized BoS are clarified in **Figure 6.2B**.

Experimental data were used to construct an initial guess for state space trajectories (i.e. values of $\boldsymbol{q}$ and $\dot{\boldsymbol{q}}$) prior to running the DC operation for approximating stability margins. These data were provided by one trial from a participant who made evident use of the counterbalance strategy in question. The kinematic data collected were resampled through a combination of interpolation and signal decimation such that the output consisted of 26-29 discrete frames (nodes) over a 2-second period initialized at onset of the perturbation used to evoke balance recovery. Guesses for control and muscle activation histories were completed using NLP which yielded trajectories that could have produced the experimental data in question. For later simulations, in the case the experimental data-based guess was not successful in attaining a local minimum, previously successful simulations were recycled into the program as an initial guess (e.g. using S simulations for P_{mid}/P_{peak} conditions).

6.4.2 Trajectory Optimization for Lateral Feasible Stability Regions

The goal of the DC-based trajectory optimization used was to minimize the cost function

$$\min\ \zeta = \left[\dot{c}_{t_0} - \dot{p}_x(t_0)\right]^{\beta} \tag{6.11}$$

where

$$\beta = \begin{cases} 1, & \text{upper boundary,} \\ -1, & \text{lower boundary,} \end{cases} \tag{6.12}$$

We aimed to determine the maximum or minimum, rightward initial CoM velocity (relative to the initial platform velocity) that could be terminated successfully from an initial CoM position c_{t_0}. Maximum rightward velocities that could be terminated without loss of balance to the right defined the upper boundary of the FSR. Minimum rightward velocities were those that would

Table 6.1 Model parameters to define system dynamics and nonlinear programming constraints. Segment inertial properties not shown below were adapted from anthropometric table(s) (Winter 2009).

Model Parameter	Values + units
Height	1.80 m
Total Body Mass (m_T)	75.0 kg
Platform Mass	10^8 kg
CoM height at $\bar{\bar{c}} = 0.5$ (c_y)	$c_y\big\|_{\bar{\bar{c}}=0.5}$ = 1.01 m
ω_0	2.74 s^{-1}
Base of Support	
Single Foot Width	0.099 m
Pelvis Width	0.344 m
Total BoS Width	0.542 m
Ankle Joints	
K_A	0.05($m_T g c_y$) N·m rad^{-1}
B_A	1.5 N·m·s rad^{-1}
Peak joint torque {Ev, In}	{0.43, 0.35} N·m m_T^{-1}
Range of motion {Ev, In}	{0.34, 0.63} rad
Hip Joints	
K_H	0.025($m_T g c_y$) N·m rad^{-1}
B_H	3.33 N·m·s rad^{-1}
Peak joint torque {Ab, Ad}	{1.29, 0.75} N·m m_T^{-1}
Range of motion {Ab, Ad}	{0.71, 0.45} rad

Terms: Ev, eversion; In, inversion; Ab, abduction; Ad, adduction

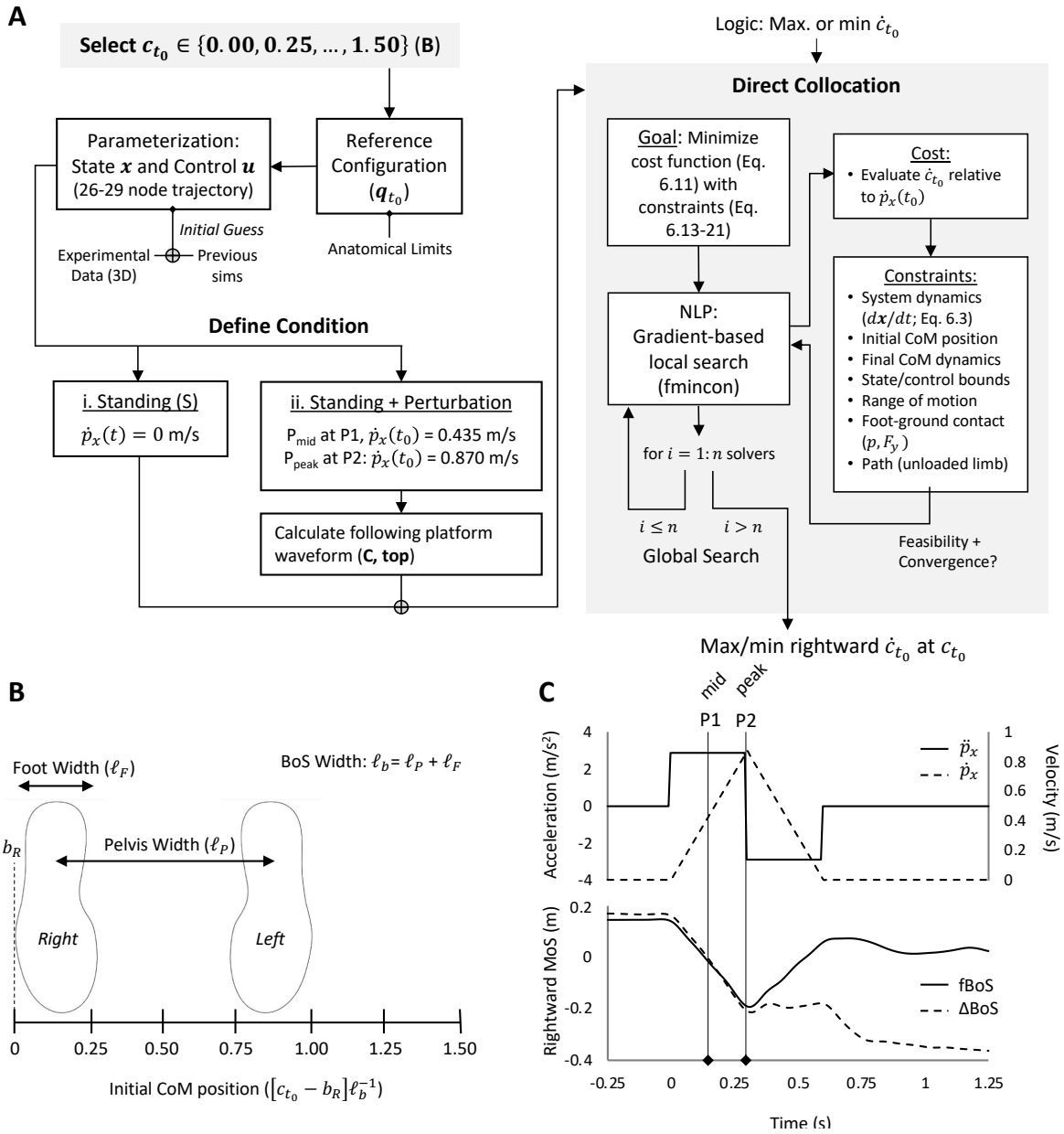

Figure 6.2 (A) Schematic outlining the optimization routine to yield feasible stability region (FSR) for lateral counterbalance, i.e. maximum or minimum rightward CoM velocity $\dot{c}_{t_0}$ initialized at relevant CoM position c_{t_0}. (**B**) Definition of the normalized CoM locations (with respect to the right base of support, BoS, boundary) used to initialize each forward dynamics simulation. (**C,** top) Acceleration (*solid*) and velocity (*dashed*) waveforms of the leftward platform perturbation used in in simulations and the physical experiment. (bottom) Representative data of rightward MoS (difference between right BoS boundary and extrapolated CoM position) for a fixed BoS (fBoS) and change in BoS (ΔBoS; i.e. cross-over step) balance control strategy. The time events targeted within estimation of stability margins (as shown in **A)** in addition to data analyses are labelled P1 and P2.

Initial CoM c_{t_0} ($[c - b_R]\ell_b^{-1}$)	Reference configuration q_{t_0}		
	S	S′	S″
0			
0.25			
0.50			
0.75			
1.00			
1.25		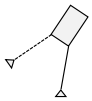	
1.50			

Figure 6.3 Illustration of the reference configurations $\boldsymbol{q}_{t_0}$ of the generalized coordinates corresponding to each initial CoM position used. For CoM positions equal to or greater than 1, two categories of configurations were defined according to the foot used within unilateral stance (S', left foot; S", right foot).

prevent loss of balance to the left when the CoM was initially positioned outside the physical BoS (lower boundary). As the model was not permitted to transition from single to double support, the BoS considered for termination criteria was in fact different from the standardized BoS; it was the width of the right foot alone. Thus, the goal of optimization was to find the FSR that results in a stable unilateral or single support posture.

Rather than impose several weighted expressions to the cost function akin to previous work (Yang et al. 2007, 2008, 2009), the use of DC allowed us to impose numerous linear and non-linear algebraic constraints on both the control and state space. The following series of notes will address each of the constraints that were imposed for forward dynamics simulations:

i. Sequential state values were limited to the system dynamics f (Equation 6.3) between nodes k and $k+1$; this was verified through forward integration (trapezoidal) over a fixed step size h_k. Step sizes were dependent on the maximum permitted time for balance recovery (two seconds) and the density of the mesh used (26-29)

$$\begin{gathered} \dot{\boldsymbol{x}} = f_k(\boldsymbol{x}_k, \boldsymbol{u}_k) \\ \boldsymbol{x}_{k+1} - \boldsymbol{x}_k - 0.5h_k(f_k + f_{k+1}) = 0 \end{gathered} \tag{6.13}$$

The 24×1 state space vector of the system $\boldsymbol{x} = (\boldsymbol{q}, \dot{\boldsymbol{q}}, \boldsymbol{a})^T$ contained information pertaining to the generalized coordinates and muscle activations.

ii. General state and control vector boundaries were imposed as:

$$\begin{gathered} \boldsymbol{x}_{\min} \leq \boldsymbol{x}_k(t) \leq \boldsymbol{x}_{\max} \\ 0 \leq \boldsymbol{u}_k(t) \leq 1 \end{gathered} \tag{6.14}$$

iii. The initial horizontal position of the CoM had to match the pre-specified, fixed position c_{RC} and given reference configuration $\boldsymbol{q}_{RC}$ (see Chapter *6.4.1* and **Figure 6.3**).

$$\begin{gathered} c_{t_0} - c_{RC} = 0 \\ \boldsymbol{q}_{t_0} - \boldsymbol{q}_{RC} = 0 \end{gathered} \tag{6.15}$$

iv. Terminal CoM dynamics (at final node t_f) had to meet the following conditions for stable *unilateral* stance (CoM within right foot BoS):

$$\begin{gathered} \min\{b_L - c, c - b_R\}_{t_f}^{U} \geq 10^{-3}\ \text{m} \\ \dot{c}_{t_f} - \dot{p}_{t_f} = 0 \\ \ddot{c}_{t_f} - \ddot{p}_{t_f} = 0 \end{gathered} \tag{6.16}$$

v. Relative hip and ankle joint angles were bound according to experimental data (Boone and Azen 1979) (**Table 6.1**)

$$\lfloor \varphi_i, \varphi_k \rfloor_{\min} \leq \lfloor \varphi_i, \varphi_k \rfloor \leq \lfloor \varphi_i, \varphi_k \rfloor_{\max} \tag{6.17}$$

vi. Negative values of the vertical ground reaction force F_y applied to the right foot were not permitted. Calculations of F_y using inverse dynamics were as follows:

$$F_y = \sum_{i=2}^{6} m_i(\ddot{c}_{y,i} - g) \geq 0\ \text{N} \tag{6.18}$$

Above, $\ddot{c}_{y,i}$ was specifically the vertical acceleration of the *i*th segment CoM. Values of λ_{Φ_1} had to remain positive but were not bound as negative values would trigger the transition to unilateral stance. Horizontal ground reaction force F_x was also calculated as:

$$F_x = \sum_{i=2}^{6} m_i \ddot{c}_{x,i} \tag{6.19}$$

Using both F_x and F_y, the constraint that restricted position of the CoP μ to within the physical BoS boundaries during unilateral stance was defined:

$$\begin{gathered} \mu = \frac{1}{F_y}\left(\tau_1 - \frac{\mathrm{a}_y}{2}\left(F_x - \sum_{i=3}^{6} m_i \ddot{c}_{x,i}\right)\right) \\ \min\{b_L - \mu, \mu - b_R\}^{U} \geq 10^{-4}\ \text{m} \end{gathered} \tag{6.20}$$

vii. Path constraints were imposed to avoid lower limb or ground collision during unilateral stance:

$$p_x - \sum_{i=1}^{4} \ell_i \cos(\varphi_i) \geq 0.20 \text{ m}$$
$$\mathrm{a}_y + \sum_{i=1}^{4} \ell_i \sin(\varphi_i) + \frac{1}{2}\ell_F \begin{pmatrix} +\sin(\pi - \varphi_4), & \text{right,} \\ -\sin(\pi - \varphi_4), & \text{left,} \end{pmatrix} \geq 10^{-3} \text{ m} \quad 6.21$$

Measurements within the laboratory were used as an estimate of a reasonable permitted distance between ankle joint centres. Vertical path constraints to the left foot considered the location of the heads of the metatarsals hence the inclusion of foot width ℓ_F.

For the perturbation conditions a series of additional constraints were defined; Equation 6.14 was adjusted such that the platform's state (p_x and $\dot{p}_x$) was bound to the correct displacement/velocity waveform.

Trajectories of both the state and control were parameterized into N nodal points evenly positioned across the time interval $[t_0\ t_f]$. Final time t_f was bound between 0.50 s and 2.00 s (Equation 6.14). The vector of parameters adjusted (state and control trajectories) within the rewritten cost function (Equation 6.11) $\zeta(\boldsymbol{z})$ were input into the NLP solver as

$$\boldsymbol{z} = \left(\boldsymbol{x}_1, \boldsymbol{u}_1 \ldots, \boldsymbol{x}_N, \boldsymbol{u}_N, t_f\right)^T \quad 6.22$$

A global solution for ζ was approximated using the Global Optimization Toolbox in MATLAB that performed a search of feasible solutions using multiple iterations of MATLAB's fmincon local solver. This solver uses the gradient of the constraint and cost functions estimated as their central finite difference to converge towards a neighboring, local optimal solution.

6.5 Results

6.5.1 Hof vs Adjusted Lateral Feasible Stability Region

The maximum and minimum rightward velocities that correspond to each initial CoM position that could be successfully corrected within our biomechanical model are outlined in **Table 6.2**. These values provided estimates of the FSR for conditions with (P_{mid}, P_{peak}) and without (S) the presence of a support-surface perturbation. Evidently, addition of the counterbalance component to balance recovery generated a consistent increase in the FSR for $c_{t_0} \in [0,1]$ when compared to the Hof et al. (2005) (**Figure 6.4A)**. For example, at a normalized CoM position 0.5, our model produced an upper boundary 116 % (3.50 cm) larger than that derived using the Hof IP model. Across all values of c_{t_0} for double support configurations; the counterbalance model derived FSR suggested 3.50 to 5.50 cm of additional xCoM excursions that were possible to achieve while maintaining upright balance. Another point of interest is the similar linearity of the FSR for our model relative to the Hof model over this same range of 0 to 1.

There was an apparent dependence of the FSR on the definition of the reference configuration at extreme values of c_{t_0}. The two possible sets of reference configurations used (see **Figure 6.3**) for $c_{t_0} > 1$ (S′, S″) yielded highly dissimilar boundaries. For simulations initiated in a left leg support (S′), maximal velocities at $c_{t_0} = 1$ were in fact reduced from the S-based boundaries (**Figure 6.4B**). The opposite was observed for simulations initiated in the more egregious right leg support configuration (S″). As S″ at $c_{t_0} = 1$ was initiated such that with the CoM was outside the unilateral BoS (right foot), the lower boundary could not be 0 as it was for S′

Representative data from the simulation initialized with $c_{t_0} = 0.75$ and no platform perturbation are displayed in **Figure 6.5**. These data outline relative joint position, active torques, CoM, CoP, and vertical ground reaction force trajectories generated from forward dynamics simulations**.** The solution returned by the DC method of trajectory optimization satisfied all constraints defined in Chapter 6.4. All simulations terminated with a positive static MoS (CoM position within physical unilateral BoS boundaries) and CoM momentum halted. The

optimal strategies generated also suggested immediate unloading of the opposing foot for all values of c_{t_0}.

6.5.2 Effect of Support-Surface Perturbation

Addition of the support-surface perturbations to the lateral counterbalance model produced considerably different estimates of the FSR (**Figure 6.6**). These effects were most notable for the P_{peak} condition (initialized at $\dot{p}_x$ = 0.870 m/s) relative to S. At peak velocity of the platform, the upper boundary CoM velocities that defined the FSR were on average 17 cm larger at each initial CoM position when compared that of the S condition. Surprisngly, nearly no difference from the S condition were detected for the P_{mid} FSR boundaries.

6.5.3 Experimental Evaluations of Margin of Stability Variants

Applying the FSR output from simulated movements to evaluations of MoS during quiet standing further highlighted the significantly larger stable xCoM excursions capable with addition of a counterbalance mechanism as opposed to the assumption of IP-based mechanics (p < 0.001; **Table 6.3**). Of the ten subjects from which data were analysed, a total of six displayed some degree of the counterbalance strategy following a lateral perturbation (fBoS n = 6); reactive stepping was also observed in six subjects (ΔBoS n = 6). Note that two subjects executed both strategies; though for the ANOVAs performed in the current study, they were treated as independent cases. One of these two subjects was also identified as a substantial outlier within the ΔBoS group at event P_{peak}; thus, they were removed from the statistical analyses and the remaining sample for ΔBoS was n = 5.

Not surprisingly, a main effect of FSR used for MoS calculations was detected for all perturbation conditions (p < 0.001). Post-hoc testing revealed that for each main effect (conditions P1 and P2), all pairwise comparisons of margins were significant (p < 0.001) with the exception of the comparison between P_{mid} and S for the P2 condition (p = 0.503). Only in the P_{peak} condition was a main effect of postural strategy observed (p = 0.017); for all margins used, the MoS was significantly lower when reactive stepping was used. Interestingly, not accounting for the perturbation with the estimated FSR (S) yields largely negative MoS for both strategies.

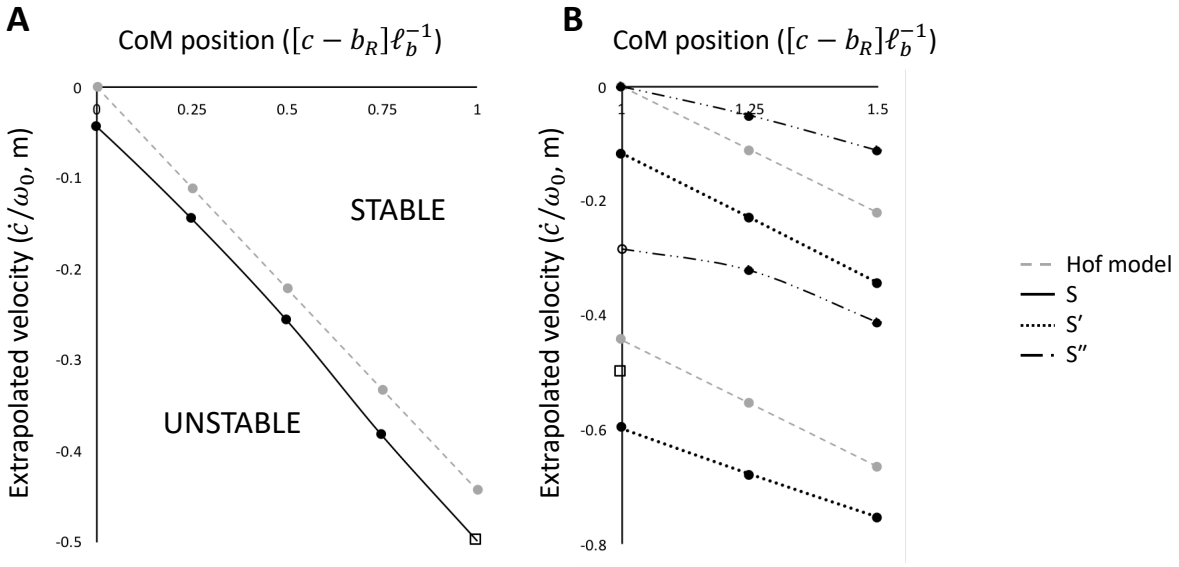

Figure 6.4 Lateral center of mass (CoM) phase-space showing the feasibility stability region (FSR); the maximum (upper boundary, more negative) and minimum (lower boundary) feasible velocities for a given model/task. The lower boundary is only calculated for positions of CoM equal to or greater than 1. Position of CoM with respect to the right base of support (BoS) boundary c_{t_0} was normalized to a standardized BoS width; extrapolated CoM velocity (rightward) was the spatial transform of CoM velocity proposed by Hof et al. (2005) via normalization to pendulum eigenfrequency. The tasks displayed are stance without a perturbation highlighting: (**A**) the FSR of our model for $0 \leq c_{t_0} \leq 1$ according to the predicted values from Hof et al. (2005) (*grey, dashed*) and the bilateral standing model simulated (S; *black, solid*). Stable and unstable regions within the displayed phase-space are shown with respect to the upper FSR boundary; (**B**) the FSR for $c_{t_0} \geq 1$ according to Hof again (*grey, dashed*), in addition to the unilateral stance model variants (S', *dotted*; S", *solid+dotted*). The open square on **A** and **B** highlight the piecewise nature of these velocity boundaries between prescribed model configurations despite equivalent values of c_{t_0}.

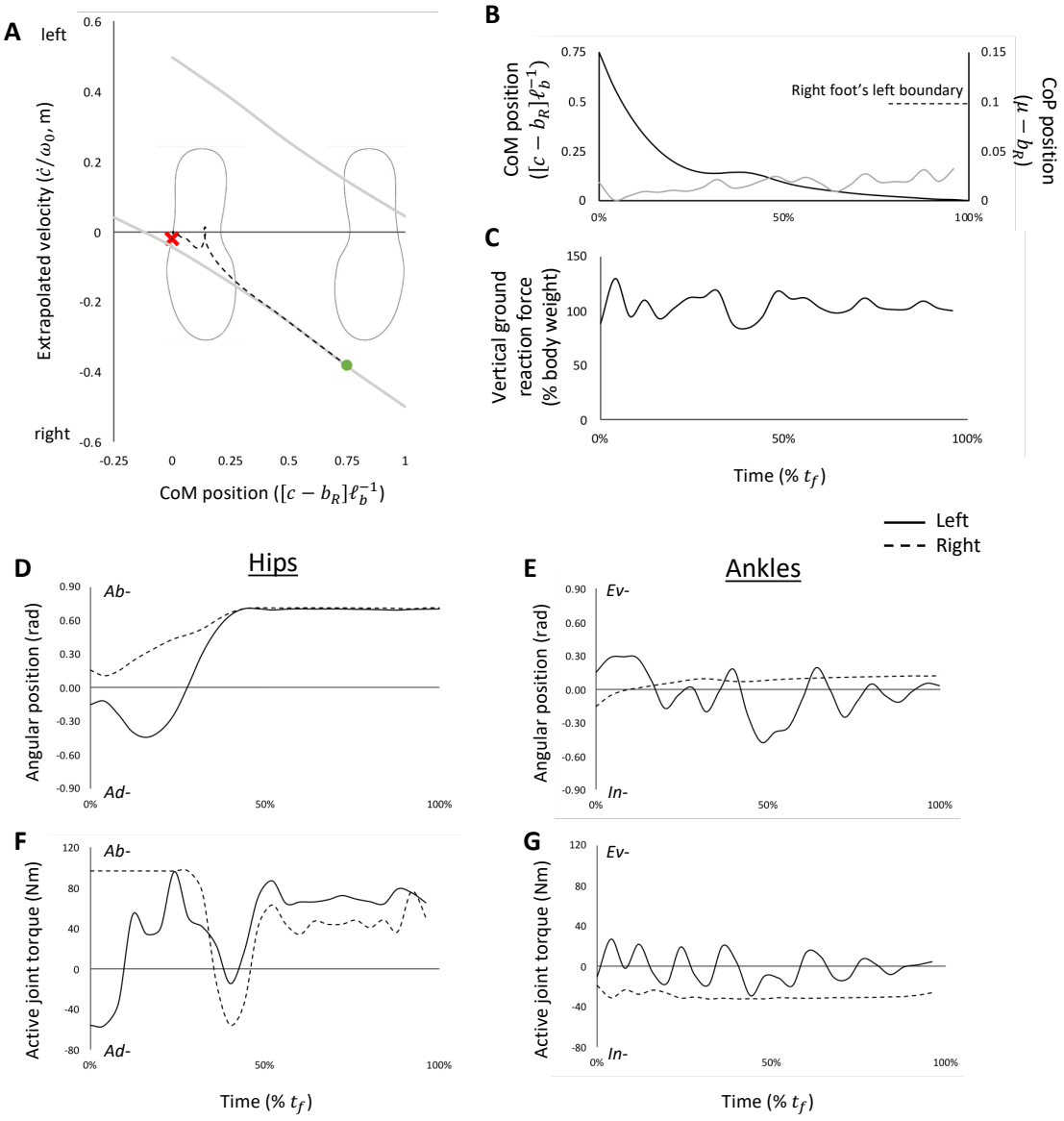

Figure 6.5 Representative data from a single simulation where no support-surface perturbation was used and lateral CoM position was initialized at 0.75. Discrete time series were normalized as a percent of total/final time of simulation t_f. (**A**) Phase-space navigation of the CoM during the balance recovery from start (*green circle*) to end (*red cross*). The feasible stability region (FSR) determined for the standing condition according to both rightward and leftward velocities are shown (*grey, solid*).(**B**) Time series CoM position (*black*; *left axis*), shown originally in A, and centre of pressure position (CoP; *grey*; *right axis*) under the right foot (i.e single support). (**C**) Vertical ground reaction force as a percent of body weight. Lastly, (**D**, **E**) angular positions (rad) of the right (*dashed*) and left (*solid*) hips and ankles in addition to (**F**, **G**) hip and ankle net joint moments (N·m) constructed through direct collocation.

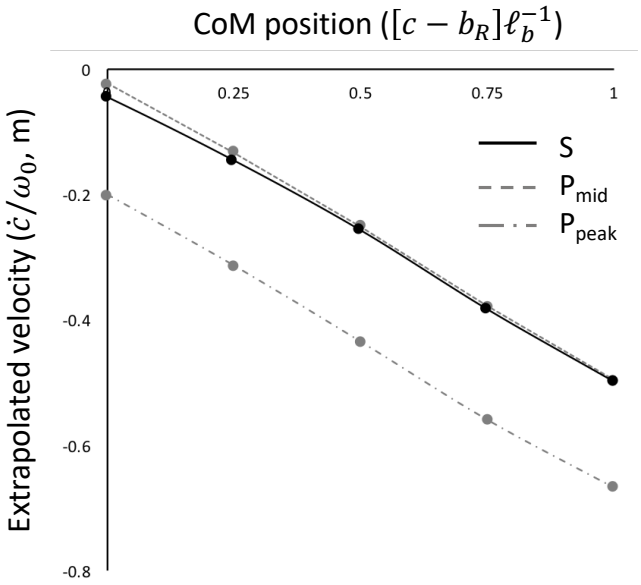

Figure 6.6 Lateral center of mass (CoM) phase-space showing the feasible stability regions (FSR) with and without addition of support-surface perturbations. Position of CoM with respect to the right base of support (BoS) boundary c_{t_0} was normalized to standardized BoS width; extrapolated CoM velocity (rightward) was the spatial transform of CoM velocity proposed by Hof et al. (2005) via normalization to pendulum eigenfrequency. Margins for conditions displayed include the Standing (S; no perturbation, *solid*), P_{mid} (*dashed*), and P_{peak} (*solid+dotted*) conditions. Perturbation conditions were initialized at different instances within the platform's acceleration waveform to highlight the temporal dependence of the FSR on active perturbations (see **Figure 6.2**).

Table 6.2 The feasible stability regions (FSR) for simulated lateral balance recovery. These negative values are the boundary rightward CoM velocities (i.e. initial velocities $\dot{c}_{t_0}$, relative to platform velocity) at each discrete, horizontal CoM position c_{t_0} (normalized to standardized base of support width) output from forward dynamics simulations for the tasks/postures specified. Note that velocities are presented as the extrapolated spatial variant initially proposed by Hof et al. (2005) in which the corresponding units are m.

		Initial CoM position (c_{t_0})						
Model/Task		0	0.25	0.50	0.75	1.00	1.25	1.50
Standing	S	-0.043	-0.144	-0.256	-0.382	-0.498	—	—
	S′	—	—	—	—	-0.284 /0	-0.322 /-0.050	-0.414 /-0.112
	S″	—	—	—	—	-0.597 /-0.117	-0.677 /-0.228	-0.752 /-0.342
Perturbation	P_{mid}	-0.023	-0.130	-0.250	-0.378	-0.497	—	—
	P_{peak}	-0.199	-0.312	-0.434	-0.558	-0.665	—	—

#/# notation indicates maximum/minimum feasible rightward velocities for $c_{t_0} \geq 1$
Note: body height for the model used was 1.80 m

Table 6.3 Evaluations (from experimental data) of the dynamic lateral margin of stability (MoS; cm) using the feasible stability regions defined by the Hof et al. (2005) model (Hof) and the the counterbalance model proposed in the current study with and without simultaneous perturbations (S, P_{mid}, P_{peak}). Values (mean ± SD) are presented for both quiet standing and perturbed conditions (i.e. at different instances of initial platform velocity, P1 and P2); the latter includes individuals who evoked a change in BoS (ΔBoS) or fixed BoS strategy (fBoS).

	Stability Margins			
Condition	Hof	S	P_{mid}	P_{peak}
Quiet Stance *	21.67 ± 0.55	25.09 ± 0.600	—	—
Perturbation (P1) *				
fBoS	3.55 ± 1.87	6.78 ± 1.88	5.92 ± 0.99	—
ΔBoS	2.39 ± 1.12	5.61 ± 1.12	5.32 ± 1.62	—
*Perturbation (*P2*)* *†				
fBoS	-14.27 ± 2.48	-10.71 ± 2.35	—	5.77 ± 2.54
ΔBoS	-17.74 ± 0.86	-14.05 ± 0.86	—	2.23 ± 0.86

* significant main effect of model, $p < 0.05$
† significant main effect of balance recovery strategy, $p < 0.05$

By isolating the FSR at P2, positive MoS was observed for all fBoS responses. Although a positive mean MoS was also observed for ΔBoS responses, only these responses yielded instances of a negative MoS. No significant interactions were observed between FSR and strategy ($p > 0.05$) once Greenhouse-Geisser corrections were applied for each grouping of data that violated the assumption of sphericity.

6.6 Discussion

The purpose of the current study was to numerically estimate the lateral xCoM positions (i.e. FSR) that yield a loss of balance when the mode of recovery is a lateral counterbalance strategy. Few works within the scientific literature have addressed this postural strategy and how it benefits whole-body CoM control within the strict framework of dynamic stability margins. Overall, our results indicate that the boundaries that define the dynamic MoS of this strategy are larger than those based on the IP model (Pai and Patton 1997; Hof et al. 2005). Furthermore, our results were in agreement with the current literature that dictates FSR boundaries are dependent on the temporal characteristics of a support-surface perturbation (Pai et al. 2000). These perturbations are used in many experimental paradigms to trigger balance recovery. As we hypothesized, the position within the time-domain of a perturbation waveform has a direct and quantifiable impact on the maximum, feasible (horizontal) velocities that can be corrected at any given initial CoM position. Using the P_{peak} FSR to calculate the MoS within experimental data produced the most viable approximations of stability relative to the other dynamic models/conditions examined.

As introduced prior, the dynamic stability margins (or FSR) were characterized using the definition common in the current literature (Pai and Patton 1997; Hof et al. 2005). Upon reaching unstable locations within the CoM phase-space (**Figure 6.5**), the CNS must revert to alternate mechanisms of postural control that may include expanding the BoS boundary(ies) in the direction of balance-loss. Our results further highlight the relative linearity of the S-based FSR suggesting replication of these boundaries may require only the addition of a constant to the Hof FSR. Since prior work using higher degree of freedom models has reported non-linear bounds (Iqbal and Pai 2000; Yang et al. 2007, 2008, 2009), it may be that the strict requirement

of the initial configuration to mimic double support within the current study attenuated any non-linearity. Rather, if all postures were free to assume a unilateral stance configuration, it may be that the FSR adopts a similar profile to other models. This notion of configuration is further reinforced by the mathematical irregularities we observed as piecewise components at extreme values of c_{t_0}, especially at the non-differentiable point $c_{t_0} = 1$. These observations suggest the following two factors: *i*) there is a strict reliance on the characterization of segment pose *with* CoM position in determination of stable regions; *ii*) the anatomy of frontal plane motion provides an additional layer of complexity regarding lateral fixed-BoS strategy stability when compared to its sagittal counterpart (Iqbal and Pai 2000). The first point may be of especial importance. If two different postures with similar CoM positioning yield two different boundaries of stability, it is then advantageous to identify optimal postures when training at-risk individuals to better avoid falling.

The FSR that define calculations of MoS within our model of lateral balance control differed largely from those suggested within the literature. Evidently from our comparisons, the approximations reported by the analytical methods of Hof et al. (2005) underestimate the dynamic stability margins that dictate whether it is possible to maintain a fixed BoS and not step at certain CoM states. The FSR for a multi-link system that may generate knee/hip strategies (i.e. counter-rotations) within the sagittal plane also underestimates these boundaries (Iqbal and Pai 2000). As limb unloading (passive or active) is not an intrinsic component of sagittal fixed-BoS posture, the CNS is limited in how it may control the CoM state. Differences from previous sagittal models and the potential for unique configurations of the whole-body then strengthen the need for specialized models of lateral balance control strategies. These strategies include execution of the counterbalance maneuver used within our model or a similar strategy the relies on lateral bend of the trunk (not included in the current study). It should be noted that analytical work has prior suggested the possibility for the CoM position to exceed physical BoS boundaries by approximately 4 cm when using a lateral counterbalance strategy (Otten 1999; Hof 2007). Our work effectively translates these prior disseminations into the FSR and validates them in relation to the CoM phase-plane. Though of greater novelty within the current study is the

coupling of balance recovery with a method of perturbation used within a true laboratory environment. This effectively improved the task-specificity of the FSR and evaluated MoS.

An interesting observation amongst our observations was the presence of non-zero velocities at $c_{t_0} = 0$ (i.e. when CoM was positioned over physical, right BoS boundary). This was likely due to the ability to rapidly translate the initial CoM position via abduction of the unloaded limb and is related to the results proposed by Hof et al. (2007). It's unclear whether altering the initial configuration such that the leg is already abducted (i.e. initialize in unilateral stance) would influence these observations; however, given the pose dependence of the adjusted MoS (**Figure 6.4B**), this is a likely outcome.

To our knowledge, only the work of Pai et al. (2000) has explicitly quantified the time dependence of the FSR or MoS on support-surface perturbations. However, no authors to our knowledge have constructed the FSR using the extrapolated velocity measure proposed by Hof et al. (2005) such that the MoS may be restructured for alternate postural tasks. Simulation-based approaches provide the benefit of isolating specific instances within the perturbation waveform to initialize balance recovery such that the capabilities of a system may be better understood. Our analyses, like Pai and colleagues, show the direct dependence of the FSR on not only the existence of an active perturbation, but the timing of the change of accelerations associated with the perturbation. It can then be stated that the perturbation acts as both a destabilizing and assistive mechanism; it is inherently a component of the postural strategy. Thus, researchers who utilize these variations of external perturbations should make considerations within either their analyses or interpretations of data. However, research defining a method for adjusting the xCoM or MoS according to perturbation characteristics has yet to be published.

Within our model, no explicit restrictions were placed on the initial transition from bilateral to unilateral stance; it was free to transition at any time interval. Despite this, DC yielded a response that immediately entered unilateral stance such that initialization of the simulations were similar to those that begin at lift-off during gait (Yang et al. 2007, 2008, 2009). This event has been acknowledged as an important marker of postural response success following slips in gait (You et al. 2001; Yang et al. 2008). In fact, in examining representative

data for fBoS and ΔBoS responses (**Figure 6.3C** top), it appears that larger separation of the xCoM trajectories occurs beyond peak perturbation velocity. In this scenario, it may be more beneficial to localize MoS to the event of foot lift-off; however, this would then require further exploration into the FSR at intervals within the perturbation waveform. Regardless, the reason behind the observed drive to initialize each simulation into single support may be the quality of our initial guess for trajectory optimization. A method of estimating controls and muscle activation based on computed muscle control may have yielded different results; although the use of the global search was intended to mitigate this possibility.

Previous studies estimating dynamic stability via CoM state have prioritized the direct shooting method of trajectory optimization (Yang et al. 2007, 2008, 2009). The current study highlighted the potential for DC as an efficient means of estimating the boundaries of the FSR for a given task which may be translated towards adapting the Hof et al. (2005) MoS. However, we cannot make any conclusions into the difference(s) between using direct shooting and DC for defining the FSR. Implementing a similar methodology as Porsa et al. (2016) may permit quantification of the differences according to computer processing times and the characteristics of the optimal solution. If it is true that DC is the more efficient direct method in terms of duration and yields similar solutions to shooting, it may encourage more researchers to then quantify the FSR across a greater number of dynamic tasks.

As within most studies and biomechanical models, there are limitations that require acknowledgement. Foremost, a more expansive data set across populations is necessary to validate the proposed margins within an experimental setting. This may prove difficult with the unpredictability of whether a person may elect to use the counterbalance strategy. Refinement of the model proposed within the current study may also be beneficial. More complex foot-floor interaction components (Bauby and Kuo 2000; Porsa et al. 2016), imposing a neural delay on muscle activation trajectories (Versteeg et al. 2016), or addition of separate trunk-pelvis segments are interesting possibilities. The latter has been acknowledged as difficult to develop with the current information in the literature (Versteeg et al. 2016). Transition to musculoskeletal modelling may also be an avenue that could provide enhanced estimates of the FSR; though one must be careful in adding complexity for the sake of it. It could be that a high complexity model

may propose greater computational challenges without adding any substantial changes to the original estimates of stability margins. Most interesting regarding the potential future directions of this current study is expansion of our model degrees of freedom to three-dimensions. The additional degrees of freedom would allow us to address coupling of sagittal and frontal plane balancing mechanisms that may be used by the CNS (e.g. flexion of the knee during counterbalancing).

6.7 Conclusion

In conclusion, the current study proposed a novel model of lateral balance control that could utilize the counterbalance strategy, an often-overlooked postural response in the literature. Using this model, we empirically determined the dynamic FSR that correspond to our model and integrated it with the the xCoM concept proposed by Hof et al. (2005) to propose estimates of the lateral MoS that better reflect the bounds of fixed-BoS lateral balance control. Following the lead of Pai and colleagues, the proposed FSR and MoS is a specialized approach to quantification of the state of dynamic stability for lateral fixed-BoS balance control that require multiple degrees of freedom (Pai and Patton 1997; Iqbal and Pai 2000; Yang et al. 2007, 2008, 2009). Additionally, this study highlighted the implicit dependence of the MoS on characteristic waveform of a support-surface perturbation (Pai et al. 2000). In general, these new applications of stability margins provide additional tools and knowledge for researchers concerned with the abilities of the CNS in prevention of falls, most importantly for high-risk populations that are typically associated with lateral instability.

6.8 Acknowledgments

The authors would like to acknowledge funding provided by a NSERC Discovery Grant (awarded to LAV), NSERC Canada Graduate Scholarship-Master's award (awarded to KAI), and Canadian Foundation for Innovation and Ontario Research Fund Research Infrastructure grants for equipment. The authors would also like to thank Dr. Scott Brandon for assistance during the development of the biomechanical model proposed and again extend appreciation to Dr. John Zettel for the use of the robotic platform.

Chapter 7. General Discussion

7.1 Overview of Results

Over the past decade, there has been an increase in the use of dynamic measures of stability in gait and posture research; these measures were heavily influenced by the original works by Patton and Pai (1997) and Hof et al. (2005). However, there remains numerous areas related to dynamic MoS calculations and balance recovery that require further insight. In this thesis, we took explicit interest in the influence of CoM estimates on stability metrics evaluated with experimental data and the efficacy of the Hof MoS for evaluations of evidently high degree of freedom postural strategies in the frontal plane. Thus, the general purpose of this dissertation was to supplement the current body of literature on the feasible stability regions (FSR) and reinforce the notion of a need for task-specific MoS calculations. Focus was placed primarily on the fixed-BoS strategies that do not utilize any change in the BoS boundary corresponding to the direction of balance-loss. Two studies that combined experimental data analyses and mathematical modelling were conducted to address this purpose; the following sections will outline the observations disseminated in addition to their contributions to the literature.

7.1.1 Accuracy of simplified CoM estimates are dependent on perturbation direction

Study 1 (Chapter *4*) was conducted to address the lacking information pertaining to simplifying the anthropometric model used to estimate xCoM kinematics for fixed-BoS balance control strategies. Prior research in dynamic stability has investigated reduced CoM models for only responses that require a change in the BoS (Tisserand et al. 2016b). Participants were exposed to multidirectional support-surface perturbations that would evoke fixed-BoS or change in BoS balance control strategies according to perturbation magnitude. For low magnitude perturbations that evoked fixed-BoS recovery, the dynamic MoS was calculated using the xCoM concept, introduced by Hof et al. (2005), at peak perturbation velocity. The results of this study demonstrated that the effects of simplification were heavily dependent on the plane of postural perturbation (**Table 4.3**, **Figure 4.2**). The largest influence of the CoM model variant used was

evident in the sagittal plane suggesting that, without making predictive corrections that account for excluded segments, at most the arm segments may be ignored in CoM estimates. However, frontal plane perturbations combined with the MoS within the equivalent plane reveal a greater lenience with simplified model variations; the pelvis CoM alone showed an impressive ability to estimate MoS of the whole-body anthropometric model. Use of the pelvis segment as an estimate of whole-body CoM has shown good fidelity for tasks such as gait (Yang and Pai 2014; Huntley et al. 2017b) though, like Tisserand et al. (2016b) suggested, it may not be a suitable option for balance recovery outside of locomotion. Ultimately, our results reinforce the context-dependence on the degree to which CoM estimates may be simplified. Though, researchers should still consider their definition of a functionally different outcome (Jamkrajang et al. 2017) as a consistent difference between model variations may be less than that considered "functional" despite being statistically significant. In the case of the results we presented, it is clear that the > 5 cm error observed for HTP and CoMp models would be considered functional. However, the smaller magnitudes of error observed for the simplified models within the frontal plane are not as definitive. It may that a clinical researcher would be wearier of those small errors if they present the risk of losing sensitivity of the measure; though this was not of focus within study 1. However, Hahn and Chou (2003) examined a similar research question using over-ground walking and reported a reduced ability to discern older adults with diagnosed balance disorders from healthy older adults when using single segments to estimate whole-body CoM. With that said, further experiments are then needed to better identify the relationship between the detection of poor balance control and the errors in dynamic MoS we observed for healthy, young adult balance recovery.

In general, the results of Study 1 provide information for many researchers who may wish to reduce the complexity of their whole-body analysis to benefit their participants through reduced setup times (important for certain populations e.g. older adults, clinical) or minimize the time of analyses such that a greater quantity of data may be collected. Many researchers have already made use of simplified estimates within their analyses (Kubo and Ulrich 2006; Worden and Vallis 2016). It should also be noted that the fixed-BoS responses observed following the lower perturbations utilized relatively few degrees of freedom emulating the IP model visually.

However, the fixed-BoS responses we observed unexpectedly following the larger perturbations clearly demonstrated segmental rotations that violated the IP mechanics. Additionally, calculations of the anteroposterior MoS following sagittal perturbations yielded negative values suggesting an unstable IP. However, we were not able to then clarify the state of stability for the higher-complexity motor control strategies that were being executed while still maintaining a fixed BoS. These anecdotal observations led us to question how to apply the dynamic MoS accurately for higher-complexity control strategies.

7.1.2 Lateral counterbalance strategy expands the feasible stability region

In the literature, the changes in FSR associated with counterbalance mechanisms are poorly understood. Previous work has addressed only those responses in the sagittal plane not considering the unique properties of limb unloading during frontal plane postural sway (Iqbal and Pai 2000). Thus, we proposed a biomechanical model that expanded the degrees of freedom of a typical IP model such that the lateral counterbalance was a valid mode of balance recovery. Using a similar methodology as (Yang et al. 2007, 2008, 2009) but supplementing DC for the direct shooting method of trajectory optimization, the maximal (upper boundary) and minimal (lower boundary) initial rightward velocities were determined for maintaining upright balance at a series of initial CoM positions. These velocities established the boundaries of the FSR for the xCoM.

The results of study 2 (Chapter 6) revealed that the counterbalance strategy expands the boundaries of the FSR for lateral balance (**Figure 6.5**) beyond those proposed for the ankle strategy (Hof et al. 2005) and hip strategy in the sagittal plane (Iqbal and Pai 2000). However, these boundaries were in agreement the limited work that has attempted to identify the capabilities of lateral balance control (Otten et al. 1999; Hof et al. 2007). Applications of the adjusted MoS metric proposed in Study 2 to the experimental data collected in Study 1 highlighted how much greater the hypothetical MoS is for lateral stability during quiet standing (i.e. 116 % greater; **Table 6.3**). Thus, applying the MoS proposed by Hof et al. (2005) in which stable dynamics are constrained to the length of the BoS underestimate the predicted feasible CoM states in lateral standing balance.

7.1.3 Margin of stability calculations are dependent on future states of platform perturbations

Previous simulation-based studies have incorporated perturbations to investigate how the CNS may prioritize certain fixed-BoS control strategies (Kuo 1995, 2005; Pai and Iqbal 1999; Pai et al. 2000; Versteeg et al. 2016). The work by Pai et al. (2000) in particular, examined the strict relationship between perturbation waveform and FSR. The importance of the forced changes in acceleration of the platforms reference frame have been discussed by previous authors concerned with balance control (Maki and McIlroy 2005; Egerton et al. 2011). Thus, to further condense the application of the adjusted MoS proposed to our laboratory environment, which uses support-surface perturbations to evoke balance recovery, we adopted a similar paradigm as Pai et al. (2000) and determined how the FSR change depending on the location within the perturbation waveform (time-series). A reminder that the dynamic MoS is effectively defined in the current thesis as the position of the xCoM with respect to the FSR boundaries. By targeting the peak perturbation velocity event P2 and the half-peak velocity event P1 during the acceleration phase, we were able to highlight that changes in the upper boundary of the FSR were linked to the waveform; e.g., the highest feasible velocities occurred at the peak event. Surprisingly, the event P1 detailed a similar FSR to no perturbation simulations. This suggests that, despite the initial duration of accelerations that should destabilize the individual, the following deceleration phase manages to return the boundaries towards values equivalent to a no perturbation scenario. Given the intent of Pai et al. (2000) was only to predict stepping reactions, exact bounds of the FSR according to perturbation were not disseminated. This made it difficult to ascertain whether results between studies were equivalent. It can be hypothesized however that differences would be the product of the model parameters used and the fact that both models acted in different planes with different degrees of freedom. Thus, further testing is required to tease the effects of perturbation characteristics on the FSR with finer detail.

An interesting point of observation within our data set was the consistency of control strategy evocation. Most participants would make use of either a strict counterbalance strategy or a variation of reactive stepping; the type of reactive stepping was typically consistent within

subjects (e.g. used only a lateral side-step). Surprisingly, one participant used distinctly different balance recovery strategies following each exposure to the leftward perturbations. From a dynamic systems theory standpoint, participants who consistently used a single strategy may have theoretically converged upon a sufficient attractor state (Thelen 2000). Given then that multiple strategies could be used with success, this suggests the existence of multiple attractor states within the framework of this lateral perturbation task despite a controlled magnitude. The participant who did not use a consistent strategy can then be assumed to having not converged upon a *single* feasible solution (state). Rather, they have used multiple different solutions that are all feasible or successful (though not necessarily optimal) suggesting they either have multiple attractor states or are potentially searching for a state. Similarities may be drawn to a child who is still developing stable motor patterns and showing large variability when repeating a task (Hinton and Vallis 2016)

7.2 Future Directions and General Limitations

From the results of Study 1, we believe it necessary to reinforce that the results disseminated should be applied only for the fixed-BoS responses similar to those we observed (i.e. primarily ankle strategies). Addressing more complex strategies as discussed in Study 2 in addition to those that require a change in BoS within multiple planes require further investigations. Given the multitudes of whole-body anthropometric models that exist (Catena et al. 2017) in addition to proposed, simplified models designed to target whole-body CoM estimates during specific tasks (Yang and Pai 2014; Tisserand et al. 2016b), future directions should also concern examining existing CoM variations under a similar experimental scheme. Lastly, to reinforce the idea of task-specific metrics, we believe that developing simplified CoM estimates based solely upon the mechanics of a task (e.g. a double-inverted pendulum during balance recovery) are a potential step in balancing fidelity of outcomes with data collection time(s). Such metrics may function similar to a vector offset to a pelvis local coordinate system (Yang and Pai 2014) or a series of critical anatomical landmarks that generate accurate estimates (Hahn and Chou 2003).

Regarding our model of lateral balance control using counterbalancing, there were four specific areas of change or refinement that could be addressed in the future. Model parameters

such as properties of the torsional springs/dampers used in addition to the initial foot position are of interest. Evidence has shown that there is a direct relationship between stability in the frontal plane and stance width as less muscular effort is required to minimize CoM displacements with a wider BoS (Bingham et al. 2011). Foot contact within the model and simulations may better produce a transition from bilateral to unilateral stance. It may be that adopting a foot-roll component (Bauby and Kuo 2000) with addition of ample Coulomb damping (friction) between the foot and surface may better replicate the postural control strategy(ies) in question. In a similar vein, additional degrees of freedom such as separate trunk-pelvis links in addition to freedom to rotate within a three-dimensional environment could assist in yielding estimates of FSR with greater accuracy in relation to the capabilities of the musculoskeletal system. Furthermore, validation of these FSR within a larger and more expansive data set that addresses multiple populations would be an ideal scenario. Greater exposures to each condition may also then yield the attractor state that each individual adopts for the large magnitude, lateral perturbation task used in this dissertation. From a motor learning perspective, it may then be possible to observe how individuals navigate the CoM phase-space to arrive at a given attractor (e.g. utilizing a series of potential FSR). However, from a purely application-based approach, a more consistent response would provide a better means of experimentally validating many of these modelled FSR's, especially in the case of a strategy used as variably between individuals as the counterbalance strategy.

Chapter 8. References

Addison O, Inacio M, Bair W-N, et al (2017) Role of Hip Abductor Muscle Composition and Torque in Protective Stepping for Lateral Balance Recovery in Older Adults. Arch Phys Med Rehabil 98:1223–1228. doi: 10.1016/j.apmr.2016.10.009

Aimola E, Santello M, La Grua G, Casabona A (2011) Anticipatory postural adjustments in reach-to-grasp: effect of object mass predictability. Neurosci Lett 502:84–88. doi: 10.1016/j.neulet.2011.07.027

Ali F, Menzinger M (1999) On the local stability of limit cycles. Chaos 9:348–356. doi: 10.1063/1.166412

Anderson FC, Pandy MG (2001) Dynamic optimization of human walking. J Biomech Eng 123:381–390

Armstrong C, Swarbrick CM, Pye SR, O'Neill TW (2005) Occurrence and risk factors for falls in rheumatoid arthritis. Ann Rheum Dis 64:1602–1604. doi: 10.1136/ard.2004.031195

Asada H, Leonard J (2005) 2.12 Introduction to Robotics. Massachusetts Institute of Technology: MIT OpenCourseWare

Bair W-N, Prettyman MG, Beamer BA, Rogers MW (2016) Kinematic and behavioral analyses of protective stepping strategies and risk for falls among community living older adults. Clin Biomech (Bristol, Avon) 36:74–82. doi: 10.1016/j.clinbiomech.2016.04.015

Bauby CE, Kuo AD (2000) Active control of lateral balance in human walking. J Biomech 33:1433–1440

Beaudette SM, Graham RB, Brown SHM (2014) The effect of unstable loading versus unstable support conditions on spine rotational stiffness and spine stability during repetitive lifting. J Biomech 47:491–496. doi: 10.1016/j.jbiomech.2013.10.055

Bernstein NA (1967) The co-ordination and regulation of movements. London: Pergamon Press

Betts JT (2010) Practical Methods for Optimal Control and Estimation Using Nonlinear Programming, Second. Society for Industrial and Applied Mathematics

Bhatt T, Wang T-Y, Yang F, Pai Y-C (2013) Adaptation and generalization to opposing perturbations in walking. Neuroscience 246:435–450. doi: 10.1016/j.neuroscience.2013.04.013

Bhatt T, Wening JD, Pai Y-C (2006) Adaptive control of gait stability in reducing slip-related backward loss of balance. Exp Brain Res 170:61–73

Bierbaum S, Peper A, Arampatzis A (2013) Exercise of mechanisms of dynamic stability improves the stability state after an unexpected gait perturbation in elderly. AGE 35:1905–1915. doi: 10.1007/s11357-012-9481-z

Bingham JT, Choi JT, Ting LH (2011) Stability in a frontal plane model of balance requires coupled changes to postural configuration and neural feedback control. J Neurophysiol 106:437–448. doi: 10.1152/jn.00010.2011

Bishop MD, Brunt D, Kukulka C, et al (2003) Braking impulse and muscle activation during unplanned gait termination in human subjects with parkinsonism. Neurosci Lett 348:89–92

Boone DC, Azen SP (1979) Normal range of motion of joints in male subjects. J Bone Joint Surg Am 61:756–759

Bradley E, Kantz H (2015) Nonlinear time-series analysis revisited. Chaos: An Interdisciplinary Journal of Nonlinear Science 25:097610. doi: 10.1063/1.4917289

Brunt D, Andersen JC, Huntsman B, et al (1992) Postural responses to lateral perturbation in healthy subjects and ankle sprain patients. Med Sci Sports Exerc 24:171–176

Caderby T, Yiou E, Peyrot N, et al (2017) Effects of Changing Body Weight Distribution on Mediolateral Stability Control during Gait Initiation. Front Hum Neurosci 11:127

Casadio M, Morasso PG, Sanguineti V (2005) Direct measurement of ankle stiffness during quiet standing: implications for control modelling and clinical application. Gait Posture 21:410–424. doi: 10.1016/j.gaitpost.2004.05.005

Catena RD, Chen S-H, Chou L-S (2017) Does the anthropometric model influence whole-body center of mass calculations in gait? Journal of Biomechanics 59:23–28. doi: 10.1016/j.jbiomech.2017.05.007

CIHI (2010) Series on Seniors: Seniors and Falls

Cinelli M, Patla A, Stuart B (2008) Age-related differences during a gaze reorientation task while standing or walking on a treadmill. Exp Brain Res 185:157–164. doi: 10.1007/s00221-007-1266-8

Cummings SR, Melton LJ (2002) Epidemiology and outcomes of osteoporotic fractures. Lancet 359:1761–1767. doi: 10.1016/S0140-6736(02)08657-9

De Groote F, Kinney AL, Rao AV, Fregly BJ (2016) Evaluation of Direct Collocation Optimal Control Problem Formulations for Solving the Muscle Redundancy Problem. Ann Biomed Eng 44:2922–2936. doi: 10.1007/s10439-016-1591-9

Delabastita T, Desloovere K, Meyns P (2016) Restricted Arm Swing Affects Gait Stability and Increased Walking Speed Alters Trunk Movements in Children with Cerebral Palsy. Front Hum Neurosci 10:354

Dempster WT (1955) THE ANTHROPOMETRY OF BODY ACTION. Annals of the New York Academy of Sciences 63:559–585. doi: 10.1111/j.1749-6632.1955.tb32112.x

Diener HC, Horak FB, Nashner LM (1988) Influence of stimulus parameters on human postural responses. J Neurophysiol 59:1888–1905. doi: 10.1152/jn.1988.59.6.1888

Dingwell JB, Cusumano JP, Cavanagh PR, Sternad D (2001) Local dynamic stability versus kinematic variability of continuous overground and treadmill walking. J Biomech Eng 123:27–32

Dingwell JB, Kang HG (2007) Differences between local and orbital dynamic stability during human walking. J Biomech Eng 129:586–593. doi: 10.1115/1.2746383

Do MC, Breniere Y, Brenguier P (1982) A biomechanical study of balance recovery during the fall forward. J Biomech 15:933–939

Egerton T, Brauer SG, Cresswell AG (2011) Changes in stepping response to lateral perturbations immediately following a single bout of physical activity. Physiother Res Int 16:141–150. doi: 10.1002/pri.490

Farley CT, Morgenroth DC (1999) Leg stiffness primarily depends on ankle stiffness during human hopping. Journal of Biomechanics 32:267–273. doi: 10.1016/S0021-9290(98)00170-5

Federolf P, Roos L, Nigg BM (2013) Analysis of the multi-segmental postural movement strategies utilized in bipedal, tandem and one-leg stance as quantified by a principal component decomposition of marker coordinates. J Biomech 46:2626–2633. doi: 10.1016/j.jbiomech.2013.08.008

Flores P (2015) A New Approach to Eliminate the Constraints Violation at the Position and Velocity Levels in Constrained Mechanical Multibody Systems. In: Flores P, Viadero F (eds) New Trends in Mechanism and Machine Science. Springer International Publishing, Cham, pp 385–393

Fujimoto M, Bair W-N, Rogers MW (2017) Single and multiple step balance recovery responses can be different at first step lift-off following lateral waist-pull perturbations in older adults. J Biomech 55:41–47. doi: 10.1016/j.jbiomech.2017.02.014

Fujimoto M, Bair W-N, Rogers MW (2015) Center of pressure control for balance maintenance during lateral waist-pull perturbations in older adults. J Biomech 48:963–968. doi: 10.1016/j.jbiomech.2015.02.012

Gage WH, Winter DA, Frank JS, Adkin AL (2004) Kinematic and kinetic validity of the inverted pendulum model in quiet standing. Gait Posture 19:124–132. doi: 10.1016/S0966-6362(03)00037-7

Gittoes MJR, Kerwin DG (2006) Component inertia modeling of segmental wobbling and rigid masses. J Appl Biomech 22:148–154

Hahn ME, Chou LS (2003) Can motion of individual body segments identify dynamic instability in the elderly? Clin Biomech (Bristol, Avon) 18:737–744

Hasson CJ, Van Emmerik REA, Caldwell GE (2008) Predicting dynamic postural instability using center of mass time-to-contact information. J Biomech 41:2121–2129

Havens KL, Mukherjee T, Finley JM (2018) Analysis of biases in dynamic margins of stability introduced by the use of simplified center of mass estimates during walking and turning. Gait & Posture 59:162–167. doi: 10.1016/j.gaitpost.2017.10.002

Hinton DC, Vallis LA (2016) Children Age 7 Complete Complex Gait and Postural Tasks Differently Than Adults Under Dual-Task Conditions. J Mot Behav 48:193–204. doi: 10.1080/00222895.2015.1072494

Hof AL (2007) The equations of motion for a standing human reveal three mechanisms for balance. J Biomech 40:451–457

Hof AL, Curtze C (2016) A stricter condition for standing balance after unexpected perturbations. J Biomech 49:580–585. doi: 10.1016/j.jbiomech.2016.01.021

Hof AL, Gazendam MGJ, Sinke WE (2005) The condition for dynamic stability. J Biomech 38:1–8

Hof AL, Vermerris SM, Gjaltema WA (2010) Balance responses to lateral perturbations in human treadmill walking. Journal of Experimental Biology 213:2655–2664. doi: 10.1242/jeb.042572

Horak FB, Nashner LM (1986) Central programming of postural movements: adaptation to altered support-surface configurations. J Neurophysiol 55:1369–1381

Hoshiyama M, Watanabe S, Kaneoke Y, et al (1993) Effect of optokinetic stimulation on human balance recovery in unexpected forward fall. Neurosci Res 18:121–127

Hsiao ET, Robinovitch SN (1998) Common protective movements govern unexpected falls from standing height. J Biomech 31:1–9

Huntley AH, Inkol KA, Vallis LA (2017a) Slip and Trip Perturbations During an Object Transport Task Requiring a Lateral Change in Support. J Mot Behav 1–9

Huntley AH, Schinkel-Ivy A, Aqui A, Mansfield A (2017b) Validation of simplified centre of mass models during gait in individuals with chronic stroke. Clinical Biomechanics 48:97–102. doi: 10.1016/j.clinbiomech.2017.07.015

Huntley AH, Zettel JL, Vallis LA (2017c) Older adults exhibit altered motor coordination during an upper limb object transport task requiring a lateral change in support. Hum Mov Sci 52:133–142. doi: 10.1016/j.humov.2017.01.014

Hurt CP, Rosenblatt NJ, Grabiner MD (2011) Form of the compensatory stepping response to repeated laterally directed postural disturbances. Exp Brain Res 214:557–566. doi: 10.1007/s00221-011-2854-1

Inkol KA, Huntley AH, Vallis LA (2018a) Do perturbation-evoked responses result in higher reaction time costs depending on the direction and magnitude of perturbation? Exp Brain Res 236:1689–1698. doi: 10.1007/s00221-018-5249-8

Inkol KA, Huntley AH, Vallis LA (2018b) Repeated Exposure to Forward Support-Surface Perturbation During Overground Walking Alters Upper-Body Kinematics and Step Parameters. Journal of Motor Behavior 1–13. doi: 10.1080/00222895.2018.1474336

Iqbal K, Pai Y (2000) Predicted region of stability for balance recovery: motion at the knee joint can improve termination of forward movement. J Biomech 33:1619–1627

Jamkrajang P, Robinson MA, Limroongreungrat W, Vanrenterghem J (2017) Can segmental model reductions quantify whole-body balance accurately during dynamic activities? Gait Posture 56:37–41. doi: 10.1016/j.gaitpost.2017.04.036

Jeong BY (1991) Respiration effect on standing balance. Arch Phys Med Rehabil 72:642–645

Karatsolis K, Nikolopoulos CS, Papadopoulos ES, et al (2009) Eversion and inversion muscle group peak torque in hyperpronated and normal individuals. The Foot 19:29–35. doi: 10.1016/j.foot.2008.06.006

Kubo M, Ulrich B (2006) Coordination of pelvis-HAT (head, arms and trunk) in anterior-posterior and medio-lateral directions during treadmill gait in preadolescents with/without Down syndrome. Gait Posture 23:512–518

Kuo AD (1995) An optimal control model for analyzing human postural balance. IEEE Trans Biomed Eng 42:87–101

Kuo AD (2005) An optimal state estimation model of sensory integration in human postural balance. J Neural Eng 2:S235-249. doi: 10.1088/1741-2560/2/3/S07

Lord SR, Rogers MW, Howland A, Fitzpatrick R (1999) Lateral stability, sensorimotor function and falls in older people. J Am Geriatr Soc 47:1077–1081

Lugade V, Lin V, Chou L-S (2011) Center of mass and base of support interaction during gait. Gait Posture 33:406–411. doi: 10.1016/j.gaitpost.2010.12.013

Maki BE, Edmondstone MA, McIlroy WE (2000) Age-related differences in laterally directed compensatory stepping behavior. J Gerontol A Biol Sci Med Sci 55:M270-277

Maki BE, McIlroy WE (2007) Cognitive demands and cortical control of human balance-recovery reactions. Journal of Neural Transmission 114:1279–1296. doi: 10.1007/s00702-007-0764-y

Maki BE, McIlroy WE (1997) The role of limb movements in maintaining upright stance: the "change-in-support" strategy. Phys Ther 77:488–507

Maki BE, McIlroy WE (2005) Change-in-support balance reactions in older persons: an emerging research area of clinical importance. Neurol Clin 23:751–783, vi–vii. doi: 10.1016/j.ncl.2005.01.002

Maki BE, McIlroy WE, Perry SD (1996) Influence of lateral destabilization on compensatory stepping responses. J Biomech 29:343–353

Marigold DS, Bethune AJ, Patla AE (2003) Role of the unperturbed limb and arms in the reactive recovery response to an unexpected slip during locomotion. J Neurophysiol 89:1727–1737

Martelli D, Vashsita V, Micera S, Agrawal SK (2015) Locomotor adaptations following repeated waist-pull perturbations. IEEE, pp 636–641

Masani K, Popovic MR, Nakazawa K, et al (2003) Importance of body sway velocity information in controlling ankle extensor activities during quiet stance. J Neurophysiol 90:3774–3782. doi: 10.1152/jn.00730.2002

McGrath M, Howard D, Baker R (2017) A Lagrange-based generalised formulation for the equations of motion of simple walking models. J Biomech 55:139–143. doi: 10.1016/j.jbiomech.2017.02.013

Micheau P, Kron A, Bourassa P (2003) Evaluation of the lambda model for human postural control during ankle strategy. Biol Cybern 89:227–236. doi: 10.1007/s00422-003-0412-z

Mildren RL, Zaback M, Adkin AL, et al (2018) Learning to balance on a slackline: Development of coordinated multi-joint synergies. Scandinavian Journal of Medicine & Science in Sports. doi: 10.1111/sms.13208

Miljkovic N, Lim J-Y, Miljkovic I, Frontera WR (2015) Aging of skeletal muscle fibers. Ann Rehabil Med 39:155–162. doi: 10.5535/arm.2015.39.2.155

Millard M, McPhee J, Kubica E (2012) Foot Placement and Balance in 3D. Journal of Computational and Nonlinear Dynamics 7:021015. doi: 10.1115/1.4005462

Millard M, Wight D, McPhee J, et al (2009) Human foot placement and balance in the sagittal plane. J Biomech Eng 131:121001. doi: 10.1115/1.4000193

Mille M-L, Johnson ME, Martinez KM, Rogers MW (2005) Age-dependent differences in lateral balance recovery through protective stepping. Clin Biomech (Bristol, Avon) 20:607–616. doi: 10.1016/j.clinbiomech.2005.03.004

Morasso PG, Sanguineti V (2002) Ankle muscle stiffness alone cannot stabilize balance during quiet standing. J Neurophysiol 88:2157–2162. doi: 10.1152/jn.2002.88.4.2157

Moyer BE, Redfern MS, Cham R (2009) Biomechanics of trailing leg response to slipping - evidence of interlimb and intralimb coordination. Gait Posture 29:565–570. doi: 10.1016/j.gaitpost.2008.12.012

Nashner LM, Shupert CL, Horak FB, Black FO (1989) Organization of posture controls: an analysis of sensory and mechanical constraints. Prog Brain Res 80:411–418; discussion 395-397

Nishihori T, Aoki M, Jiang Y, et al (2012) Effects of aging on lateral stability in quiet stance. Aging Clin Exp Res 24:162–170. doi: 10.3275/7626

Norrie RG, Maki BE, Staines WR, McIlroy WE (2002) The time course of attention shifts following perturbation of upright stance. Experimental Brain Research 146:315–321

O'Connor SM, Xu HZ, Kuo AD (2012) Energetic cost of walking with increased step variability. Gait Posture 36:102–107. doi: 10.1016/j.gaitpost.2012.01.014

Otten E (1999) Balancing on a narrow ridge: biomechanics and control. Philosophical Transactions of the Royal Society B: Biological Sciences 354:869–875. doi: 10.1098/rstb.1999.0439

Pai YC, Iqbal K (1999) Simulated movement termination for balance recovery: can movement strategies be sought to maintain stability in the presence of slipping or forced sliding? J Biomech 32:779–786

Pai YC, Maki BE, Iqbal K, et al (2000) Thresholds for step initiation induced by support-surface translation: a dynamic center-of-mass model provides much better prediction than a static model. J Biomech 33:387–392

Pai YC, Patton J (1997) Center of mass velocity-position predictions for balance control. J Biomech 30:347–354

Pai YC, Rogers MW, Patton J, et al (1998) Static versus dynamic predictions of protective stepping following waist-pull perturbations in young and older adults. J Biomech 31:1111–1118

Pandy MG, Anderson FC, Hull DG (1992) A parameter optimization approach for the optimal control of large-scale musculoskeletal systems. J Biomech Eng 114:450–460

Papadimitropoulos EA, Coyte PC, Josse RG, Greenwood CE (1997) Current and projected rates of hip fracture in Canada. CMAJ 157:1357–1363

Patton JL, Pai Y, Lee WA (1999) Evaluation of a model that determines the stability limits of dynamic balance. Gait Posture 9:38–49

Pearsall DJ, Reid JG, Ross R (1994) Inertial properties of the human trunk of males determined from magnetic resonance imaging. Ann Biomed Eng 22:692–706

Peebles AT, Reinholdt A, Bruetsch AP, et al (2016) Dynamic margin of stability during gait is altered in persons with multiple sclerosis. J Biomech 49:3949–3955

Perry SD, Santos LC, Patla AE (2001) Contribution of vision and cutaneous sensation to the control of centre of mass (COM) during gait termination. Brain Res 913:27–34

Peterka RJ (2003) Simplifying the complexities of maintaining balance. IEEE Engineering in Medicine and Biology Magazine 22:63–68. doi: 10.1109/MEMB.2003.1195698

Peterson CL, Kautz SA, Neptune RR (2011) Braking and propulsive impulses increase with speed during accelerated and decelerated walking. Gait Posture 33:562–567. doi: 10.1016/j.gaitpost.2011.01.010

Peterson DS, Dijkstra BW, Horak FB (2016) Postural motor learning in people with Parkinson's disease. J Neurol 263:1518–1529

Porsa S, Lin Y-C, Pandy MG (2016) Direct Methods for Predicting Movement Biomechanics Based Upon Optimal Control Theory with Implementation in OpenSim. Annals of Biomedical Engineering 44:2542–2557. doi: 10.1007/s10439-015-1538-6

Rietdyk S (1999) Postural responses to unexpected multidirectional upper body perturbations. PhD Thesis, University of Waterloo

Rietdyk S, Patla A., Winter D., et al (1999) Balance recovery from medio-lateral perturbations of the upper body during standing. Journal of Biomechanics 32:1149–1158

Rogers MW, Hain TC, Hanke TA, Janssen I (1996) Stimulus parameters and inertial load: effects on the incidence of protective stepping responses in healthy human subjects. Arch Phys Med Rehabil 77:363–368

Rogers MW, Mille M-L (2003) Lateral stability and falls in older people. Exerc Sport Sci Rev 31:182–187

Rosenblatt NJ, Grabiner MD (2010) Measures of frontal plane stability during treadmill and overground walking. Gait Posture 31:380–384. doi: 10.1016/j.gaitpost.2010.01.002

Sivakumaran S, Schinkel-Ivy A, Masani K, Mansfield A (2018) Relationship between margin of stability and deviations in spatiotemporal gait features in healthy young adults. Hum Mov Sci 57:366–373. doi: 10.1016/j.humov.2017.09.014

Stanmore EK, Oldham J, Skelton DA, et al (2013) Risk factors for falls in adults with rheumatoid arthritis: a prospective study. Arthritis Care Res (Hoboken) 65:1251–1258. doi: 10.1002/acr.21987

Statistics Canada (2010) Canada year book. Statistics Canada., Ottawa, Ont.

Sugimoto D, Mattacola CG, Mullineaux DR, et al (2014) Comparison of Isokinetic Hip Abduction and Adduction Peak Torques and Ratio Between Sexes: Clinical Journal of Sport Medicine 24:422–428. doi: 10.1097/JSM.0000000000000059

Suzuki Y, Nomura T, Casadio M, Morasso P (2012) Intermittent control with ankle, hip, and mixed strategies during quiet standing: a theoretical proposal based on a double inverted pendulum model. J Theor Biol 310:55–79. doi: 10.1016/j.jtbi.2012.06.019

Tang PF, Woollacott MH (1998) Inefficient postural responses to unexpected slips during walking in older adults. J Gerontol A Biol Sci Med Sci 53:M471-480

Thelen E (2000) Motor development as foundation and future of developmental psychology. International Journal of Behavioral Development 24:385–397. doi: 10.1080/016502500750037937

Tisserand R, Robert T, Chabaud P, et al (2016a) Elderly Fallers Enhance Dynamic Stability Through Anticipatory Postural Adjustments during a Choice Stepping Reaction Time. Front Hum Neurosci 10:613

Tisserand R, Robert T, Dumas R, Chèze L (2016b) A simplified marker set to define the center of mass for stability analysis in dynamic situations. Gait & Posture 48:64–67. doi: 10.1016/j.gaitpost.2016.04.032

van der Kooij H, Jacobs R, Koopman B, van der Helm F (2001) An adaptive model of sensory integration in a dynamic environment applied to human stance control. Biol Cybern 84:103–115. doi: 10.1007/s004220000196

van Meulen FB, Weenk D, Buurke JH, et al (2016) Ambulatory assessment of walking balance after stroke using instrumented shoes. Journal of NeuroEngineering and Rehabilitation 13:

Versteeg CS, Ting LH, Allen JL (2016) Hip and ankle responses for reactive balance emerge from varying priorities to reduce effort and kinematic excursion: A simulation study. J Biomech 49:3230–3237. doi: 10.1016/j.jbiomech.2016.08.007

Ward SR, Eng CM, Smallwood LH, Lieber RL (2009) Are current measurements of lower extremity muscle architecture accurate? Clin Orthop Relat Res 467:1074–1082. doi: 10.1007/s11999-008-0594-8

Welch TDJ, Ting LH (2014) Mechanisms of Motor Adaptation in Reactive Balance Control. PLoS ONE 9:e96440. doi: 10.1371/journal.pone.0096440

Winter D (1995) Human balance and posture control during standing and walking. Gait & Posture 3:193–214. doi: 10.1016/0966-6362(96)82849-9

Winter DA (2009) Biomechanics and motor control of human movement, 4th ed. Wiley, Hoboken, N.J

Winter DA, Patla AE, Prince F, et al (1998) Stiffness control of balance in quiet standing. J Neurophysiol 80:1211–1221

Winter DA, Patla AE, Rietdyk S, Ishac MG (2001) Ankle muscle stiffness in the control of balance during quiet standing. J Neurophysiol 85:2630–2633. doi: 10.1152/jn.2001.85.6.2630

Worden TA, Beaudette SM, Brown SHM, Vallis LA (2016) Estimating Gait Stability: Asymmetrical Loading Effects Measured Using Margin of Stability and Local Dynamic Stability. J Mot Behav 48:455–467

Worden TA, Vallis LA (2017) Examining Transfer Effects of Dual-Task Training Protocols for a Complex Locomotor Task. J Mot Behav 1–17. doi: 10.1080/00222895.2017.1327409

Worden TA, Vallis LA (2016) Stability control during the performance of a simultaneous obstacle avoidance and auditory Stroop task. Exp Brain Res 234:387–396. doi: 10.1007/s00221-015-4461-z

Yang F, Anderson FC, Pai Y-C (2007) Predicted threshold against backward balance loss in gait. J Biomech 40:804–811. doi: 10.1016/j.jbiomech.2006.03.015

Yang F, Anderson FC, Pai Y-C (2008) Predicted threshold against backward balance loss following a slip in gait. J Biomech 41:1823–1831. doi: 10.1016/j.jbiomech.2008.04.005

Yang F, Espy D, Pai Y-C (2009) Feasible stability region in the frontal plane during human gait. Ann Biomed Eng 37:2606–2614. doi: 10.1007/s10439-009-9798-7

Yang F, Pai Y-C (2014) Can sacral marker approximate center of mass during gait and slip-fall recovery among community-dwelling older adults? Journal of Biomechanics 47:3807–3812. doi: 10.1016/j.jbiomech.2014.10.027

You J, Chou Y, Lin C, Su F (2001) Effect of slip on movement of body center of mass relative to base of support. Clin Biomech (Bristol, Avon) 16:167–173

Zettel JL, McIlroy WE, Maki BE (2008) Effect of competing attentional demands on perturbation-evoked stepping reactions and associated gaze behavior in young and older adults. J Gerontol A Biol Sci Med Sci 63:1370–1379

Zettel JL, McIlroy WE, Maki BE (2002a) Can stabilizing features of rapid triggered stepping reactions be modulated to meet environmental constraints? Exp Brain Res 145:297–308. doi: 10.1007/s00221-002-1083-z

Zettel JL, McIlroy WE, Maki BE (2002b) Environmental constraints on foot trajectory reveal the capacity for modulation of anticipatory postural adjustments during rapid triggered stepping reactions. Exp Brain Res 146:38–47. doi: 10.1007/s00221-002-1150-5

Chapter 9. Appendices

9.1 Marker Setup and Tracking

A modified version of the Winter et al. (1998) 14-segment anthropometric model was utilized to estimate whole-body CoM kinematics for the experimental data set collected within Study 1 (Chapter 4). This data set was analyzed in both Study 1 and 2 (Chapters 4 and 5). The positions of each retroreflective marker within the 13-segment variation of the Winter model used in addition to a list of said segments are displayed in **Figure 9.1**.

During testing, markers were either affixed to the skin/clothing of the participant or were digitized to rigid clusters of 3-4 non-collinear markers. The use of the latter mitigated the potential effects of marker occlusion on data quality. Marker digitization was performed in Visual3D software using a 10-second quiet-standing reference trial collected for each participant prior to commencement of the experimental protocol. Clusters were fixed to the pelvis, thighs, and feet to locate relevant bony landmarks for each segment (**Figure 9.1**). Segmental local coordinates systems (LCS) were generated for each segment using these clusters; anatomical landmarks relevant to each segment existed at a fixed point within the respective LCS. Note that segmental rotations were not analyzed in Study 1 and 2; thus, the LCS were used only as a means of reducing the likelihood of marker occlusion lowering data quality. As such, segments tracked using physical markers were limited in the measurable degrees of freedom. Transformations of local markers positions (x, y, z) to the lab global reference frame (GCS) were completed as

$$(x', y', z')^{T} = \boldsymbol{R}\,(x, y, z)^{T} + \boldsymbol{o} \qquad 9.1$$

where $\boldsymbol{R} \in \mathbb{R}^{3\times3}$ and $\boldsymbol{o} \in \mathbb{R}^{3\times1}$ define the angular and linear orientation of the segment LCS within the GCS and (x', y', z') is the transformed position vector.

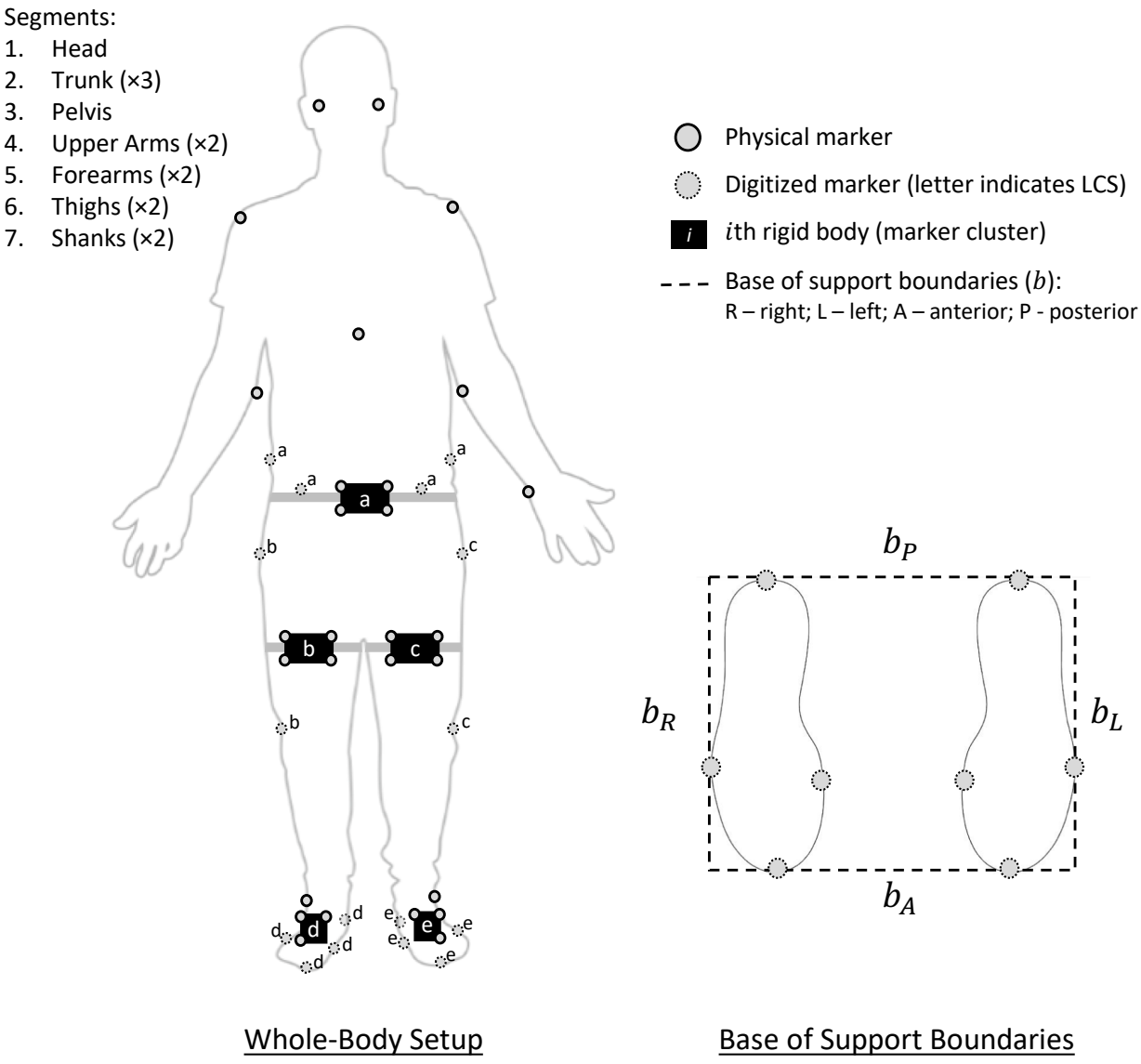

Figure 9.1 Schematic outlining the marker setup (whole-body and geometric BoS representation) used to collect 3D kinematic data for Studies 1 and 2. Superscript letters for digitized markers indicate the rigid cluster of markers that said marker belongs to. i.e. digitized to that cluster's local coordinate system.

9.2 Solution for Model Equations of Motion

The equations of motion (EOM) for the two-dimensional system introduced in Study 2 **(**Chapter 6; see **Figure 6.1**) which provide non-linear dynamics for the state space equation $\dot{\boldsymbol{x}} = f(\boldsymbol{x}, \boldsymbol{u}, t)$ were determined using Lagrangian mechanics.

Determination of the EOM first required definition of the Lagrangian function

$$L(\dot{\boldsymbol{q}}, \boldsymbol{q}) = T(\dot{\boldsymbol{q}}, \boldsymbol{q}) - V(\boldsymbol{q}) \tag{9.2}$$

Net kinetic T and potential energy V of the N rigid bodies within the system are expressed as functions of an n×1 vector of generalized coordinates $\boldsymbol{q}$ that summarize the system's n degrees of freedom. They were evaluated respectively as

$$T = \sum_{i=1}^{N} \frac{1}{2} \left(m_i \dot{\boldsymbol{r}}_i^T \dot{\boldsymbol{r}}_i + \dot{\boldsymbol{\varphi}}_i \boldsymbol{I}_i \dot{\boldsymbol{\varphi}}_i^T \right) \tag{9.3}$$

$$V = \sum_{i=1}^{N} m_i g r_{y,i} \tag{9.4}$$

Definition of T requires linear and angular segment velocities ($\dot{\boldsymbol{r}}$, $\dot{\boldsymbol{\varphi}}$) in addition to segmental mass m and inertia tensors $\boldsymbol{I}$; V requires gravitation acceleration g and vertical segment CoM position r_y. Both $\boldsymbol{r}$ and $\boldsymbol{\varphi}$ of each segment CoM in addition to their time derivatives exist within a three-dimensional Cartesian reference frame x, y, z (see **Figure 6.1** for reference) and can be expressed in terms of $\boldsymbol{q}$ for a system that operates within two dimensions as

$$\boldsymbol{r}_i(\boldsymbol{q}) = \begin{pmatrix} X + \bar{\ell}_i \cos q_i \\ Y + \bar{\ell}_i \sin q_i \\ 0 \end{pmatrix}, \qquad \dot{\boldsymbol{r}}_i(\dot{\boldsymbol{q}}, \boldsymbol{q}) = \begin{pmatrix} \dot{X} - \bar{\ell}_i \dot{q}_i \sin q_i \\ \dot{Y} + \bar{\ell}_i \dot{q}_i \cos q_i \\ 0 \end{pmatrix}, \tag{9.5}$$

$$\boldsymbol{\varphi}_i(\boldsymbol{q}) = \begin{pmatrix} 0 \\ 0 \\ q_i \end{pmatrix}, \qquad \dot{\boldsymbol{\varphi}}_i(\dot{\boldsymbol{q}}) = \begin{pmatrix} 0 \\ 0 \\ \sum_{k=1}^{i} \dot{q}_k \end{pmatrix} \tag{9.6}$$

Note that in Equation 9.4, X and Y indicate the position and velocity of the segment origin thus presenting linked-segment kinematics along an open-chain as cumulative. Basic trigonometry utilizing segment CoM position $\bar{\ell}_i$ from anthropometric table(s) was used to estimate segment kinematics, excluding platform/BoS translations (i.e. q_i for $i > 1$).

Once L is defined, the system dynamic EOM can be defined for an open or closed-chain using the Euler-Lagrange equation

$$\frac{d}{dt}\left(\frac{\partial L}{\partial \dot{q}_i}\right) - \frac{\partial L}{\partial q_i} - \sum_j^m \lambda_j \frac{\partial \Phi_j}{\partial q_i} = Q_i \tag{9.7}$$

Here, Q_i, an element of control vector $\boldsymbol{Q}$, are the non-conservative force(s)/torque corresponding to the ith element of $\boldsymbol{q}$. However, within the formulations used in Study 2, $\boldsymbol{Q}$ contained *both* non-conservative forces (e.g. muscle joint actuation, viscous damping) in addition to conservative components (torsional elastic potential energy). Additionally, stated in Equation 9.6, the d×1 vector $\boldsymbol{\Phi}$ containing d holonomic constraint functions of the form $\Phi_j(\boldsymbol{q}) = 0$; each constraint function has a corresponding Lagrange multiplier λ_j.

Equation 9.6 can effectively be rewritten as the following second-order ODE for an open-chain

$$\boldsymbol{M}(\boldsymbol{q})\ddot{\boldsymbol{q}} + \boldsymbol{C}(\boldsymbol{q}, \dot{\boldsymbol{q}})\dot{\boldsymbol{q}} + \boldsymbol{G}(\boldsymbol{q}) = \boldsymbol{Q} \tag{9.8}$$

or closed-chain

$$\boldsymbol{M}(\boldsymbol{q})\ddot{\boldsymbol{q}} + \boldsymbol{C}(\boldsymbol{q}, \dot{\boldsymbol{q}})\dot{\boldsymbol{q}} + \boldsymbol{G}(\boldsymbol{q}) - \boldsymbol{\mathcal{J}}(\boldsymbol{q})^T\lambda = \boldsymbol{Q} \tag{9.9}$$

and simplified algebraically to a series of first-order ODEs for forward dynamics simulations, e.g.

$$\begin{aligned} \boldsymbol{q}_1 &= \boldsymbol{q} \\ \boldsymbol{q}_2 &= \dot{\boldsymbol{q}}_1 \\ \dot{\boldsymbol{q}}_2 &= \boldsymbol{M}(\boldsymbol{q}_1)^{-1}[\boldsymbol{Q} + \boldsymbol{\mathcal{J}}(\boldsymbol{q}_1)^{\boldsymbol{T}}\lambda - \boldsymbol{C}(\boldsymbol{q}_1, \boldsymbol{q}_2)\boldsymbol{q}_2 - \boldsymbol{G}(\boldsymbol{q}_1)]. \end{aligned} \tag{9.10}$$

This technique provides explicit benefits through simplification of the algebra necessary to isolate and solve for $\ddot{\boldsymbol{q}}$ in addition to organization of large scale EOM.

To elaborate further on the structure of Equations 9.7-8, $\boldsymbol{M} \in \mathbb{R}^{n\times n}$ is the inertial mass matrix derived as

$$\boldsymbol{M}(\boldsymbol{q}) = \sum_{i=1}^{N} \left(m_i \boldsymbol{\Psi}_i^T \boldsymbol{\Psi}_i + \boldsymbol{\Upsilon}_i^T \boldsymbol{I}_i \boldsymbol{\Upsilon}_i \right) \tag{9.11}$$

where

$$\boldsymbol{\Psi}_i = \frac{\partial \left(\dot{r}_x, \dot{r}_y, \dot{r}_z \right)_i}{\partial (\dot{q}_1, \ldots, \dot{q}_n)}; \quad \boldsymbol{\Upsilon}_i = \frac{\partial \left(\dot{\varphi}_x, \dot{\varphi}_y, \dot{\varphi}_z \right)_i}{\partial (\dot{q}_1, \ldots, \dot{q}_n)} \tag{9.12}$$

are the linear ($\boldsymbol{\Psi}_i \in \mathbb{R}^{3\times n}$) and angular ($\boldsymbol{\Upsilon}_i \in \mathbb{R}^{3\times n}$) Jacobian matrices that contain the partial derivatives of segmental $\dot{\boldsymbol{r}}$ and $\dot{\boldsymbol{\varphi}}$ (Equations 9.4-5) with respect to $\dot{\boldsymbol{q}}$ (Asada and Leonard 2005). The constructed $\boldsymbol{M}$ matrix was characteristically symmetric ($\boldsymbol{M} = \boldsymbol{M}^T$) such that

$$\boldsymbol{M} = \begin{pmatrix} M_{ij} & \ldots & M_{in} \\ \vdots & \ddots & \vdots \\ M_{in} & \cdots & M_{nn} \end{pmatrix} \tag{9.13}$$

Elements of $\boldsymbol{C} \in \mathbb{R}^{n\times n}$, which provide the effects of Coriolis/centripetal forces within linked non-inertial reference frames, were defined using the Christoffel symbols corresponding to $\boldsymbol{M}$ (Asada and Leonard 2005). These elements are defined according to the following sequence of partial derivatives:

$$C_{ij}(\boldsymbol{q}, \dot{\boldsymbol{q}}) = \frac{1}{2} \sum_{k=1}^{n} \left(\frac{\partial M_{ij}}{\partial q_k} + \frac{\partial M_{ik}}{\partial q_j} - \frac{\partial M_{kj}}{\partial q_i} \right) \dot{q}_k. \tag{9.14}$$

The gravitational toppling column vector $\boldsymbol{G} \in \mathbb{R}^{n\times 1}$, which highlights gravitational potential energy produced by each rigid body, was determined by the gradient of $V(\boldsymbol{q})$:

$$\boldsymbol{G}(\boldsymbol{q}) = \nabla V(\boldsymbol{q}) \tag{9.15}$$

Lastly, the constraint vector $\boldsymbol{\Phi}$ was used to construct the final element, $\boldsymbol{\mathcal{J}} \in \mathbb{R}^{d\times n}$, the Jacobian of $\boldsymbol{\Phi}$ with respect to $\boldsymbol{q}$. The expression $\boldsymbol{\mathcal{J}}(\boldsymbol{q})^T \lambda$, which includes the $d\times 1$ vector of Lagrange

multipliers λ, provided a means of constraining the system to a closed-chain (i.e. double-support or bilateral stance). The complete expressions for each of $\boldsymbol{M}$, $\boldsymbol{C}$, $\boldsymbol{G}$, and $\mathbf{Q}$ as used within Study 2 are detailed in *Appendix 9.3*.

To formulate the open-chain as a closed-chain, Equation 9.8 was rearranged to account for λ, when necessary, as

$$\begin{pmatrix} \boldsymbol{M} & -\boldsymbol{\mathcal{J}}^{\boldsymbol{T}} \\ \boldsymbol{\mathcal{J}} & 0 \end{pmatrix} \begin{pmatrix} \ddot{\boldsymbol{q}} \\ \lambda \end{pmatrix} = \begin{pmatrix} \boldsymbol{Q} - \boldsymbol{C}\dot{\boldsymbol{q}} - \boldsymbol{G} \\ -\dot{\boldsymbol{\mathcal{J}}}\dot{\boldsymbol{q}} \end{pmatrix} \tag{9.16}$$

This method requires rewriting of the holonomic constraints as accelerations via differentiation of $\boldsymbol{\mathcal{J}}$ (Flores 2015):

$$\boldsymbol{\mathcal{J}}\ddot{\boldsymbol{q}} = -\dot{\boldsymbol{\mathcal{J}}}\dot{\boldsymbol{q}} \tag{9.17}$$

Thus, forward integration of the system dynamics was then able to estimate both generalized accelerations $\ddot{\boldsymbol{q}}$ and constraints forces λ.

9.3 Euler-Lagrange Matrix Expressions

The following section will outline the components calculated for the dynamics of the six segment, five degrees of freedom biomechanical model that fit the Euler-Lagrange equation (Equation 9.7). The dynamics and degrees of freedom of the model were described by a 5×1 column vector $\boldsymbol{q}$ in addition to its first and second time derivates:

$$\boldsymbol{q} = \begin{pmatrix} p_x \\ \varphi_1 \\ \varphi_2 \\ \varphi_3 \\ \varphi_4 \end{pmatrix}, \qquad \frac{d\boldsymbol{q}}{dt} \equiv \dot{\boldsymbol{q}} = \begin{pmatrix} \dot{p}_x \\ \dot{\varphi}_1 \\ \dot{\varphi}_2 \\ \dot{\varphi}_3 \\ \dot{\varphi}_4 \end{pmatrix}, \qquad \frac{d^2\boldsymbol{q}}{dt^2} \equiv \ddot{\boldsymbol{q}} = \begin{pmatrix} \ddot{p}_x \\ \ddot{\varphi}_1 \\ \ddot{\varphi}_2 \\ \ddot{\varphi}_3 \\ \ddot{\varphi}_4 \end{pmatrix} \tag{9.18}$$

Thus, the following text will outline the expressions derived within each element of $\boldsymbol{M} \in \mathbb{R}^{5\times5}$, $\boldsymbol{C} \in \mathbb{R}^{5\times5}$, $\boldsymbol{G} \in \mathbb{R}^{5\times1}$, and $\boldsymbol{Q} \in \mathbb{R}^{5\times1}$ in relation to the generalized kinematics.

$$\boldsymbol{M} = \begin{pmatrix} M_{11} & \dots & M_{15} \\ \vdots & \ddots & \vdots \\ M_{15} & \dots & M_{55} \end{pmatrix}$$

$M_{11} = \sum_{i=1}^{6} m_i$

$M_{12} = -\left(\bar{\ell}_3 m_3 + \ell_3 \sum_{i=4}^{6} m_i\right) \sin(\varphi_1)$

$M_{13} = -\bar{\ell}_4^h m_4 \cos(\varphi_2) - \left(\bar{\ell}_4^w m_4 + \ell_4 \sum_{i=5}^{6} m_i\right) \sin(\varphi_2)$

$M_{14} = -\left(\bar{\ell}_5 m_5 + \ell_5 m_6\right) \sin(\varphi_3)$

$M_{15} = -\bar{\ell}_6 m_6 \sin(\varphi_4)$

$M_{22} = I_3 + \bar{\ell}_3^2 m_3 + \ell_3^2 \sum_{i=4}^{6} m_i$

$M_{23} = \ell_3 \left(\left(\bar{\ell}_4^w m_4 + \ell_4 \sum_{i=5}^{6} m_i\right) \cos(\varphi_1 - \varphi_2) + \bar{\ell}_4^h m_4 \sin(\varphi_1 - \varphi_2)\right)$

$M_{24} = \ell_3 \left(\bar{\ell}_5 m_5 + \ell_5 m_6\right) \cos(\varphi_1 - \varphi_3)$

$M_{25} = \ell_3 \bar{\ell}_6 m_6 \cos(\varphi_1 - \varphi_4)$

$M_{33} = I_4 + m_4(\bar{\ell}_4^{h\,2} + \bar{\ell}_4^{w\,2}) + \ell_4^2 \sum_{i=5}^{6} m_i$

$M_{34} = \ell_4 \left(\bar{\ell}_5 m_5 + \ell_5 m_6\right) \cos(\varphi_2 - \varphi_3)$

$M_{35} = \ell_4 \bar{\ell}_6 m_6 \cos(\varphi_2 - \varphi_4)$

$M_{44} = I_5 + \bar{\ell}_5^2 m_5 + \ell_5^2 m_6$

$M_{45} = \ell_5 \bar{\ell}_6 m_6 \cos(\varphi_3 - \varphi_4)$

$M_{55} = I_6 + \bar{\ell}_6^2 m_6$

$M_{12} = M_{21}, \quad M_{13} = M_{31}, \quad M_{14} = M_{41}, \quad M_{15} = M_{51}, \quad M_{23} = M_{32}$

$M_{24} = M_{42}, \quad M_{25} = M_{52}, \quad M_{34} = M_{43}, \quad M_{35} = M_{53}, \quad M_{45} = M_{54},$

$$\boldsymbol{C} = \begin{pmatrix} C_{11} & \dots & C_{15} \\ \vdots & \ddots & \vdots \\ C_{51} & \dots & C_{55} \end{pmatrix}$$

$$C_{12} = -\left(\bar{\ell}_3 m_3 + \ell_3 \sum_{i=4}^{6} m_i\right) \cos(\varphi_1)\dot{\varphi}_1$$

$$C_{13} = \left(\bar{\ell}_4^h m_4 \sin(\varphi_2) - \left(\bar{\ell}_4^w m_4 + \ell_4 \sum_{i=5}^{6} m_i\right) \cos(\varphi_2)\right)\dot{\varphi}_2$$

$$C_{14} = -\left(\bar{\ell}_5 m_5 + \ell_5 m_6\right) \cos(\varphi_3)\, \dot{\varphi}_3$$

$$C_{15} = -\bar{\ell}_6 m_6 \cos(\varphi_4)\dot{\varphi}_4$$

$$C_{23} = \ell_3 \left(\left(\bar{\ell}_4^w m_4 + \ell_4 \sum_{i=5}^{6} m_i\right) \sin(\varphi_1 - \varphi_2) - \bar{\ell}_4^h m_4 \cos(\varphi_1 - \varphi_2)\right) \dot{\varphi}_2$$

$$C_{24} = \ell_3 \left(\bar{\ell}_5 m_5 + \ell_5 m_6\right) \sin(\varphi_1 - \varphi_3)\dot{\varphi}_3$$

$$C_{25} = \ell_3 \bar{\ell}_6 m_6 \sin(\varphi_1 - \varphi_4)\dot{\varphi}_4$$

$$C_{32} = \ell_3 \left(-\left(\bar{\ell}_4^w m_4 + \ell_4 \sum_{i=5}^{6} m_i\right) \sin(\varphi_1 - \varphi_2) + \bar{\ell}_4^h m_4 \cos(\varphi_1 - \varphi_2)\right)\dot{\varphi}_1$$

$$C_{34} = \ell_4 \left(\bar{\ell}_5 m_5 + \ell_5 m_6\right) \sin(\varphi_2 - \varphi_3)\dot{\varphi}_3$$

$$C_{35} = \ell_4 \bar{\ell}_6 m_6 \sin(\varphi_2 - \varphi_4)\dot{\varphi}_4$$

$$C_{42} = -\ell_3 \left(\bar{\ell}_5 m_5 + \ell_5 m_6\right) \sin(\varphi_1 - \varphi_3)\, \dot{\varphi}_1$$

$$C_{43} = -\ell_4 \left(\bar{\ell}_5 m_5 + \ell_5 m_6\right) \sin(\varphi_2 - \varphi_3)\dot{\varphi}_2$$

$$C_{45} = \ell_5 \bar{\ell}_6 m_6 \sin(\varphi_3 - \varphi_4)\, \dot{\varphi}_4$$

$$C_{52} = -\ell_3 \bar{\ell}_6 m_6 \sin(\varphi_1 - \varphi_4)\dot{\varphi}_1$$

$$C_{53} = -\ell_4 \bar{\ell}_6 m_6 \sin(\varphi_2 - \varphi_4)\dot{\varphi}_2$$

$$C_{54} = -\ell_5 \bar{\ell}_6 m_6 \sin(\varphi_3 - \varphi_4)\dot{\varphi}_3$$

$$C_{11} = \mathrm{C}_{21} = \mathrm{C}_{22} = \mathrm{C}_{31} = \mathrm{C}_{33} = \mathrm{C}_{41} = \mathrm{C}_{44} = \mathrm{C}_{51} = \mathrm{C}_{55} = 0$$

$$\boldsymbol{G} = \begin{pmatrix} G_1 \\ \vdots \\ G_5 \end{pmatrix}$$

$$G_1 = 0$$

$$G_2 = g\left(\bar{\ell}_3 m_3 + \ell_3 \sum_{i=4}^{6} m_i\right) \cos(\varphi_1)$$

$$G_3 = g\left(-\bar{\ell}_4^h m_4 \sin(\varphi_2) + \left(\bar{\ell}_4^w m_4 + \ell_4 \sum_{i=5}^{6} m_i\right)\cos(\varphi_2)\right)$$

$$G_4 = g\left(\bar{\ell}_5 m_5 + \ell_5 m_6\right)\cos(\varphi_3)$$

$$G_5 = \bar{\ell}_6 m_6 g \cos(\varphi_4)$$

$$\boldsymbol{Q} = \begin{pmatrix} F_p \\ \tau_1 - \tau_2 \\ \tau_2 - \tau_3 \\ \tau_3 - \tau_4 \\ \tau_4 \end{pmatrix}$$

$$\tau_1 = \gamma_1^{Ev} - \gamma_1^{In} - B_A\dot{\varphi}_1 - K_A c_y\big|_{\bar{c}=0.5}(\varphi_1 - \pi)$$

$$\tau_2 = \gamma_2^{Ab} - \gamma_2^{Ad} - B_H(\dot{\varphi}_2 - \dot{\varphi}_1) - K_H\lfloor\varphi_1, \varphi_2\rfloor c_y\big|_{\bar{c}=0.5}$$

$$\tau_3 = \gamma_3^{Ab} - \gamma_3^{Ad} - B_H(\dot{\varphi}_3 - \dot{\varphi}_2) - K_H\lfloor\varphi_2, \varphi_3\rfloor c_y\big|_{\bar{c}=0.5}$$

$$\tau_4 = \gamma_4^{Ev} - \gamma_4^{In} - B_A(\dot{\varphi}_4 - \dot{\varphi}_3) - K_A(\lfloor\varphi_3, \varphi_4\rfloor - \pi)c_y\big|_{\bar{c}=0.5}$$

*A reminder that $\lfloor\varphi_i, \varphi_j\rfloor$ denotes the relative joint angle defined by absolute angles i and j. For consistency, we defined angle of the left foot $\lfloor\varphi_3, \varphi_4\rfloor$ such that it was equivalent to definitions of φ_1.